THE TRAVELING WAVE: A CONCEPT FOR ENHANCING UNDERWATER VEHICLE PERFORMANCE

31 December 1991

DTIC
ELECTE
JUL 14 1992
S
A
D

Prepared for:

DARPA Submarine Technology Program
HYDRODYNAMIC PROGRAM AREA
COTR: Mr. Gary Jones

Mr. K. J. Moore	- CORTANA
Dr. M. Noori	- CORTANA
Dr. J. Wilson	- CORTANA
Dr. J. M. Wu	- ERCI
Dr. A. Rubel	- GRUMMAN
Dr. M. Stern	- GRUMMAN
Mr. R. Balasubramanian	- SPECTREX

92-18341

REPORT DOCUMENTATION PAGE

Form Approved
OMB No. 0704-0188

Public reporting burden for this collection of information is estimated to average 1 hour per response, including the time for reviewing instructions, searching existing data sources, gathering and maintaining the data needed, and completing and reviewing the collection of information. Send comments regarding this burden estimate or any other aspect of this collection of information, including suggestions for reducing this burden, to Washington Headquarters Services, Directorate for Information Operations and Reports, 1215 Jefferson Davis Highway, Suite 1204, Arlington, VA 22202-4302, and to the Office of Management and Budget, Paperwork Reduction Project (0704-0188), Washington, DC 20503.

1. AGENCY USE ONLY (Leave blank)	2. REPORT DATE 31 DEC 1991	3. REPORT TYPE AND DATES COVERED FINAL 08/88 to 12/91

4. TITLE AND SUBTITLE

The Traveling Wave: A Concept for Enhancing Underwater Vehicle Performance

5. FUNDING NUMBERS

C - MDA972-88-C-0064
TA - II.B

6. AUTHOR(S)

Mr. K.J. Moore, Dr. M. Noori, Dr. J. Wilson, Dr. J.M. Wu, Dr. A. Rubel, Dr. M. Stern, Dr. R. Balasubramanian

7. PERFORMING ORGANIZATION NAME(S) AND ADDRESS(ES)

Cortana Corporation
520 N. Washington Street, Suite 200
Falls Church, VA 22046

8. PERFORMING ORGANIZATION REPORT NUMBER

9. SPONSORING/MONITORING AGENCY NAME(S) AND ADDRESS(ES)

Defense Advanced Research Projects Agency
Submarine Technology Program
3701 North Fairfax Drive
Arlington, VA 22203-1714

10. SPONSORING/MONITORING AGENCY REPORT NUMBER

11. SUPPLEMENTARY NOTES

12a. DISTRIBUTION/AVAILABILITY STATEMENT

APPROVED FOR PUBLIC RELEASE
DISTRIBUTION UNLIMITED

12b. DISTRIBUTION CODE

13. ABSTRACT (Maximum 200 words)

Over the past 25 years, Soviet researchers have been investigating the potential of a traveling wave, imposed at the surface of a body, to reduce the drag of the body. The Soviets contend that when properly posed, the traveling wave will produce a system of entrained vortices which lead to a significant reduction in shear stress without a concomitant penalty in pressure drag.

The possibility of using vortical flow to reduce drag has been known in the United States for a number of years. Suitably positioned transverse slots can result in entrained vortices and a significant reduction in base drag over the closure of a bluff body. In addition, experiments at NASA Langley have shown that ordered periodic vorticity injected into a turbulent boundary layer near the wall results in 20 to 25 percent drag reduction over nominal flat plate values.

While the Soviet literature presents some theory and some experimental results, it is often incomplete and difficult to follow. The parameter space for successful implementation of the traveling wave has been, until now, elusive. Identification of the appropriate parameter space requires an understanding of the physics of the traveling wave. The purpose of the research reported has been to develop an understanding of the traveling wave phenomenon through analytical and computational investigations. This report presents the results of research to date and maps out a plan for determining the feasibility of implementing the traveling wave for drag reduction on underwater vehicles.

14. SUBJECT TERMS Drag reduction; Submarines; Vortices; Foreign Technology	15. NUMBER OF PAGES 171
	16. PRICE CODE

17. SECURITY CLASSIFICATION OF REPORT UNCLASSIFIED	18. SECURITY CLASSIFICATION OF THIS PAGE UNCLASSIFIED	19. SECURITY CLASSIFICATION OF ABSTRACT UNCLASSIFIED	20. LIMITATION OF ABSTRACT UL

NSN 7540-01-280-5500

Standard Form 298 (Rev. 2-89)
Prescribed by ANSI Std. Z39-18
298-102

EXECUTIVE SUMMARY

BACKGROUND

Over the past 25 years, Soviet researchers have been investigating the potential of a traveling wave, imposed at the surface of a body, to reduce the drag of the body. The Soviets contend that when properly posed, the traveling wave will produce a system of entrained vortices which lead to a significant reduction in shear stress without a concomitant penalty in pressure drag.

The possibility of using vortical flow to reduce drag has been known in the United States for a number of years. Suitably positioned transverse slots can result in entrained vortices and a significant reduction in base drag over the closure of a bluff body. In addition, experiments at NASA Langley have shown that ordered periodic vorticity injected into a turbulent boundary layer near the wall results in 20 to 25 percent drag reduction over nominal flat plate values.

PURPOSE

While the Soviet literature presents some theory and some experimental results, it is often incomplete and difficult to follow. The parameter space for successful implementation of the traveling wave has been, until now, elusive. Identification of the appropriate parameter space requires an understanding of the physics of the traveling wave. The purpose of the research reported herein has been to develop an understanding of the traveling wave phenomenon through analytical and computational investigations. This report presents the results of our research to date and maps out a plan for determining the feasibility of implementing the traveling wave for drag reduction on underwater vehicles.

SPECIFIC CONTENT

This report begins with a brief review of traveling wave-related research from the late 1950s to the present day. Soviet researchers at the Institute of

i
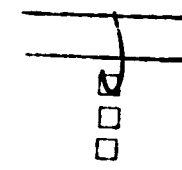
Hydromechanics in Kiev have been active in this field over a number of years, and both experimental and theoretical studies have been reported. Merkulov was the first to identify the possible advantages of secondary flow with controlled vortices in reducing drag. Other related experimental studies have been performed in France, Japan and the United Kingdom. In the late 1970s and into the 1980s researchers at NASA Langley investigated compliant surfaces and fixed wavy walls with small amplitude.

In Chapter II the basic physics of the traveling wave is discussed in the context of related investigations of other unsteady flow phenomena. It is important to distinguish between the behavior of a traveling wave and that of a translating wavy wall. In the former case, a progressive wave on a body surface results from the displacement of any point on the surface in a plane normal to the direction of wave propagation. There is no displacement of points on the surface parallel to the propagating wave, in contrast to the translating wavy wall situation. Insight into traveling wave parameter space was initially gained with excursions from the von Kármán street solution. The traveling wave results in vortex generation at the wave troughs and establishment of a secondary flow condition which cannot be classified as conventional laminar, transitional or turbulent flow, but rather constitutes a new regime described as "controlled vortical flow." The critical parameters in establishing stable vortical flow of this type have been identified as the amplitude-to-wavelength ratio of the traveling wave, a/λ, and the ratio of wave velocity to freestream velocity, c/U_∞ and the wavelength Reynolds number, Re_λ.

A number of computational approaches have been identified for simulation of traveling wave behavior, namely the spectral method, the discrete element method, and the use of finite difference codes such as ARC2D. Numerical results have been obtained for various wave profiles and critical parameter values $a/\lambda > 0.1$ and $c/U_\infty > 0.4$. The simulations are incomplete due to resource limitations, but the data provide useful insights into the physics of the traveling wave and have enhanced understanding of the associated phenomena.

Drag characteristics of a traveling wave wall mid-region (neglecting leading edge and trailing edge effects) have been determined for Reynolds numbers,

based on wavelength, in the range 10^3 to 5×10^4. The plate lengths investigated were on the order of 30 wavelengths. Results of our investigations indicate that a rapid increase in drag, associated with vortex formation, is expected near the leading edge of the flexible plate. Over a short distance, less than a wavelength, the drag decreases, with some fluctuations, to an equilibrium value. Steady state values of both skin friction drag and pressure drag are reduced, compared to values for a flat plate. Drag levels are found to vary significantly with wall geometry (a/λ, wave profile) and with flow parameters (c/U_∞). The value of drag also depends upon inflow Reynolds number, that is, the character of the developed boundary prior to the first wave. A concern shared by the investigators involves the imposition of periodic boundary conditions for the computational investigation. It is recognized that one must be extremely careful in drawing conclusions from calculations performed in this manner.

An important factor in assessing potential practical implementation of the traveling wave is the trade-off between the energy required for wall activation and the energy reduced through drag reduction. Rough estimates of hydrodynamic power expenditure for a traveling wave vortex system have been obtained analytically. Preliminary hydrodynamic energy calculations have been performed using the spectral code. Also, there is a need to investigate in more detail the acoustic phenomena associated with the traveling wave, particularly in the context of possible practical applications. Both additional energy and noise calculations are clearly required.

The results of analytical and numerical studies of traveling wave behavior have indicated the need for an experimental proof-of-concept investigation. Parameter ranges of interest have been identified based on the theoretical results. The design and materials aspects of active wall systems have been investigated with a view to constructing a traveling wave test device. Recommendations are made based on "lessons learned" from existing devices and information on state-of-the-art actuator systems. Mechanical actuation is the most feasible method presently available to "actively" generate waves with amplitudes on the order of 1 cm. (This target value has been defined on the basis of theoretical results and Reynolds numbers for typical submarines.) A mechanically-driven active wall device would be noisy and cumbersome, and
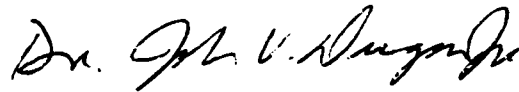
thus unsuited to practical submarine applications. However, valuable data on traveling wave behavior that could illuminate the properties required for a more practical "passive" coating would be obtained using a test device of this type for water tunnel experiments. A laboratory-scale experimental investigation has been identified as a possible next step in furthering current understanding of the physics of the traveling wave. Preliminary designs and order-of-magnitude cost estimates for active wall test devices have been obtained.

Given state-of-the-art actuator materials/systems, the installation of an active wall traveling wave device on an underwater vehicle is problematic, at least if wave amplitudes on the order of 1 cm are required. However, an auto-oscillatory system based on a passive elastic coating may provide a means of implementing the traveling wave concept. In this instance, a suitable combination of elastic properties and flow parameters would result in energy exchange between the fluid and coating such that a traveling wave develops on the coating surface. At this time, an auto-oscillatory system appears to offer the greatest potential for implementation.

ACKNOWLEDGEMENTS

CORTANA CORPORATION

Dr. John V. Dugan, Jr.
Program Manager,
DARPA Advanced Submarine
Technology and Integration Program

TABLE OF CONTENTS

LIST OF FIGURES

Page

LIST OF TABLES

I. INTRODUCTiON

PRESENT RESEARCH OBJECTIVES

This report is primarily intended to present an overview of past developments, results of current research, and to serve as a guideline for a basic understanding of the physics of the traveling wave. One of the initial objectives of this study is to understand the concept of the traveling wave which originated in Soviet literature, and to fill the holes and shortcomings associated with it. For example, some of the parameters which were not discussed in detail in the Soviet literature are the wall profile and optimum values for amplitude to wavelength ratios for specific wave to freestream velocity ratio (c/U_∞). In this report, both the wall profile and relationship between critical parameters are examined for several periodic cases.

Another objective of the ongoing research is to obtain a detailed understanding of the physics and the mechanics of the traveling wave concept. Once the physics and critical *hydrodynamic control parameters* are understood, experimental verification can proceed. At this time it can be shown that under specific conditions, which are dictated by a stability analysis and relate the wall and flow parameters, it is possible to produce and maintain a secondary flow over a traveling wave. The secondary flow is associated with entrapment of vortices in the wave troughs, where they can be stabilized. Initial identification of the main parameters and the quantitative relationships between them is nearly complete. Procedures to calculate the total drag for the trapped vortices and a parametric relationship between the vortex location and minimum drag (or thrust) level are presented.

A further objective of this research is to identify the limits of the implementation of the traveling wave on underwater vehicles. It is possible that this technology may be limited to small-scale vehicles or is suitable only for turbulent flow. Although implementation of a wave traveling with a certain velocity requires some energy expenditure, indications are that the overall efficiency of the whole system may, in some circumstances, be better than that of a regular planar surface. Obviously, the most important objective is to calculate, in detail if

possible, analytically and numerically the energy requirement and energy balance to maintain the activated wall. A comparison of the hydrodynamic energy expenditure with that of the flat plate, at the same condition, can give a good estimate of the energy requirements. Understanding the mechanisms that govern the traveling wave concept will help to formulate a viable model. By an organized team effort, a plan of attack has been established to resolve the various questions associated with refining this concept and to arrive at the selection of parameters for a proof-of-concept experiment. Experimental verification and data collection will be reported subsequently.

HISTORICAL BACKGROUND

Overview

The following introduction includes a chronological history of the research conducted on the traveling wave concept. This report includes a brief analysis of previous research which relates to the active wall and traveling wave concept. We wish to emphasize the fact that the main concern of the previous research was not always to trap the vortex and generate a secondary flow field. In all these studies, the goal was to reduce the resistance to the fluid motion or to produce thrust.

Early Period (up to 1975)

The emergence of the traveling wave concept began with Kramer's (1957, 1960, 1965) extensive studies on dolphin locomotion. Although he did not identify the traveling wave concept, his goal was to reduce the drag of a submerged body by covering it with a specially designed compliant coating. He called this technique "stabilization by distributed damping." His basic hypothesis was that the anisotropic nature of the coating and the viscosity of the substrate fluid would control and damp out enhancement of laminar instabilities in the flow over the vehicle. This would result in a delay of transition to turbulent flow so that the boundary layer would remain in a condition between laminar and turbulent (i.e. transition), thus producing considerable drag reduction. While many Western researchers attempted experiments to imitate Kramer's

work, it now appears that only Soviet researchers recognized the significance of Kramer's insight that the coating should be anisotropic in the direction of flow such that natural perturbations would be translated in an ordered fashion along the surface and in the direction of flow.

Following Kramer's study, the pioneering theoretical studies on the problem were done by Benjamin (1960, 1963) and Landahl (1962). Benjamin's theoretical studies included treatments of shearing flows bounded by a simple harmonic wavy surface, and his main objective was to calculate the normal and tangential stresses on the boundary. In spite of extensive valuable studies by him and other researchers, it appears that only a small group of Soviet researchers identified the advantages of a secondary flow with controlled vortices that is presently of interest.

The fundamental idea of vortex shielding was explained best by Merkulov (1967) who considered the possible mechanisms for reducing hydrodynamic resistance by a traveling wave. His theoretical studies attempted to determine the flow conditions under which a traveling wave, with specific parameters, will propagate in a secondary flow regime such that the freestream is in contact with the secondary flow rather than a rigid surface. Basically, this study examined, with a detailed mathematical derivation, the oscillation of an elastic plate with an ideal fluid flow along the direction of oscillation.

In 1970 Kendall performed a series of experimental wind tunnel studies on the turbulent boundary layer over a wall subjected to a traveling wave propagation. Due to the nature of his experimental setup and his parameter range, he was not concerned with the generation of secondary flow and vortex formation. Later in 1970, Merkulov and Savchenko performed an experimental, as well as a theoretical, study of a viscous fluid flow along a traveling wave. There, for the first time, the description of the phenomena was referred to as the "traveling wave theory." One of the most interesting findings from this report is presented in graphical form in Figure 1. This Figure presents the coefficient of friction as a function of Reynolds number for various traveling wave relative phase velocities. The number on each curve indicates the value of c/U_∞. The relative phase velocity appears to be defined as the ratio of the wave velocity c to the freestream velocity U_∞ in this case. Unfortunately, in other cases it is defined as

3

c/(U∞ -c). Hence, there is uncertainty in the actual values presented in this graph and some inconsistencies with later published data by Savchenko, one of the two authors. It is evident from the graph that the drag at zero phase velocity corresponding to a flow over a solid wavy wall is considerably in excess of drag on a smooth flat plate. However, C_d rapidly decreases with increase in the phase velocity.

$C_d \times 10^{-3}$
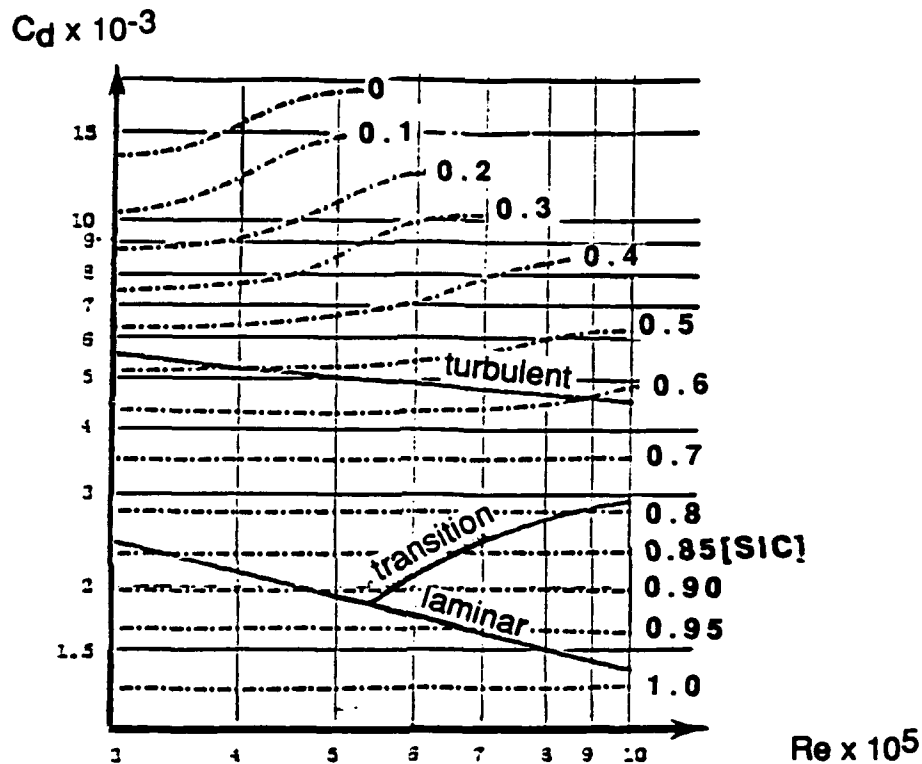
Figure 1. C_d of Reynolds Number at Various Relative Velocities
(Merkulov & Savchenko, 1970)

In their study Merkulov and Savchenko specifically identified the occurrence of a secondary flow in each traveling wave trough or cell, where a closed vortex is formed and the local flow is vortical. They also addressed the fact that the replacement of the normal turbulent boundary layer by a spatially periodic array of vortices results in a fundamental alteration to the relevant Reynolds number of the flow; therefore, the characteristic length is no longer described by the body length, but instead can be related to the wavelength of the periodic structure. Since the flow was periodic, the length of the body was claimed to be inconsequential, because the flow in each cell was independent of the total

number of cells or the location of any cell in the sequence. In addition to their experimental study, they raised the question of energy requirements. Based on their experimental evidence, they claimed that an insignificant energy expenditure will be required to maintain the secondary flow system in comparison to maintaining a turbulent boundary layer over a flat plate.

Some of the most significant experimental research in the traveling wave phenomenology outside the Soviet Union has been conducted in France. Rousseau (1972) demonstrated that traveling waves were used by dolphins, by placing a strain gauge on the skin of a dolphin and measuring the well-defined cyclical strain variations with very low frequencies (in the order of 10 Hz). Subsequently, Mattout (1972) conducted an experiment with water flow over a mechanically activated surface and succeeded in attaining a reduction in frictional drag. The reductions reported were in the range of 7 to 25 percent for the passive and active wall, respectively. In these studies the researchers did not identify the generation of the secondary flow and vortex formations. However, the reported reduction in drag with both positive and negative wave velocities suggests that a secondary flow was established in at least some instances.

Japanese researchers also have shown some interest in the traveling wave concept. Taneda and Tomonari (1974) have performed extensive experimental studies on the flow along a wavy rubber plate. The experiment was carried out in a low speed wind tunnel and in a small water tank. The Reynolds number based on the rubber plate length was of the order of 10^5. In this study, they showed that upon the proper choice of freestream (U_∞) and phase velocities (c), one can trap the vortices in troughs of waves and generate a vortical secondary flow. Figure 2 shows a representative flow pattern.

Recent Period

Related studies in unsteady or "vortex thrust" flows have followed Merkulov's initial research in the Soviet Union. These research studies consisted of flapping wing type engine (Savchenko 1971), viscous flow around flexible bodies, (Nikishova and Babenko 1975), and flow around an elastic cylinder (M. Ilgamov, 1975). The physics of these kinds of flow are in principle similar to the

5

physics of the traveling wave flow; however, the scales are much larger and the effect is to provide thrust rather than control the boundary layer. As will be shown in later sections of this report, scale is an important aspect of a traveling wave system.
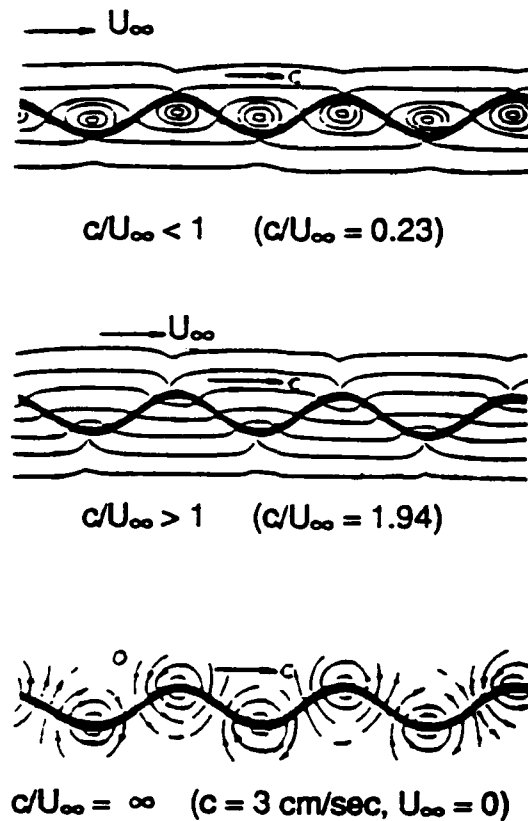
Figure 2. Variation of Streamline Flow Pattern with c/U_∞
(Taneda et al. 1974)

Savchenko (1979) conducted experimental, analytic, and numerical calculations of the flow over a wall with a traveling wave. He reported agreement between the experimental and numerical results (Figure 3). The closed vortices were assumed to behave like roller bearings, and a simplified energy calculation was performed based on this model. In his study the non-dimensional wave velocity is defined as $c/(U_\infty - c)$. In terms of energy saving, for typical flow and wall parameters and for a Reynolds number on the order of 10^7 based on a characteristic plate length, Savchenko calculated, in a simplified

form, the energy expenditure to maintain the vortical flow system to be only one-eighth that of a turbulent boundary layer.
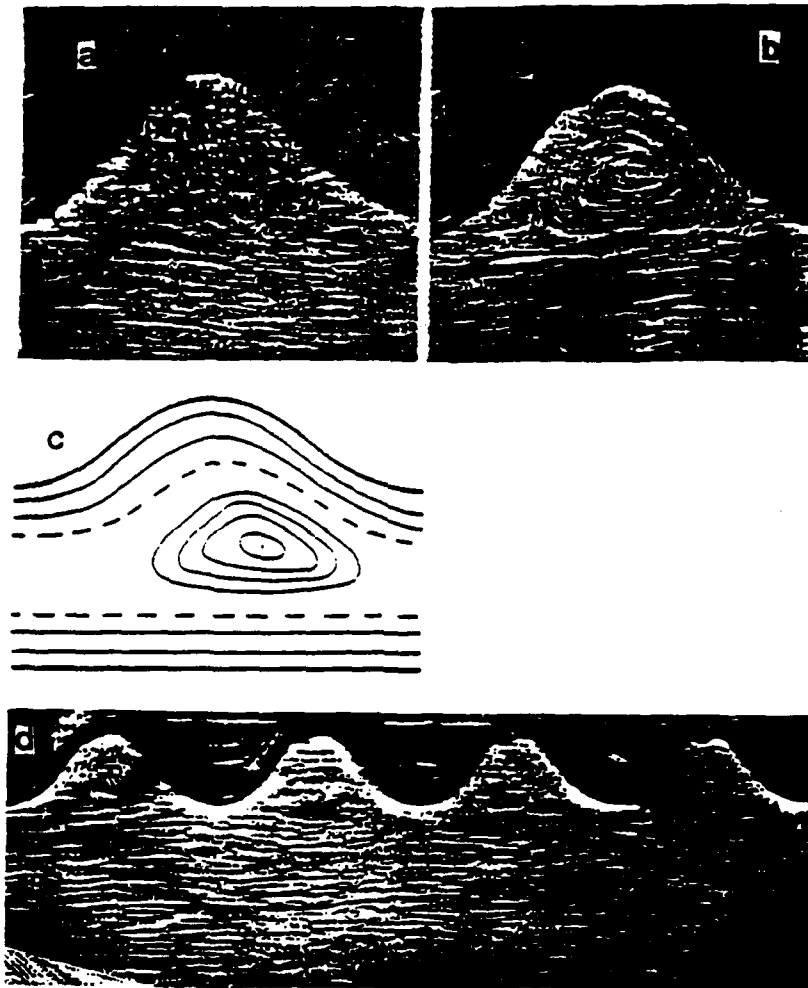
Figure 3. Flow Pattern Along Traveling Wave: a - Flow in Depression Between Wave Crests at c = 0; b - at $c/(U_\infty-c) = 1/2$; c - Digital Computer Calculation of Flow Pattern; d - Flow Along Surface of Model at $c/(U_\infty-c) = 1/2$

In the late 1970s and into the 1980s, Bushnell et al., conducted a series of experimental, numerical and theoretical studies on flow over both compliantly coated and fixed wavy walls at NASA. They investigated laminar and low speed turbulent flows over various wavy rigid surfaces having wavelengths on the order of the boundary-layer thickness. Due to the parameter range (small amplitude-to-wavelength ratio), they did not observe any ordered vortex formation and secondary flow effects, although they identified several configurations which produced an indication of a small drag reduction. However, as will be discussed later in this report, Bushnell's work and his experience and that of his teammate, R. Balasubramanian, provided the basis for numerical calculations in the present research.

This review of previous research reveals the fact that many of the Soviet studies of flow over a deformable surface were indeed focused on the traveling wave concept and the generation of controlled vortical flow. On the other hand, Western researchers were not specifically concerned with the vortical flow. Table 1 presents a summary of the several research efforts relating directly or indirectly to the traveling wave concept. This Table presents the name, year and nature of the research. It can be seen from the Table that much of the Soviet research is indeed associated with vortex formation. The main topics of the Soviet research relating to the traveling wave concept are listed in Table 2. However, for comparison purposes, a list of some of the Western related studies of the flow over a traveling wave is presented in Table 3.

Table 3 presents the parameter space for several earlier Western studies. Most of these studies were in a parameter space where no vortical flow has been identified. It will be shown that the two critical ratios identified, a/λ and c/U_∞, for all of these studies except for Taneda et al. (1974) vary from the present study by more than an order of magnitude. Based upon the present work, these other studies investigated only situations where these critical values were out of the proper range of vortex entrapment. As shown later in this report, in order to establish an ordered vortical flow a/λ must be ≥ 0.1 and < 0.3 and c/U_∞ must be in the order of 0.5. To date, only the importance of c/U_∞, the later value, is indicated in the Soviet literature. To add to the confusion, the Soviets often use the value of $c/(U_\infty - c)$ rather than c/U_∞. While displaying empirical examples of its importance, the literature has yet to provide a supporting rationale. It should

8

be noted that values of 0.5 and 1.0 for c/U_∞ - c are 0.33 and 0.5, respectively, for c/U_∞. Thus, the results of Soviet and Western research, including the results presented herein, regarding the implications of wave velocity relative to the freestream velocity are consistent.

Table 1. History of Traveling Wave Related Research

INVESTIGATOR	NATURE OF STUDY	VORTEX FORMED?
Kramer (1955-65)	Experimental (Anisotropic Compliant Coating)	No
Benjamin (1959-64)	Theoretical (Rigid Wavy Surface)	No
Merkulov (1967)	Theoretical	Yes
Kendall (1969)	Experimental	No
Merkulov & Savchenko (1970)	Numerical/Experimental	Yes
Mattout (1972)	Experimental	No
Taneda, et al. (1974)	Experimental	Yes
Ilgamov, et al. (1975, 1978, 1983)	Experimental/Theoretical	Unknown
Savchenko (1979)	Theoretical/Numerical	Yes
Bushnell, et al. (1980s)	Numerical/Experimental (Small amplitude)	No
Berkovskiy & Puchkova (1981)	Theoretical/Numerical	Yes
Tyndall (1988)	Theoretical/Experimental	Yes
Wu, et al. (1990)	Theoretical	Yes
Present Study (1990, 1991)	Theoretical/Numerical	Yes

Table 2. Some of the Main Topics of Soviet Studies

- Demonstration of Secondary Flow
- Identification of Critical Parameters for Vortex Entrapment
- Discussion on Stability Problem
- Basic Energy Calculation
- Various Experimental Verification Techniques

Table 3. Parameter Scales for Some of the Traveling Wave Research

Author	Media	a (mm)	λ (mm)	a/λ	L (cm)	c (m/s)	c/U_∞	f (Hz)	U_∞ (cm/s)	Re_λ
Wehrmann (1965)	-	1×10^{-3}	42	2.38×10^{-5}	4.2	2.1	6.5k	50	3.2×10^{-2}	--
Kendall (1970)	air	3.18	102	3.1×10^{-2}	122	0.3 to 3	0.19	30	$1.6\times10^{+2}$	10^4 to 10^5
Taneda et al. (1974)	air and water	15 to 50	80 to 1200	4×10^{-2} to 1.9×10^{-1}	20 to 230	0.15 to 4.5	0.23 to ∞	--	--	$\sim10^3$ to 10^5
Weinstein & Balasubramanian (1977)	-	2×10^{-2}	1.8	1.1×10^{-2}	40	0	0.0	--	25	--
Park et al. (1985)	water*	1.3×10^{-2}	10	1.3×10^{-3}	4	0.1 to 1.5	120 to 150	10 to 150	1.0	<10
Present Study (1990)	water*	--	--	$(1.0\text{-}2.5)\times10^{-1}$	-	-	0.0 to 0 7	--	--	10^3 to 5.5×10^4

* Indicates that the experimental study has not yet been conducted.

L is the total length of the plate and Re_λ is based on U_∞ and λ

II. CURRENT INTERPRETATION OF THE PHYSICS

CHARACTERISTICS OF THE TRAVELING WAVE CONCEPT

<u>Background</u>

In this section, our current understanding of the basic physics of the traveling wave will be presented. First a set of terms and definitions, as well as a general characterization of the traveling wave concept, are required. A traveling wave, as defined herein, is a progressive wave on the body surface. It will be shown that with proper physical and geometrical parameters, and a certain phase velocity, an ordered vortical flow can be established. The suitable choice of these dynamic wall parameters will produce vortices in each of the wave's troughs and maintain a secondary but periodic flow condition. The phenomenon is an inherently unsteady flow phenomenon. Further, the rotation of the vortices and the wall motion can sustain a thin shear layer at the wall which has velocity in the direction of the wall. Between the vortices and the freestream is a second Rayleigh-like layer also with a velocity gradient less than an equivalent flat plate. It is crucial to note that, due to the very special nature of the flow, assumptions derived from laminar and turbulent flow concepts in the conventional manner (for instance, flat plate or pipe flow) are not necessarily valid assumptions, and one might refer to this new flow regime as "Controlled (or Ordered) Vortical Flow," as this report does henceforth.

<u>Related Studies</u>

Japanese experimental studies of the flow around flexible bodies for a large amplitude progressive wave (Taneda et al. 1974) are consistent with Soviet published results. It was shown that for a proper set of wave parameters (amplitude, wavelength), for values of the ratio of wave phase velocity c to the freestream velocity U_∞ less than unity, a controlled vortical flow regime can be achieved. In Figure 2, page 6, patterns of streamlines along such a flow, identified by means of an electrolysis method and smoke photographs, are depicted. In a theoretical study on the kinematics of a flexible and oscillating

11

plate, Dombrov et al. (1978) showed similar flow patterns on a traveling wave with low vibrational amplitude, propagating along a plate. Figure 4 shows this theoretical pattern derived from their calculation for a phase velocity less than the freestream velocity. This result is in general agreement with Taneda's experimental results (1974).
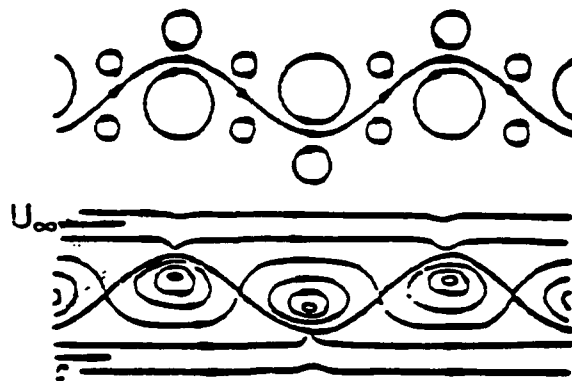
Figure 4.   Pattern of Flows Created By Dombrov et al. (1978) Theoretical Study (U_∞ is the Freestream Velocity and c is the Traveling Wave Velocity)

Kalugin and Panchuk (1970) also identified similar flow patterns. They performed a numerical computation of a two-dimensional, unsteady, viscous, incompressible flow along a traveling wave wall. They numerically solved the Navier-Stokes equation within the limit of a one-wave period assuming a periodic flow condition in an infinite channel and demonstrated the formation of the vortices and secondary flow. Figure 5 shows the resultant streamlines from their numerical calculations at different time steps for specific parameter combinations. This Figure shows the vortex formation as computational time increases. Later on in this report, very similar computational results will be shown.
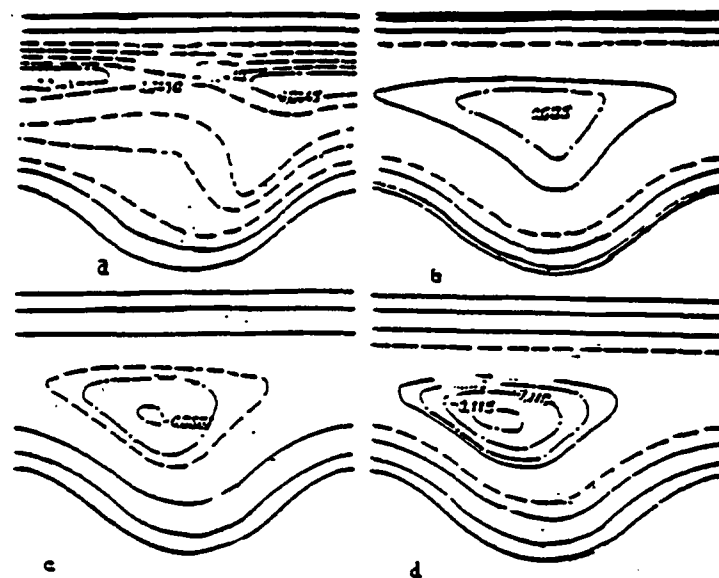
a) t=10 b) t=20 c) t=30 d) t=40

Figure 5.   Results of Numerical Computations for Various Times (Kalugin
             & Panchuk, 1970)

Among the Western research on related topics in the past 20 years, D. Bushnell
and his co-workers raised the possibility of turbulence control through altering
its structure. It is known that the introduction of unsteady transverse vorticity
with circulation opposite to the mean vorticity of the turbulent boundary layer
can measurably reduce the drag. In this regard, the NASA research by
Bushnell's colleague on the effect of introducing ordered vorticity into turbulent
wall flow (W. Goodman, 1985) is of particular interest. Studies have shown that
a cylinder adjacent to a flat plate will produce a modified Kármán-vortex street.
If the cylinder is sufficiently close to the surface, one component of the shed
vorticity will be almost completely suppressed (Figure 6). Placing such a
configuration into the outer region of a turbulent boundary layer will suppress
turbulence and reduce drag by the introduction of vorticity. Introduction of
vorticity of both positive and negative signs has been shown to reduce drag,
with opposing vorticity being somewhat more effective.   This phenomenon is
basically a method of turbulence control. Altering its structure actually "excites"

13

or "energizes" the turbulence and provides separation control. About 25% drag reduction over nominal flat plate values has been reported.

This result suggests that by altering the turbulent structure by generation of ordered vortices, the drag will be reduced. However, the problem of maintaining the vortices and their stability, in general, are issues that need to be resolved. Flow/turbulence control is precisely what is required for successful application of the traveling wave. By proper choice of the flow and wall parameters, the traveling wave will produce an ordered energy system through the controlled vortical flow and, in a simplified sense, can be visualized as acting as a roller bearing between the wall and the freestream. Rather than randomly energize the boundary layer, the traveling wave provides stable, systematic and ordered vortices that can be controlled to suit the condition for minimum drag.

(A) Cylinder

Flow →

(B) Cylinder with control plate for suppression of alternate shedding

Flow →

(C) Plate in close proximity to cylinder

Flow →
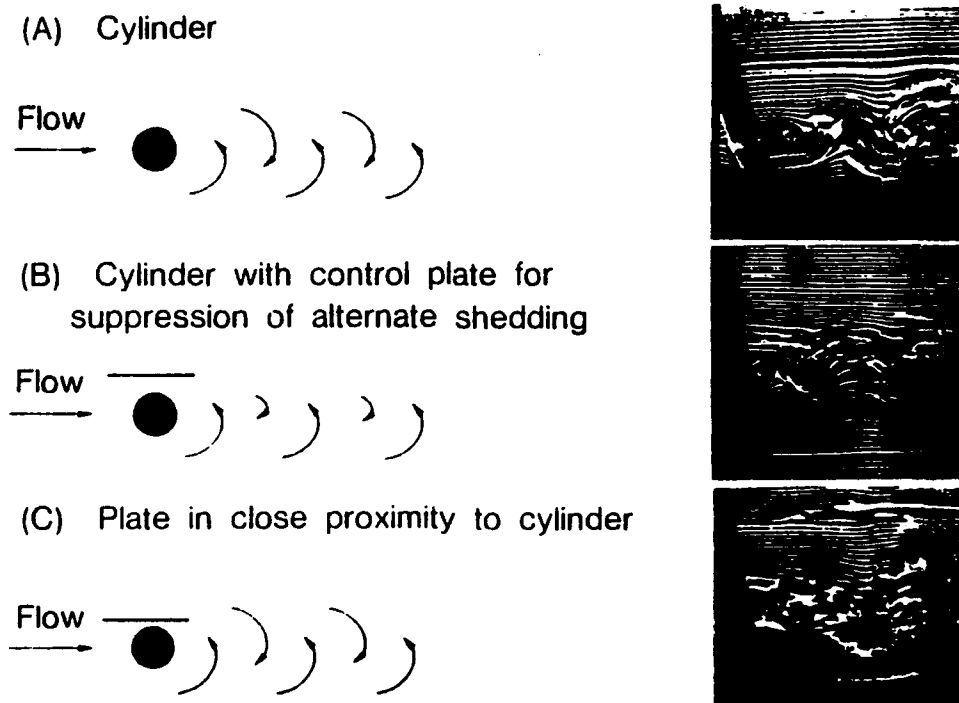
Figure 6.   Cylinder, Plate Configuration for Creation of Single Sided Vortex Street to Reduce the Drag on a Turbulent Boundary Layer (Goodman, 1985)

14

Another important related experimental investigation which can be serve to illuminate the traveling wave concept is the study on the transverse grooves on a bluff afterbody by F.G. Howard et al. (1983). That research has shown that the separation, which occurs just downstream of the shoulder of the body boattail of a non-grooved bluff afterbody, can be avoided and the flow will remain attached over a much greater region of a bluff afterbody on which transverse grooves are employed in the shoulder region. Measurements showed that the better flow attachment reduces the drag coefficient at the intermediate Reynolds number (approximately 0.3 to 1.3 x 10^5) for the grooved afterbody, Figure 7.
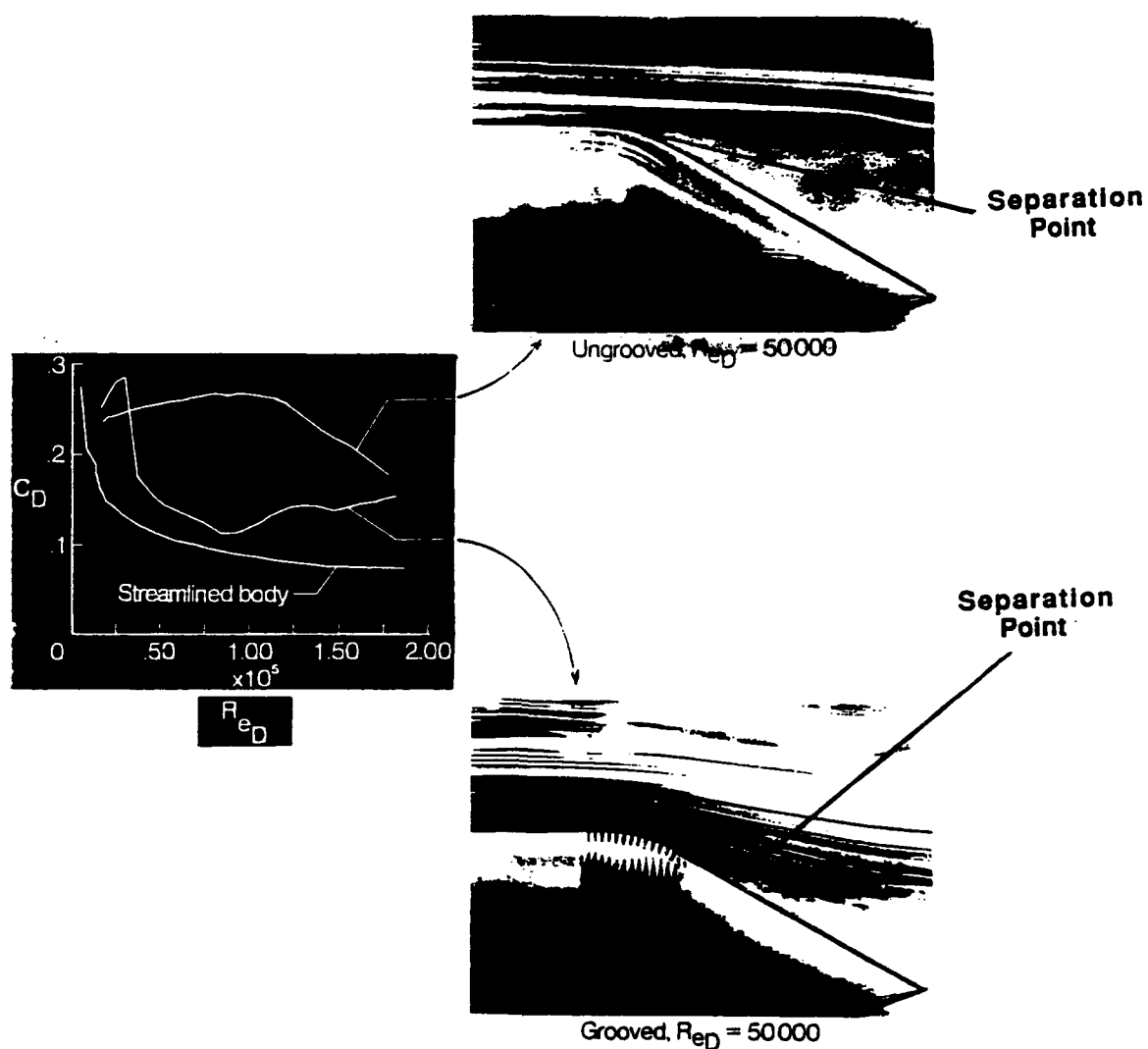
Figure 7.   Effect of Afterbody Transverse Grooves to Drag Coefficient

15

The mechanism of transverse grooves appears to be one of substituting several small regions of separation for a larger separated flow region. It is recognized that in flow over enclosed cavities, vortices can be formed within the cavity. The grooves thereby act as local low pressure areas which are located in the regions of a high longitudinal pressure gradient. These transverse grooves need to be tailored to provide a reduced drag coefficient at a particular Reynolds number. The tailoring of the grooves can be compared to the traveling wave concept, where the size of the grooves relates to the wave amplitude and wavelength of the traveling wave. In both cases, the near-wall vorticity provides a more favorable flow condition.

Statement of the Problem

Since a "traveling wave" can connote a variety of configurations versus required wavy wall, it is important to establish a precise picture of this concept. Consider a wave superimposed upon a wall boundary with flow moving over it with freestream velocity U_∞, Figure 8. Generally this wave can have two kinds of motion in the X-direction, translational motion for a rigid wall and traveling wave motion for a deformable wall:
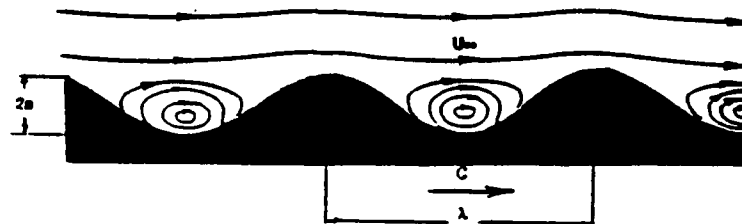
Figure 8.   Flow/Wall Geometry of a Traveling Wave Wall

1. Translational motion: at any later time the whole wall rigidly moves to a new position. In this case, all particles at the wall move with the wall velocity in the x direction only, as depicted in Figure 9a.
2. Traveling wave motion: at any later time, the wall remains stationary in the x-coordinate and only the wave passes by in x direction (a flexible wave motion). In this case, all particles at the wall move up and down in the y-

16

direction and have no x component, as depicted in Figure 9b (e.g. ocean waves).
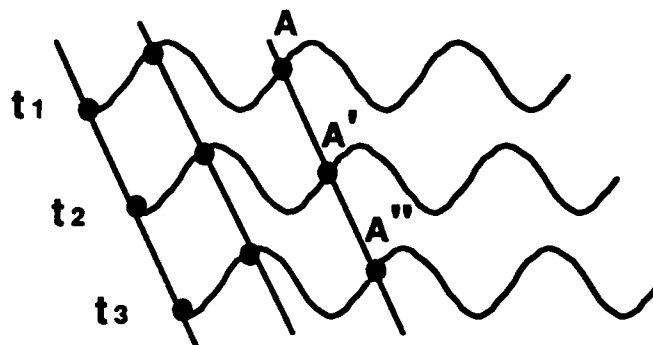
Figure 9a.   A Translating Wavy Wall, the Wave Solidly Moves with the Wall, A' and A" are Positions of a Particle A at the Wall at Later Times
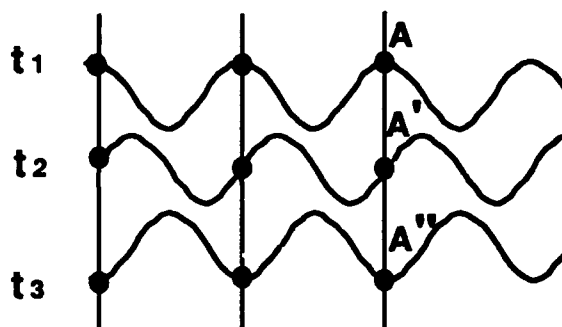
Figure 9b.   Traveling Wave, Particles at the Wall Have a Periodic Motion in y Only. (Every Point at the Wall Such as A Moves Up and Down at a Fixed x Position (A' and A"))

The critical traveling wave question is as follows: Given a specific set of flow and wall parameters, is it possible to produce and sustain stable vortices in the troughs of the wave and generate a secondary flow such that both the viscous shear forces at the wall and the pressure drag are nearly zero? Initial computations by Coleman Donaldson (1989) indicated that for a set of specific conditions, a secondary flow with reduced drag could be established. In an attempt to determine the parameter space in which a vortical flow can be sustained, our team member, J. Wu, identified the von Kármán vortex street as a well understood analogy which might provide the initial insight into identifying

critical parameters for producing a stable vortical flow. From the outset, the team recognized that the relationships obtained using von Kármán vortex street analogy and later Kelvin-Stuart cat's eye would provide guidance for discriminating among the possible physical relationships which might result in the formation of a vortical flow.

It will be shown later in this report that the first-order parameters to be considered are (see Figure 7):

U_∞ freestream (undisturbed) flow velocity,

c   wall wave (phase) velocity,

λ wavelength of the wall profile,

a   amplitude of the wall profile, and

υ fluid kinematic viscosity.

Three Distinct Regions of Traveling Wave

Before an in-depth discussion on the physics of the traveling wave is presented, it is important to specify three distinct regions which are associated with the traveling wave. These regions are leading edge, trailing edge, and mid-region.

Leading Edge

In order to initiate a traveling wave on a smooth surface, one has to provide a mechanism to initiate the vortices. This can be achieved by a transverse vortex generator or by properly shaping the onset of the wave. For example, by gradually increasing the amplitude and wavelength (Taneda, 1974), one can facilitate vortex formation (Figure 10). Note: If the a/λ ratio is out of the critical range, a vortex will not form.

Figure 10. A Gradual Increase in the Wave Amplitude as a Mechanism for Initial Vortex Formation

Another method is to allow for the vortex to form along the first several waves. This is the method used in our numerical calculation. The physics of the initial formation of the vortex and the associated mechanism will be addressed under the "leading edge" heading in this and future reports. As will be discussed later, this is the region of the surface which has the potential of radiating noise.

Trailing Edge

Similar to the leading edge, care must be taken at the trailing edge to properly disperse the vortices. It is very important to recognize that the existence of energetic vortices leaving a control volume accounts for the amount of the momentum deficit that results in "thrust" or "drag" generated by the control volume. That value can vary dramatically as a function of design efficiency. Quantitative analysis of a finite body with leading and trailing edges has been initiated and will be presented later in this report (see page 39).

Mid-Region

The focus of the present research is on the mid-region where the already-formed traveling wave has been well developed. Most of the subsequent discussions and results obtained are for this region. This is the main drag-reducing region for a well designed vehicle. Theoretically, the entrapment of identical vortices in each of the troughs of the wave, for the mid-region, corresponds to the exact periodicity of the flow along the wall and zero momentum deficit, which indicates zero total drag. Since the mid-region is the major part of the traveling wave, this report focuses on this region. This by no means should weaken the importance of the trailing and leading edges. A control volume analysis that includes the effects of leading and trailing edges is presented later in this section. Obviously, the leading and trailing edges are very important in the context of acoustic signature and system efficiency. Recognizing that the phenomenon, by nature, is an unsteady flow, the noise radiation associated with unsteady pressure forces of the initial vortex formation must be studied in detail and will be addressed later.

19

From our preliminary study of the physics of the traveling wave for the mid-region, for trapping the vortices at the wave's trough and producing a secondary flow, inviscid flow theory predicts the following relationships:

$$\frac{a}{\lambda} \approx 0.2,$$ (1)

and, therefore,

$$\frac{c}{U_\infty} \approx 0.4$$ (2)

To understand the physics of the traveling wave more thoroughly, consider a flow over a wavy wall boundary as shown in Figure 11. If such a flow can indeed be produced and sustained, the consequences could be significant. First, the maintenance of vortical flow within the deformed boundary is accomplished by energy transferred to it from the oscillating boundary and the freestream. Due to the high nonlinearity and multi-parameter nature of the problem, it would be beneficial to establish a simple yet physically correct analytical model first, in order to place numerical results in context.
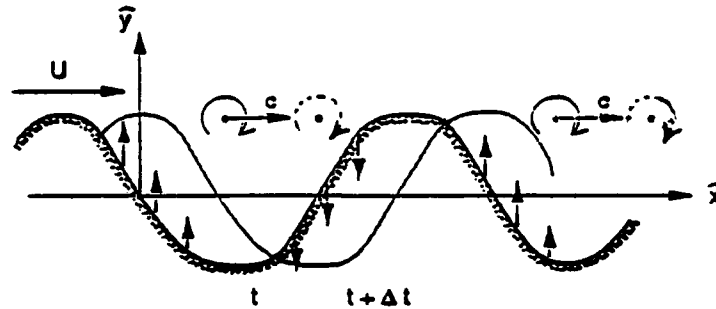
Figure 11. Vortices Trapped by Traveling Wave Wall Viewed from a Fixed Frame

Mathematical Model

In order to establish a fundamental mathematical model for the traveling wave, consider an inviscid uniform flow $U_\infty = U_\infty \dot{i}$ over a flexible wavy wall of infinite length, of which each point oscillates up and down periodically, producing a traveling (progressive) wave with phase velocity $c = c\dot{i}$ (Figure 11). The wave can be defined, in general, by

20

$$\widehat{y}_B = af\big(k\widehat{x}-\omega t\big) = af\big(k(\widehat{x}-ct)\big), \tag{3}$$

where a is the amplitude and k is the wave number defined as $k = \omega/c$, and f is a general periodic function. As boundary conditions, the wall velocity components in x and y respectively are:

$$\widehat{u}_B = 0, \tag{4}$$

$$\widehat{v}_B = \frac{\partial \widehat{y}_B}{\partial t} = -ackf'\big(k(\widehat{x}-ct)\big). \tag{5}$$

This is an unsteady flow viewed in the fixed lab or absolute frame, which can be transformed to a moving or traveling frame and viewed as a steady flow through a Galilean transformation (Figure 12).

Figure 12. Flow Pattern in Traveling Wave Frame

In this case,

$$x = \widehat{x} - ct \text{ and} \tag{6}$$

$$y = \widehat{y}, \tag{7}$$

and the boundary conditions are

$$y_B = af(kx), \tag{8}$$

$$u_B = -c \tag{9}$$

$$v_B = -ackf'(kx), \quad \text{and} \tag{10}$$

$$u = U_\infty - c \quad \text{at} \quad y = \infty \tag{11}$$

If the wavelength is assumed to be unity, then $|k| = 2\pi$. Assume the vortices have been well formed (right in troughs) and are stable, each having the strength of $-\Gamma$. J. Wu et al. (June 1990) first identified a similarity between this problem and von Kármán's vortex street. He suggested that the wall be considered a streamline and a proper row of image vortices be introduced. He then turned to the classical vortex street case to identify a consistent set of parameters which might produce a stable vortical flow.

Since the captured vortices prevent the external flow from being directly in contact with the wall, the wall is covered by an isolated thin flow-layer, governed by a local Reynolds number based on the wave amplitude, a, and vortex induced velocity, c, so that

$$Re_a = \frac{2ca}{\nu} \tag{12}$$

In comparison with the global Reynolds number,

$$Re_L = \frac{UL}{\nu} \tag{13}$$

where $L \sim N\lambda$, (N is the number of waves in the total length L and λ is the wavelength), then:

$$\frac{Re_a}{Re_L} \sim \frac{2}{N}\frac{c}{U}\frac{a}{\lambda} \ll 1 \tag{14}$$

Therefore, if Re_a governs the flow phenomena, delay of transition to turbulence with traveling wave may be anticipated.

NEW INSIGHTS

Use of an Analogy

To gain insight into the appropriate parameter space, Wu considered the von Kármán vortex street. As will be shown, this is not an exact analogy, but it did help us identify a reasonable point of departure as we began the numerical analysis.

In von Kármán's vortex street, one row of vortices induced a uniform velocity, V, to each vortex of the other row, such that

$$V = -\frac{\Gamma}{2}\tanh(\pi b), \tag{15}$$

where b is the vertical spacing between the centers of the vortices of the rows and Γ is the vortex strength. Hence, in the fixed frame the vortices move along with the whole flow. When the vortex street is formed behind a cylinder in von Kármán's case, the inviscid theory cannot predict the vortex strength Γ. It only indicates that, for a point vortex model, the vortex street will be least unstable if the ratio of the vertical spacing, b, to longitudinal spacing between vortices of the same row is equal to 0.281. More recently, there have been some studies on the linear stability of the vortex street with a finite vortex core, again showing that only specific values of b, depending on the core size, can make the street stable.

The appearance of an oscillating wall will certainly change the stability characteristics of the vortex row, at least if viscosity is taken into account. A Galilean transformation can make vortices stationary within a traveling

coordinate system and the flow becomes steady, as sketched in Figure 12. This flow pattern is significantly different from that seen in the laboratory frame; there appears to be a series of saddles, each located between successive vortices. To make this clear we use the well known complex velocity:

$$\frac{d\Omega}{dz} = u - iv = \frac{i\Gamma \sin 2\pi z_0}{\cos(2\pi z_0) - \cos(2\pi z)} - V,$$

(16)

$$z_0 = \frac{1}{4} + i\frac{b}{2}$$

(17)

where Ω is the complex velocity function, and other parameters are already defined in previous equations. If we denote

$K = \sinh(\pi b)$, and

(18)

$\delta = 2/\tanh(\pi b)$

(19)

then, the location of saddles A and B in Figure 13 can be found by separating the real and imaginary parts of the velocity terms. Then the nonlinear autonomous system for pathlines are:

$$\frac{dx}{dt} = \frac{k}{\delta} \frac{\cos^2 \tilde{x} + \sinh^2 \tilde{y} + 2K^{-1} \sin \tilde{x} \sinh \tilde{y} - \left(2 + K^2\right)}{\cos^2 \tilde{x} + \sinh^2 \tilde{y} - 2K \sin \tilde{x} \sinh \tilde{y} + K^2}$$

(20)

$$\frac{dy}{dt} = \frac{k}{\delta} \frac{2\left(K + K^{-1}\right)\cos \tilde{x} \cosh \tilde{y}}{\cos^2 \tilde{x} + \sinh^2 \tilde{y} - 2K \sin \tilde{x} \sinh \tilde{y} + K^2},$$

(21)

where

$$(\tilde{u}, \tilde{y}) = (2\pi x, 2\pi y)$$

(22)

The numerical solution of pertinent equations shows that there exist three different sub-patterns depending on the value of b: (a) when b < 0.4105, the pathline initiating from a saddle encloses a vortex and returns to the same saddle (Figure 13a); (b) when b = 0.4105, the pathline terminates at the

24

neighboring saddle of the opposite row (Figure 13b); and, (c) when b > 0.4105, the pathline connects at the neighboring saddle of the same row (Figure 13c). Both cases (a) and (c) allow for a continuous flow layer of finite width between two rows of vortices, but only case (c) is geometrically appropriate to model the traveling wave flow.

A comparison of Figure 12 and Figure 13c shows that two flows will be similar if we take the wall to be any one of the streamlines in Figure 13c which is between the two vortex rows, and if:

$$U_\infty - c = - V = \frac{\Gamma}{2} \tanh(\pi b) \tag{23}$$

This key identification uniquely determines the vortex strength:

$$\Gamma = \delta(U_\infty - c) \tag{24}$$

Therefore, once b is fixed, Γ reduces linearly as c increases relative to U_∞. When $c = U_\infty$, no vortex is produced; when $c > U_\infty$, the direction of oncoming flow viewed in the moving frame is inverted and Γ becomes negative. (For this condition no vortex was found in Taneda's (1974) experiment).

With real viscous flow in mind, in the present analysis the tangential velocity relative to the wall and pressure gradient should be as low as possible for given c/U_∞, such that no new separation will result. This requires taking the wall as the central streamline of the vortex street, since along other streamlines the velocity variation will be steeper. As b increases from 0.4105, the obtained wall shape begins to resemble a sinusoidal wave with an amplitude of less than b/2. The admissible wall amplitude, a, is limited by the condition b > 0.4105. Analytically we found a $\approx$ 0.2 when b = 0.443. This corresponds to a maximum inclination angle of 46.7°; while for the sinusoidal wave with a = 0.2, the angle is 51.5°. This variance is presented in Figure 14. This is a typical amplitude that will be used in the first set of numerical calculations. This simple sinusoidal shape is, of course, convenient for computational analysis as well as in practical

applications. Although this analogy cannot assist in estimating viscous forces, it can provide insight into wall slip velocity Δq.

The wall slip velocity Δq is the difference between vortex-induced velocity in the fluid next to the wall q_v and wall velocity q_w. It will be shown later that for the critical value of c/U_∞ of .414, the slip velocity is purely periodic. This is the logic behind selecting values of $a/\lambda = 0.2$ and $c/U_\infty = 0.4$ as initial parameters for the numerical investigation.
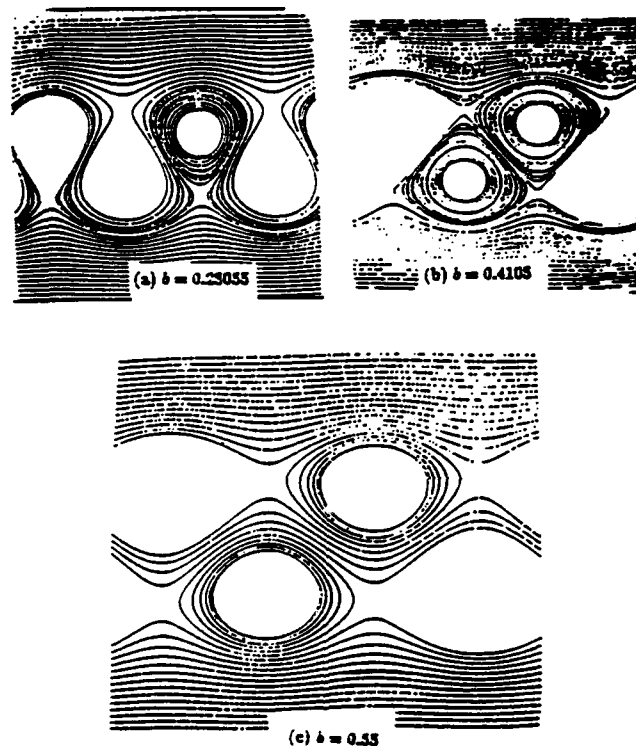
Figure 13. von Kármán Vortex Street Viewed in "Traveling Frame"
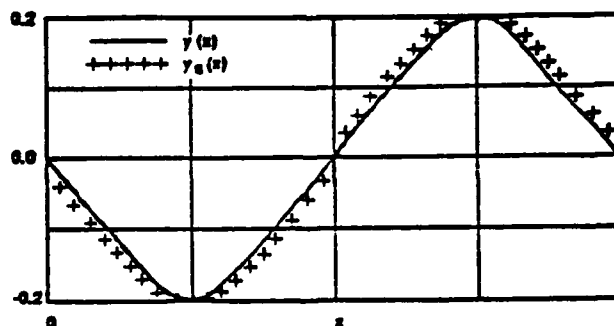
Figure 14.   Central Streamline $y = y(x)$ of Vortex Street, Viewed in the Moving Frame. As Comparison, $y_s(x)$ is Sinusoidal Wave of the Same Amplitude

26

Flow Regime

The results of computational analysis from Navier-Stokes codes have been used to verify and enhance our understanding of the physics of the traveling wave. Figure 15 shows the different flow regimes in the controlled vortical flow pattern. It can be seen that there exists an isolating layer between the wall and the vortex which acts differently from the conventional boundary layer. This is the actual near wall shear stress layer in the traveling wave problem where the maximum velocity gradient is the slip velocity and is due to the difference between the velocity of the wall q_w and the vortex-induced velocity q_v in the fluid next to the wall.
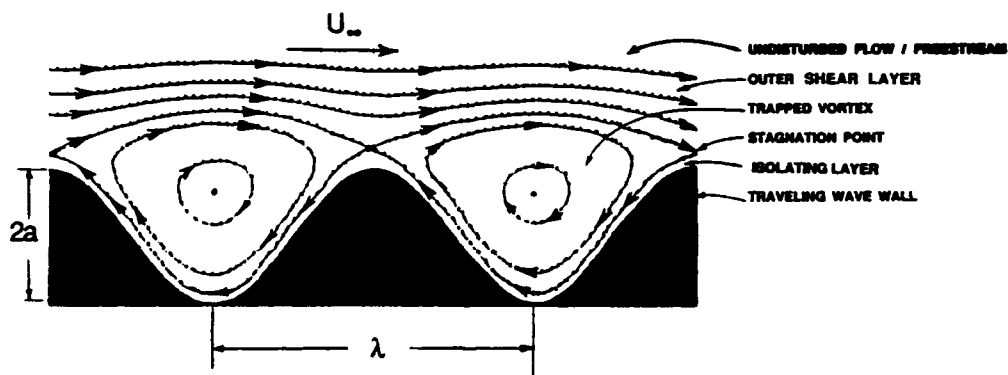
Figure 15. Elements of Traveling Wave Flow

In order to keep the drag near zero, the flow has to be periodic over the wave. With exact periodicity of the flow over the wave train, the isolating layer will not grow, but will maintain the same thickness. It can be anticipated that by properly energizing the wall, the required periodicity will be achievable in the mid-region of some practical cases.

Moreover, due to the wall motion in the same direction of vortex-induced velocity, the isolated thin layer may have a much smaller shearing stress than a conventional boundary layer. Hence with proper design, drag reduction, minimal or even no growth of the outer shear-layer, and elimination of break-away separation is anticipated.

27

To clarify this concept, let q_v be the tangential velocity induced by vortex on the wall, then in the inviscid analysis the slip velocity is given by $\Delta q = q_v - q_w$, (where q_w is the average wall velocity) which causes a wall viscous shear layer in real flows. One of the key discoveries of the present study is that, once vortices have been captured, there exists a critical c/U_∞ between 0 and 1 such that for arc length of S.

$$\frac{1}{2\pi} \int_0^{2\pi} \Delta q \, ds \approx 0.$$

(25)

Namely, the averaged slip velocity, and hence the averaged skin-friction and the growth rate of the isolated layer, can be made nearly zero by correctly choosing the wave speed.

Thus, if we have a finite body over which a large mid-region produces a traveling wave flow (say, N waves with wave-length λ, N >> 1), then for proper c/U_∞, equation 25 implies that

$$C_{D_{mid-region}} \approx 0.$$

(26)

This consequence is obviously significant. It is a departure from the conventional concept of boundary layer flow and associated skin-friction, transition and separation. This new type flow will be compared with the common flow of a smooth body later in this report.

Wall Profile Function

In the first set of numerical calculations, the wall profile was chosen to be a sinusoidal profile with $a/\lambda = 0.2$, as indicated in the preceding analysis. Although vortex entrapment and an indication of drag reduction was achieved with this wall profile, some evidence indicates that for the optimum condition to occur, a sinusoidal profile may not be the preferable choice. Several initial calculations have been made for a wide range of c/U_∞ values. The wall profile itself was varied in an attempt to reduce the velocity variations at the wall. While near-zero drag is the current objective, it is anticipated that a thrust will be

28

generated when the location of the vortex is offset from the center toward the trailing edge of the wave trough. Such a wall-vortex configuration will cause a low pressure region to be formed at the trailing edge of each wave trough and a high pressure region at each leading edge. Consequently, locating the center of the vortex further forward of center in the trough should result in a pressure drag. On the other hand, it is desired to reduce the slip velocity, Δq, to near zero to reduce the friction drag. Thus, other wall profiles, such as a sinusoidal wave with $a/\lambda = 0.1$, a Kelvin-Stuart cat's eye, and a combination of cat's eye and sinusoidal wave were each investigated.

From the outset, it was anticipated that the feasibility of low/high pressure regions may suggest a wall profile that has a low slope at the leading edge and a high slope at the trailing edge, which implied an asymmetric wall profile (Figure 16). It appeared that this kind of wall profile would assure vortex entrapment and will not permit the vortex to escape and be washed downstream. It is now understood that optimum shaping depends upon many factors which will vary based on freestream velocity and location of vortex center along the wall. Also, the dependence that the smaller the amplitude, the lesser the energy required to move the wall up and down is only a first-order condition. Locating the vortex near the expanding section of the wall will also reduce wall energy, but not necessarily drag. An important condition for the wall profile optimization is the minimum "total" energy, which may not correspond to the lowest drag/greatest thrust condition.

Figure 16.   An Asymmetric Wavy Wall Shape

Other Wall Profiles

In our attempt to establish the proper relationship between the flow and the wall parameters and to estimate the optimum wall shape for minimum drag, several non-sinusoidal wall profiles have been investigated. As a point of departure, our initial calculations were performed for a sinusoidal wall profile. However, there is not a solid base for believing that this is the best wall profile for

minimum drag. Other important factors, such as vortex stability and implementation potential of the wall wave, must also be considered. It is recognized that wall profile is irrelevant to drag as long as true periodicity is obtained. If periodicity is assumed, wall profile will only effect ease of vortex generation and system stability.

The sinusoidal profile, as discussed earlier, was just a starting point and provided an insight into the physics of the traveling wave. For example, various flow regions on a traveling wave, i.e., isolated layer, trapped vortex and outer shear layer (See Figure 15) were identified. It was also established that if the vortex-induced fluid velocity q_v matches the wall velocity q_w along the wall, the slip velocity is zero and theoretically there must be no shear stress at the wall. Thus, a critical wall design parameter could be to minimize the difference between q_w and q_v. Taking these factors into account, other possible wall profiles have been examined from the inviscid theory point of view, a good candidate for the wall profile may be derived from the "Cat's eye" shape, Figure 17.

Kelvin-Stuart Cat's Eye: The stream function Ψ of Kelvin-Stuart cat's eye flow is given by (Stuart, 1967):

$$\Psi = Ln\,(\alpha\,coshy + \beta\,cos\,x), \quad \beta = \sqrt{\alpha^2 - 1} \quad \alpha \geq 1 \tag{27}$$

where α is the single parameter. The wall profile is a relation in y and x for constant Ψ and can be given as :

$$y = -\,cosh^{-1}\left[\frac{1}{\alpha}\left(k - \beta\,cosx\right)\right], \quad \beta = \sqrt{\alpha^2 - 1} \tag{28}$$

30
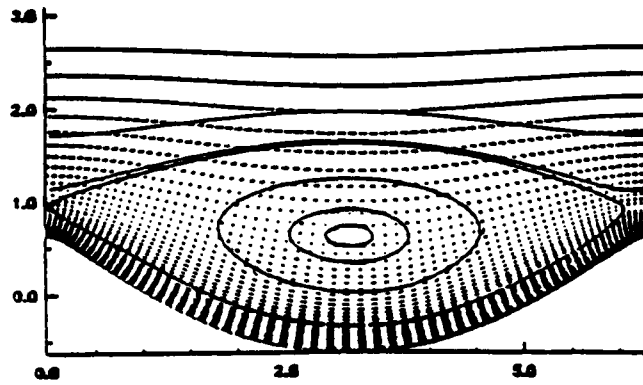
Figure 17. Vortex Entrapment in a Cat's Eye Wall Shape

Equation (27) is an exact solution of the Euler equation for ideal, homogeneous incompressible fluid with distributed vorticity (Holm, et al. 1986). This solution is non linearly stable for $1 \leq \alpha \leq 1.175$. For $\alpha = 1$, the solution degenerates to a simple shear layer, and as $\alpha \rightarrow \infty$, it becomes a row of point vortices. For each α there is a maximal possible wall amplitude, which slowly increases to $(a/\lambda)_{max} = 0.14$ as $\alpha \rightarrow \infty$. When $\alpha = 1.175$, the solution is a reasonable approximation of the traveling wave, see Figure 18. Thus, we choose $\alpha=1.175$ (the upper bound of stability) whose $(a/\lambda)_{max}=0.11$ (corresponding to the central streamline with saddles). However, according to the definition of a cat's eye curve, $(a/\lambda)_{max}$ cannot exceed 0.14. Thus, to investigate excursions outside of the basic shape, one can establish curves of general cat's eye shape for other values of a/λ by multiplying the curve of $a/\lambda=0.1$ by a corresponding constant factor. For example, curves with $a/\lambda=0.2$ can be obtained by doubling the ordinate of the curves of $a/\lambda=0.1$. Curves of $a/\lambda=0.3$ can be obtained by tripling the ordinate of the curves of $a/\lambda=0.1$ and so on. For numerical calculation we have started with $a/\lambda = 0.1$. Further discussion on development and proof of this theorem is out of the scope of this report and can be obtained from Holm et al. (1986).
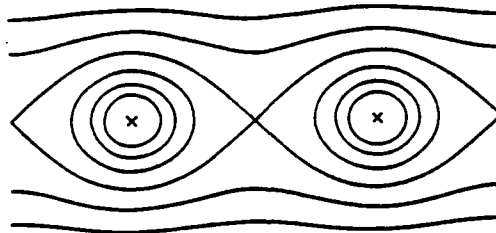
Figure 18. A Typical Streamline for Kelvin-Stuart Cat's Eye

31

Cycloid: A cycloid wall profile was also considered in this study because it was identified as a candidate mechanism for implementing a traveling wave in a future experiment. This curve is described by a point P at a distance b from the center of a circle of radius a as the circle rolls on the x axis (Figure 19). The equation of a cycloid in a parametric form is

$$x = a\varphi - b \sin \varphi \tag{29}$$

$$y = a - b \cos \varphi \tag{30}$$

where the parameters, a and b, are chosen such that the desired a/λ is achieved. It is anticipated that, due to the definition of a cycloid, it is easier than other profiles to implement in real applications (from a mechanical control view point). A comparison of the three major wall profiles is presented in Figure 20 for $a/\lambda = 0.1$ over one cavity or a single wavelength, $\lambda = 2\pi = 6.3$. It can be seen that the cycloid is fuller than both the cat's eye and sinusoidal wall profiles.
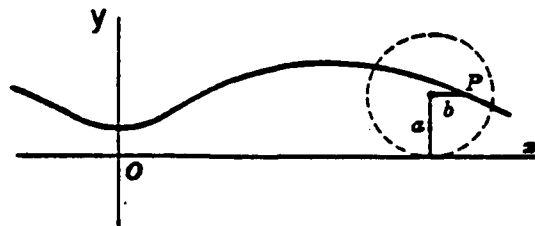
Figure 19. Definition of a Cycloid

Bedform Ripples and Dunes: Among the most discriminating features of ripples and dunes are their skewed shape and the presence of leeward vortex or separation of the flow behind the bedform, Figure 21. It is possible that further insight to alternative traveling wave profiles may be gained through examination of the mechanics of the limiting-equilibrium profiles of migrating ripples, and dunes. However, these shapes are dominated by the effect of gravity. This effect is not a consideration for the traveling wave. In the absence of a gravitational influence, these shapes could be entirely different.
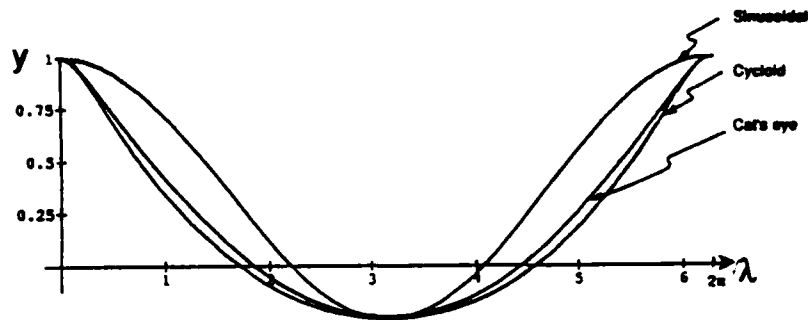
Figure 20. A Comparison of Several Wall Profiles

Depending upon the extent of the bedform, it is possible to define shapes for freestream surfaces (Haque et al., 1985, 1986). These shapes are defined theoretically, based on observed data for a large variation of the bedform sizes. Some of the analysis is based on low sediment transport rate, in which the sediment essentially moves. The sediment transport rate may be analogous to the wave (phase) velocity c and the bedform may be analogous to the wall wave profile. Further investigation is required to understand the relationship between the key parameters of this natural phenomenon and whether it has any relationship to the traveling wave concept. The potential usefulness of this or any other analogy must be evaluated carefully when considering wall profile options.

Figure 21.   Idealization of Flow Over Train of Ripples and Dunes
(K. Mahmood et al. 1988)

33

Wall Maximum Velocity

Viewed from the Galilean traveling reference frame (traveling with the wave phase speed c) the wall appears to have a velocity q_x of -c. On the other hand, due to vertical periodic motion of the wall, q_y, there always exist locations at the wall where the total wall velocity is maximum. Magnitude and location of the maximum wall velocity are very important from design considerations and are functions of wall shape and a/λ. They also play an important role in determination of the location and the value of vortex circulation Γ. A comparison of wall velocities along one wave cavity for several wall profiles is presented in Figure 22. This Figure indicates that from a Galilean traveling frame, for the same a/λ a sinusoidal wall profile has the most uniform wall velocity and cycloid has the highest wall velocity. These values for different a/λ along with the exact location of maximum velocities are provided in Table 4. Table 5 presents the values of maximum and average wall velocities along one wave cavity for several wall profiles and different a/λ. These Tables provide valuable insights necessary for identifying c/U_∞ and a/λ values which will produce low drag. The values of the entries in these Tables have been obtained by simple analysis using wall velocity components and are non-dimensionalized with respect to the phase velocity c.
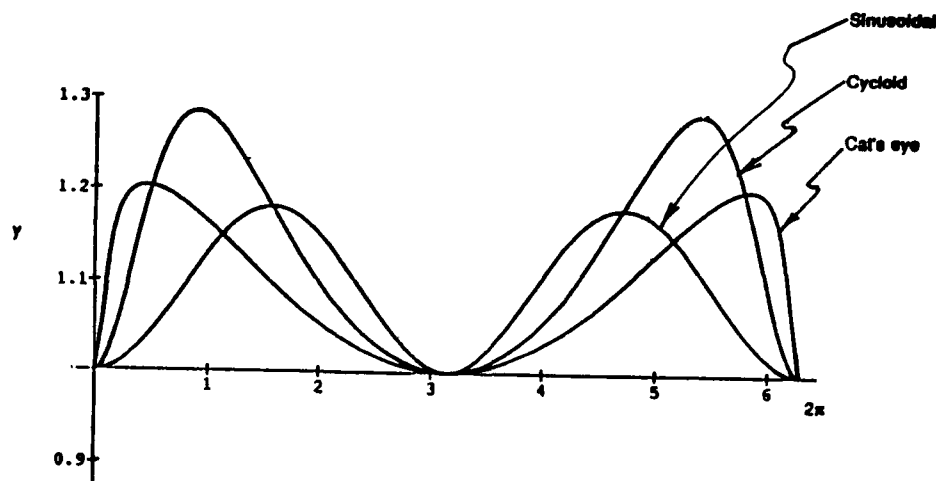
Figure 22.   A Comparison of Wall Velocities Along One Wave Cavity for $a/\lambda = 0.1$

34

Table 4. The Location of Maximum Velocities for Different Wall Profiles

Profile	x(qw) max degree	(qw) max/c		
		$a/\lambda = 0.1$	$a/\lambda = 0.2$	$a/\lambda = 0.3$
Sinusoidal	90°	1.18	1.606	2.13
Cat's eye	27°	1.203	1.67	2.24
Cycloid	51°	1.285	1.90	2.62

Table 5. Maximum and Average Wall Velocities Along One Wave Cavity

a/λ	Sinusoidal		Cat's Eye		Cycloid	
	(qw) Max	(qw) Avg	(qw) Max	(qw) Avg	(qw) Max	(qw) Avg
0.0	1.00	1.00	1.00	1.00	1.00	1.00
0.1	1.18	1.09	1.20	1.09	1.29	1.13
0.2	1.61	1.32	1.67	1.33	1.90	1.43
0.22	1.71	1.38	1.78	1.38	2.04	1.50
0.24	1.81	1.43	1.89	1.44	2.18	1.57
0.25	1.86	1.46	1.95	1.47	2.25	1.61
0.3	2.13	1.62	2.24	1.62	2.62	1.80
0.4	2.70	1.95	2.86	1.96	3.38	2.21
0.5	3.30	2.30	3.49	2.31	4.16	2.64
0.6	3.90	2.67	4.14	2.68	4.95	3.08
0.7	4.51	3.04	4.79	3.05	5.74	3.52

FIRST-ORDER OPTIMIZATION

As was mentioned earlier, three distinct layers exist in the traveling wave flow (Figure 14): 1) the isolating layer which acts as a thin viscous layer, 2) the vortex sheath, and 3) the outer layer which could be similar to a Rayleigh layer In a conventional flow across flat plate. Therefore, a simple optimization criterion is the minimization of the velocity gradient within the isolating and outer shear layers. In other words, in order to minimize these two shear layers, the vortex-induced velocity must be matched with the wall velocity at the inner layer and with the freestream velocity at the outer layer. By analyzing the results of computational simulations, it was realized that the maximum vortex-induced velocity occurs almost at the location of the maximum wall velocity; however, for calculation purposes, the average vortex velocity must be considered. The average wall velocity is an indication of the average vortex-induced velocity of the fluid next to the wall (for the inviscid case they are exactly the same). Viewed from the traveling frame, if the vortex-induced velocity has to match the wall velocity at the trough of the wave, it must have a value of c (the wave phase velocity). Since the freestream velocity viewed from the traveling frame has a value of U_∞ - c, in order to match the vortex-induced velocity to this freestream velocity , we must have U_∞ - c = c or U_∞ = 2c. This indicates that c/U_∞ = 0.5.

Obviously, in real fluid, due to viscous losses and dissipations, the optimum c/U_∞ must be greater than 0.5 to account for these effects. However U_∞ - c is very sensitive to changes in c/U_∞. This is presented in Table 6. As can be seen from this Table, a change from 0.5 to 0.6 for c/U_∞ corresponds to a change of 1.0c to 0.67c for U_∞ - c. Ideally, as noted above, it is desired to have the average wall velocity equal to U_∞ - c. Thus, given a value of a/λ for a specified wall profile, the value of c/U_∞ can be obtained from this Table.

Table 6 may be used as a tool to estimate the value of c/U_∞ for the minimum shear layer. This technique is most useful for wall profiles which provide a relatively uniform velocity along the wave and have their maximum velocity away from the wave crest, such as a sinusoid. In this condition, energy transfer from the wall to "pump" the vortex is more complete and has better efficiency. As shown before (Figure 22), the location of maximum wall velocity for a

36

sinusoidal wall profile is at 90°, whereas for the cat's eye profile this maximum velocity occurs at 27°, and for the cycloid it occurs at 51°. To illustrate this relationship, consider a sinusoidal wall profile with $a/\lambda = 0.2$; the average wall velocity is 1.32, as seen from Table 5. This is an indication of the average vortex-induced velocity which should match with U_∞ - c for the minimum drag at the outer layer. By interpolation of Table 6, this value corresponds to a c/U_∞ of about 0.43. Although this is a simplified criteria, it can serve as an optimization tool to check the relation between a/λ and c/U_∞ for a given wall profile.

Table 6. Relation Between Wave Phase Velocity c and Freestream Velocity U_∞

c/U_∞	U_∞-c
.33	2.0c
.4	1.5c
.5	1.0c
.525	.91c
.55	.82c
.575	.74c
.6	.67c
.65	.54c
.7	.43c
.75	.33c
.8	.25c
.9	.11c
.95	.05c

CONTROL-VOLUME APPROACH

Another approach to evaluating the traveling wave is control volume analysis. In this approach one does not have to consider the microstructure of the wave train and individual vortices; the whole structure of one wavelength is considered as a unit. Based on input/output variables it is possible to calculate the momentum or energy exchange. The difference between the input and

37

output energy is the momentum deficit of the control volume and accounts for the amount of drag, or thrust. The rate of vortices convecting from the control volume (output rate) is an indication of the thrust depending upon vortex orientation. Since this approach required consideration of a rather long wave train, numerical investigation (multiple wave) is likely to be very time-consuming.

Consider a sufficiently large control volume surrounding a finite body as shown in Figure 23 and observed in body-fixed coordinate. Assuming the exit control surface is sufficiently close to the downstream end of the body, the net fluid dynamic force acting on this finite body will be reflected in its wake flow. Then. this Figure contains four sub-cases: (a) a short, smooth surface body of length l, (b) a long, smooth body of length L, (c) a short, body of length l with traveling wavy wall, and (d) a long body of length L with traveling wavy wall. Except for the mid-region surfaces, the front and tail portions are exactly the same. The conventional boundary layer will be thicker for case (b) than case (a) at the end of the body. Thus, $U_{b-wake} < U_{a-wake}$. With traveling wavy wall cases of (c) and (d), the formed vortices will depart from the body approximately with the phase velocity c. And if traveling wavy-wall controlling parameters are the same, then $U_{c-wake} = U_{d-wake}$. Moreover, provided $c > 0$, we always have U_{d-wake} (= U_{c-wake}) > U_{a-wake} > U_{b-wake}. This intuitive physics tells us:

1. For the Wake Momentum Deficit
   $Wake_b > Wake_a > Wake_c = Wake_d$, and

2. The Overall Finite Body Drag
   $Drag_b > Drag_a > Drag_c = Drag_d$.

Three general observations follow: (1) Any body with sufficiently long traveling mid-region surface with legitimately chosen controlling parameters will have less drag than any smooth body of the same length. (2) While for conventional wall body, the longer length will have a larger drag, but this is not the case for traveling wave wall body, since mid-body length is relatively insignificant. Hence, it could be more beneficial to apply traveling wave technique to a longer body. (3) Critical to the success of a traveling wave body are its two ends, the power required to generate and maintain vortices, and the stability of such a

vortical flow. This approach to evaluating the potential of the traveling wave appears to be more attractive for an in-water experiment and is now being considered for validation of the numerical analysis which is addressed in the following two sections.
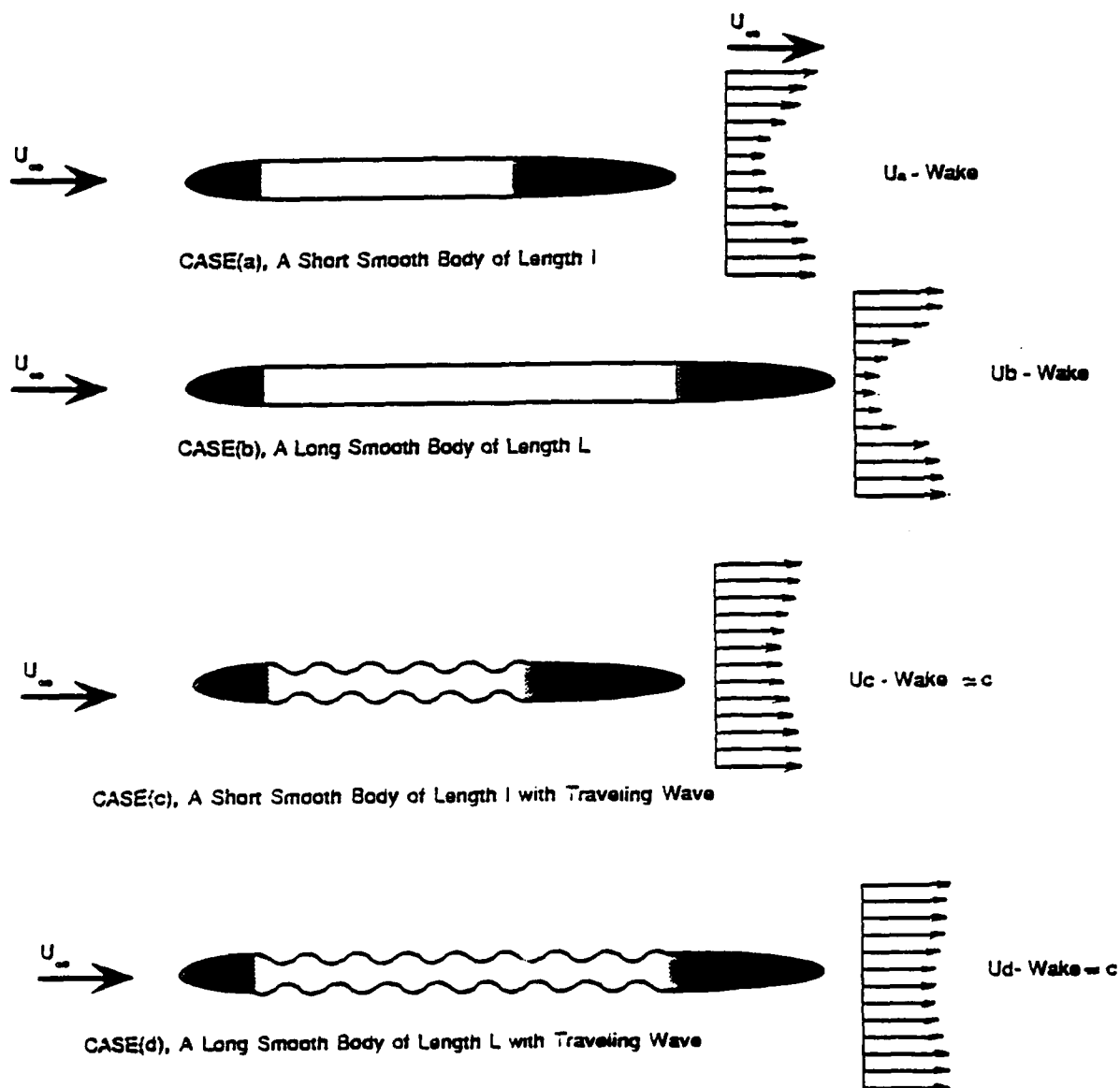
Figure 23. Schematic Similar Bodies with Different Length Surfaces

39

III. COMPUTATIONAL APPROACHES

NUMERICAL METHODS EMPLOYED

Once a reasonable set of values for the principal control parameters had been identified, a numerical approach was adopted to verify the analytical approach and to obtain insights into the fluid physics. To obtain a better understanding of the flow field, to validate the physics contained in the theoretical framework developed by Wu, and to assure the relative merits of the two chief codes, the problem was attacked using several different numerical approaches. These approaches employ several different numerical methods: a spectral method which is a fractional step procedure (Gottlieb & Orzag, 1977), a Discrete-Element/Finite Volume method (DEM), and a central difference method. Table 7 presents the different computational methods with the names of the user/developer, the nature of the codes, and resulting resolution and associated CPU. A brief discussion on the implementation of the two codes employing spectral and discrete-element methods is given in the following section.

ON THE USE OF PERIODIC BOUNDARY CONDITIONS

A full computational simulation of the traveling wave phenomenon is beyond our current capability. Such a simulation would require a set of unsteady computations with sufficient number of waves to describe the initial capture of the vortices, the near periodic behavior of the main central section, as well as the final shedding of the vortices at the trailing region. The behavior of each wave would need to be sufficiently resolved in both space and time. At this stage of the research it is reasonable to use a single wave with periodic boundary conditions as an economical means for gaining an understanding of the underlying physics of aspects of the problem, as well as to verify the numerical algorithms. The idealized central section of the traveling wave system is steady and periodic so that, when the proper combinations of shape, phase speed, amplitude, etc. are chosen, then the numerical formulation is well posed. In practice, great difficulty was encountered when following the

40

evolution of such a calculation to the steady condition   Nevertheless, the degree to which such a calculation settled toward a near steady result at nearly zero drag could be used to select a range of traveling wave parameters that are promising for further investigation. Another use of the periodic approximation involves a space-time analogy where transient solutions are used to model the spatial development of the initial region of the wave. It is recognized that these conditions are inappropriate but it is hoped that, for now, these results can give insights into the starting mechanism where the capture and stabilization of the vortices in the wave troughs is a requirement. At a later date, with the advantage of controlled experiments, these models can be honed to strengthen our capability to design a practical system.

SPECTRAL METHOD

NASA Code

The NASA spectral code was chosen because it represented the most rigorous U.S. effort to date to gain insight into the drag of deformable and wavy walls. It was the initial premise of the current researchers that the same codes applied in a much different parameter space would substantiate the possibility of an ordered vortex flow having significant potential to reduce drag. Such an approach would be necessary in order to compare the present results with previous work which had not been encouraging. After consultations with Dennis Bushnell, as well as his continued support and guidance, this code became one of our primary CFD tools.

Table 7. Summary of Numerical Methods

	SOLA	DEM	FINITE DIFFERENCE	SPECTRAL	
User/ Developer	Jimmy Wu/ ERCI	Arsev Eraslan/ ERCI	Art Rubel/ GRUMMAN	Carol May/ Cortana	R. Balasub-ramanian/ SPECTREX
Operating Machines	VAX at UTSI	VAX and Alliant at UTSI	Cray XMP at GRUMMAN	Convex DTRC	Cray II at NASA Langley
Nature of Code	First Order Finite Difference	Discrete Element Analysis	Central Difference	Spectral Method	Spectral Method
Current Resolution	25X30	40X24	59X89	39X39	64X64 & 128X128

Assumptions

The spectral algorithm used in the NASA Code solves the two-dimensional incompressible Navier-Stokes equations in Primitive Variable form (u, v, p formulation) over a half space bounded at the bottom by the wave and to infinity in direction normal to the wave. Streamwise periodicity of the flow, which is the appropriate technique for situations involving waves rather than a single cavity flow, is also employed in this code.

To enable accurate representation of the flow field and surface characterization, a Conformal Mapping technique is employed to map the physical space (z-

42

plane) conformably to a unit circle (w-plane). The center of the circle represents the points at infinity and the perimeter represents the wavy bottom of the physical plane. (Note that the points at the streamwise extremities occupy the radial line at $\phi = 0$ or 2π of this circle.) A logarithmic map ($\xi = -i \ln (w)$) maps the w-plane onto the ξ-plane and a final inverse stretching transformation ($\eta - y$) creates a computational plane. The accuracy of surface delineation is thus clearly a function of the accuracy of the conformal mapping technique alone and is monitored by printing out the surface coordinates of the wave.

The computational method employed in the spectral Navier-Stokes solver employs high accuracy Chebyshev-Fourier expansion schemes to represent all global variables. The time advance from field at ' t_n ' to ' t_{n+1} ' involves the three-step fractional step approach with the non-linear terms updated using Adams-Bashforth scheme; a freeing of CFL limitation using a semi-implicit approach for the advection terms; a fast Poisson Solver which uses direct solution techniques (Eigen - expansions approach) with spectral accuracy and a fully implicit viscous step (see Balasubramanian et al. (1980)). The spectral algorithm provides second-order accuracy in time by using Richardson-extrapolation techniques and has a very high global accuracy (for mathematical detail see Appendix A).

DISCRETE-ELEMENT METHOD (DEM)

The Discrete-Element Method (DEM) computational model represents the "control-volume" approach, which does not consider partial differential equations, except for the establishment of the convergence (consistency, stability, accuracy) of the computational algorithm to the Navier-Stokes system. The DEM algorithm was specifically developed for "vortex-dominated" flow conditions; therefore, it can be applied with a high level of confidence to deep-wave-cavity configurations.

The DEM computational algorithm utilizes "completely body-conforming" elements adjacent to the boundary enclosure surfaces; however, it considers completely Cartesian, rectangular elements in the interior flow subregions for computational efficiency and, particularly, for computational accuracy. The

43

computational algorithm has complete second-order accuracy capabilities, which can eliminate (or minimize) "numerical diffusion"; and furthermore, it has special capabilities for eliminating the third-order "numerical-dispersion" effects by introducing special "artificial-dispersion" terms which do not compete with the physical effects.

The study is based on the applications of a fast-transient, three-dimensional DEM computational model, with one-layer specification (i.e., two-dimensional). The computational features of the model, which is a complete Navier-Stokes solver for incompressible flows, is summarized in Partial Differential Equation (PDE) form, for reader convenience (for mathematical detail see Appendix B).

OTHER METHODS

At the beginning of the program, J. Wu used the Sola Code at the UTSI VAX environment. The Sola Code is a first-order, low resolution, finite element code which was used only to provide rough estimates of the solution. Besides spectral and DEM codes, other codes were also used to validate the results. Two other finite difference codes were used by Grumman which are presented in summary.

ARC2D

This code was developed at NASA Ames and is an implicit finite difference code that solves the conservation form of the compressible Navier-Stokes equations. It makes use of central space differencing. Although it can be run time-accurate, all the cases of traveling wave problems run with this code used the accelerated non-time accurate factorization algorithm. The code was run in periodic mode to check out a plane Couette flow solution. This mode was also used for the preliminary results. The Navier-Stokes equation in "thin-layer" form (i.e. streamwise stresses neglected) gave traveling wave results that were little different from the full Navier-Stokes solutions. The code was run at nominal Mach number 0.1.

Grumman In-House Upwind Code

Another Grumman-owned pilot Navier-Stokes code was also used to compute the traveling wave flow. This code is also an implicit compressible finite difference Navier-Stokes equation solver in conservation form. It, however, makes use of more modern upwind methodology for computation of spatial flux difference (i.e. Roe scheme). This code was run in accelerated non-time accurate mode with periodic boundary conditions. This code was also run at Mach number 0.1. Results from both this and the ARC2D codes were similar in nature, converging to within four decimal places to what could naively be interpreted as steady state.

IV. RESULTS OF NUMERICAL FLOW FIELD COMPUTATIONS

PARAMETER DOMAIN

Simulation studies, based on $a/\lambda > 0.1$ and $c/U_\infty > 0.4$, were performed for a variety of wall profiles including sinusoidal, Kelvin-Stuart cat's eye, and combination of sine-cat's eye profiles. These parameter values represent one of the principal differences between the present study and previous traveling wave related research studies conducted in this country (see Table 3, page 10).

Although there are concerns among our team members that there are limitations associated with imposing different periodicity schemes, the results of all our independent computational codes are generally confirmatory. However, it should be recognized that the approach is preliminary and as yet does not explicitly consider the end effects (e.g. vortex dispersion) and vortex stability. The similar results from the three different approaches give us a reasonable degree of confidence on which to base the pursuit of further investigations and a suggested range of experimental study for real parameter optimization.

At the present time the numerical calculations are not complete, but the initial results have provided many useful insights which have enhanced our understanding of the physics and mechanism of the traveling wave phenomenon. The results of the numerical computations verify the relationship between the wall and flow parameters as generally described in the Soviet literature. They show the evolution of vortex formation and confirm that for a given set of parameters vortex entrapment is achieved. Drag coefficients have been calculated and the results indicate substantial drag reduction potential of the traveling wave in comparison with a flat plate. The parameter space for the computational simulations for the two chief codes used during this research is presented in Table 8.

46

Table 8. Parameter Range in the Present Simulation Study

			c/U∞
DISCRETE ELEMENT CODE	$Re_\lambda = 5.5 \times 10^4$ $\upsilon = 1.3 \times 10^{-6}$ m^2/s	$a/\lambda = 0.2$	0.33, 0.414, 0.550 - sinusoidal
		$a/\lambda = 0.1$	0.550 - cat's eye
SPECTRAL CODE	$Re_\lambda = 1000$	$a/\lambda = 0.2$	0.01, 0.2, 0.25, 0.33 0.414, 0.5, 0.7 - sinusoidal
		$a/\lambda = 0.15$	0.7
	$\upsilon = 1.3 \times 10^{-6}$		0.3, 0.4, 0.414, 0.5, 0.6, 0.7 - sinusoidal
	m^2/s	$a/\lambda = 0.1$	0.414 - cat's eye

GRID-DISCRETISATION

Grid discretisation is critical for adequate resolution and accuracy of the computational results. However, there must be a trade-off between the grid resolution and computational run time (expense). In order to examine the trend of the flow behavior, a low resolution simulation was employed initially (32X32 grid in spectral code). It was soon realized that to get a meaningful result, the number of grids had to be increased to higher values to resolve the flow due to perturbation of the wall profile. Figure 24 presents the velocity vectors over the initial trough of a traveling wave for three different resolution simulations using spectral code. Our analysis indicates that for the a/λ ratio of 0.2, two small separation bubbles first form and quickly merge into a single vortex. It can be seen that by increasing the grid structure from 32X32 to 64X64 and then 128X128, the velocity distribution becomes more detailed. With a 32X32 simulation, even one vortex is hardly detectable, while with 128X128 simulation, it is possible to clearly see the onset and merging of two small vortices. Figure 25 presents the fine structure (128X128) of grid discretisation for one wave cavity for the spectral code. Figures 26 and 27 show the fine grid structures at the wall and two wave cavities for DEM code (128X36 for two wave cavities).

47
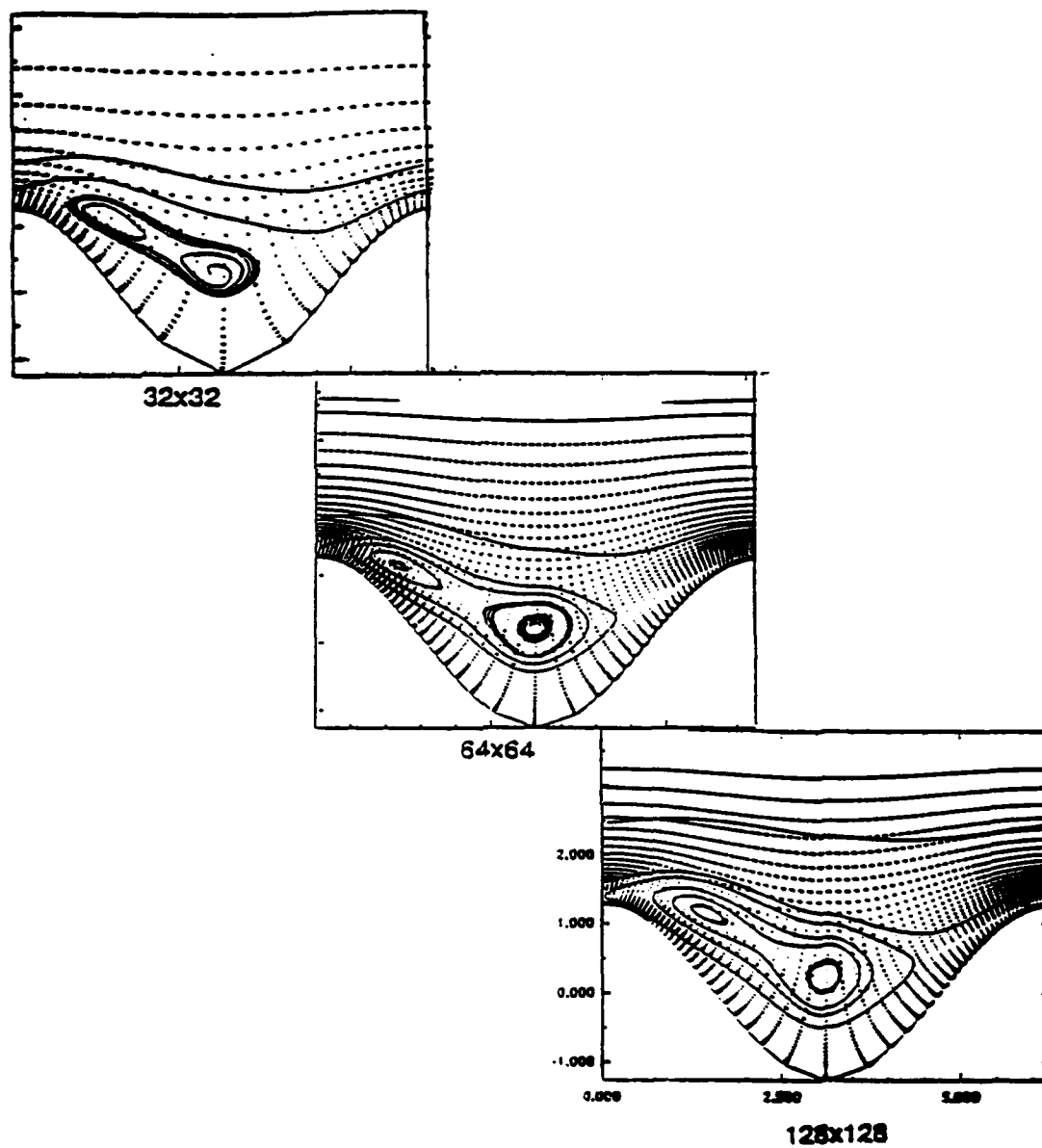
Figure 24.   Velocity Vectors for Three Different Numerical Resolutions at a Given Time - Spectral Code
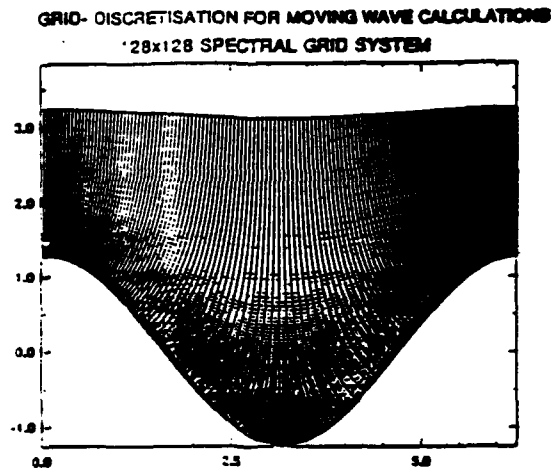
Figure 25. A Fine Structure of Grid Discretisation for SPECTRAL Code
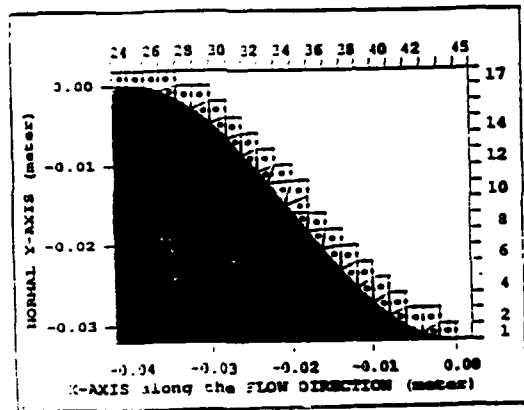
Figure 26. A Fine Structure of Grid Discretisation at the Wall for DEM Code
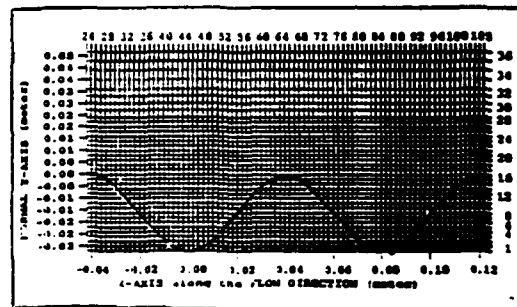
Figure 27. Two Wave Cavities Configuration for DEM Code

49

APPLICATION OF PERIODICITY

Due to the nature of the problem (periodic wall profile), and to avoid extreme computational time, periodic boundary conditions have been utilized. If the flow over a single wave were to be studied, with a prescribed leading edge and a trailing edge region, an appropriate set of boundary conditions may be to use inflow-outflow (non-periodic) boundary conditions in the streamwise direction; but, even for this case, the outflow conditions are not well understood. Hence, the result of that approach is not always accurate in practice, especially for the time-dependent flow (with vortices exiting the outflow plane). The situation is more complicated if there is more than a single wave over which solutions are required, such as a traveling wave. In this case, a more accurate method of studying flow problems of this nature is through enforcing some kind of periodic boundary conditions. Given the limitation of the current computer capability, the main reason for using periodic conditions for these situations is the fact that neither the inflow nor the outflow conditions are quite well defined for such problems. Application of periodic boundary conditions, in the spectral code for instance, imply that at the start of the computation $T=T_0$, the flow conditions correspond to some appropriate initial conditions of the flow which is allowed to evolve with time. Since the changes in the flow occur because of such an evolution, with time it becomes clear that the flow evolution never stops. Thus, the solutions can only achieve a quasi-steady state and not a true steady state as in inflow-outflow codes.

A further implication, since no steady state condition can be achieved, is that the solution at every step must be time accurate so comparisons of evolutions can be made. For the flow over the wave-train, the evolving solution consists of two major characteristics: (a) the memory of the primary flow; i.e., the initial flow condition at $T=T_0$ and its subsequent evolution; and (b) the periodic component or the perturbation due to the wave. The first one can be viewed as the effect of the leading edge if the initial flow conditions corresponding to a fully developed flow at the end of the leading edge section were prescribed in the code. It is important to note that this evolution will be affected by the presence of the traveling wave which can be viewed as a controller for such growth. If proper choice of the wave-train were made (in terms of a/λ; x/λ; c/U_∞, shape of the

50

wave), it may be possible to adjust (or even arrest) the rate of growth of the flow. One of the purposes of the research as identified in Section I is to determine this parameter range where such beneficial effects may occur.

VELOCITY VECTORS

The bulk of the calculations reported here involve drag reduction studies of rather large amplitude waves, $a/\lambda \geq 0.1$, for laminar flow conditions. The initial interest has been focused on this amplitude range based on the fluid physics analysis by Wu.

Initial studies of drag characteristics of traveling waves were done for a non-dimensional wave amplitude $a/\lambda = 0.2$ and non-dimensional wave speed $c/U_\infty = 0.4$; the Reynolds number based on wavelength $(R = U_\infty \lambda/\upsilon)$ was taken to be 1000 to 10,000 for the Spectral Code and 3 to 5.5×10^4 for the DEM code for most cases.

Figures 28 through 30 show the flow behavior for different computational time steps obtained from spectral code. A time of approximately 25 units represents one second of real time and one second of the DEM code. The velocity profiles/streamlines for one wave cavity of a sinusoidal wave are shown. It can be seen that as the time passes, the vortex begins to form at the wave trough. Apparently, there are two vortices that merge together and produce a larger stable vortex. After this vortex is formed, it will have a modest fluctuation about the center until it reaches a quasi-steady state. Similar behavior is evident from the results of the DEM code which is shown in Figures 31 to 33. These time steps are in seconds. Also in these Figures the ratio of amplitude to wavelength is $a/\lambda = 0.2$ and the phase to freestream velocity ratio is $c/U_\infty = 0.4$. Vortex entrapment was established for other values of these parameters. Figure 34 presents the velocity vectors for a sinusoidal wave with $a/\lambda = 0.1$ and $c/U_\infty = 0.4$. Results of the Cat's eye wall profile are presented in Figure 35 for $c/U_\infty = 0.4$ and $a/\lambda = 0.1$. Figure 36 presents a time-series of the sinusoidal wall profile and reveals the development of the formation of the vortices in the wave troughs.

In some cases the flow pattern comparison indicates that as time goes on, the vortex center moves slightly away from the wall. This implies a small growth of the isolating layer thickness due to the presence of very small drag. This thickness can be represented by the saddle height to wavelength ratio δ_i/λ (see Figure 15, page 27), which can be compared with the growth of the thickness of a laminar boundary layer over a flat plate. The growth of δ_i/λ is much slower (attributed to a small drag at $c/U_\infty=0.4$ condition). Further fine tuning of c/U_∞ should make this growth vanish, i.e., a zero drag condition.

PRESSURE CONTOURS

Numerical solutions of the Navier-Stokes equations give the values of velocity and pressure for all grid points in the two-dimensional region. The information on the pressure distribution is crucial for analyzing the low and high pressure areas and for estimating the drag coefficient. Figure 37 presents the graphs of pressure contours using spectral code at three different computational time units of 5, 10 and 15; and Figure 38 shows the same graph for time units of 20 and 35. These pressure contours are for a sinusoidal wall profile with $a/\lambda = 0.2$ and $c/U_\infty = 0.4$.

As can be seen from this set of figures, the center of the vortex is the low pressure area (as is expected). The pressure increases as the velocity decreases. The wave crest and the bottom of the trough correspond to the highest pressure areas (lowest velocity). Keep in mind that these results are viewed from a moving frame of reference which is traveling with the wave, so the vortices seem to be stationary with respect to this coordinate system.
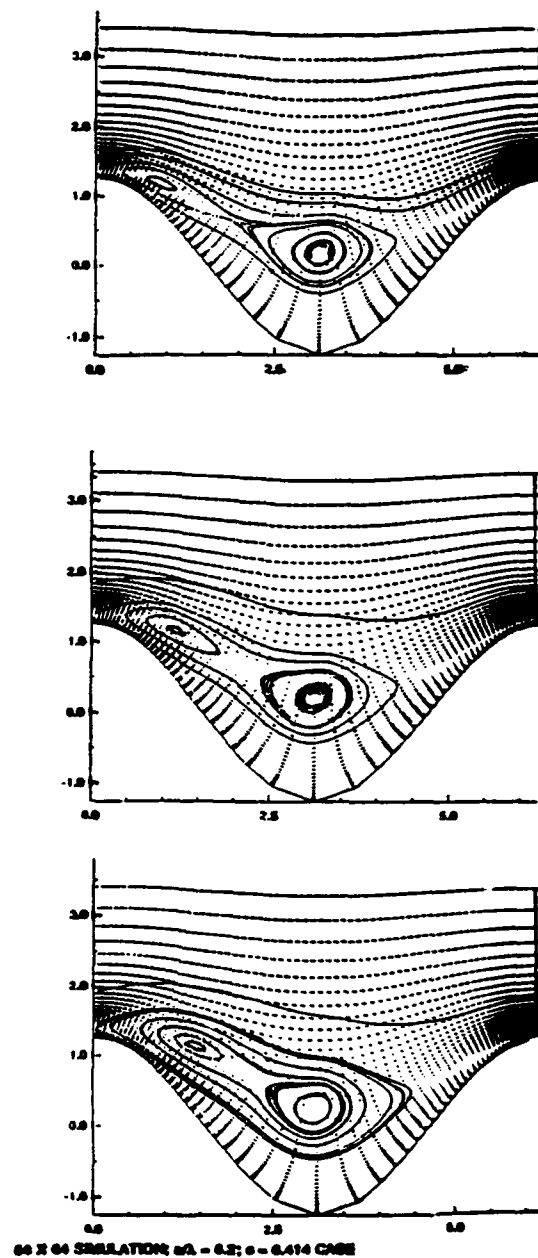
Figure 28. Velocity Distributions Over One Sinusoidal Wave Cavity for Computational Times of 2.5, 3.75 and 5.0, Using Spectral Codes

53
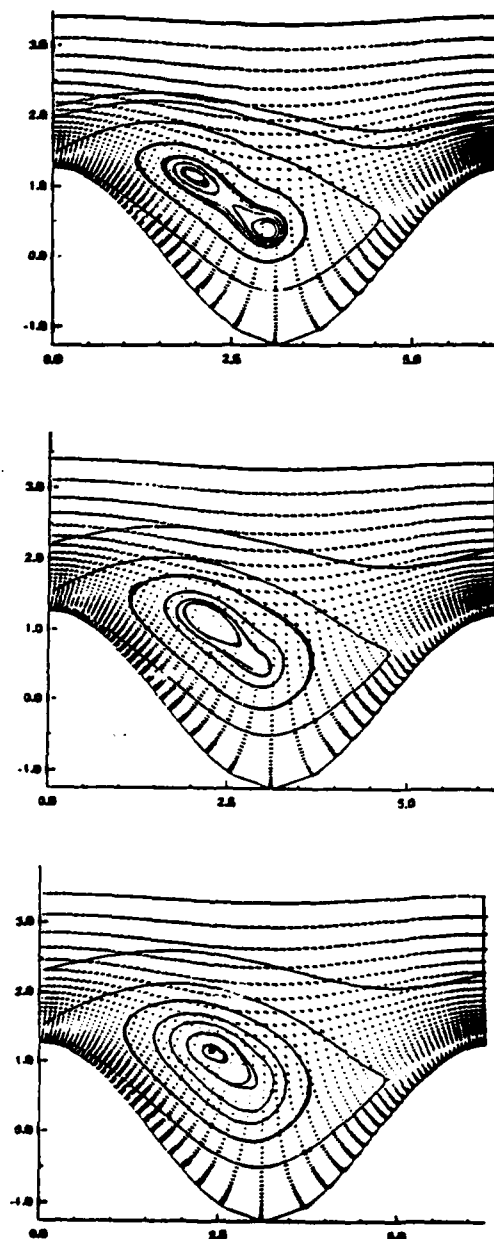
Figure 29.   Velocity Distributions Over One Sinusoidal Wave Cavity for
Computational Times of 7.5, 8.75 and 10, Using Spectral Codes
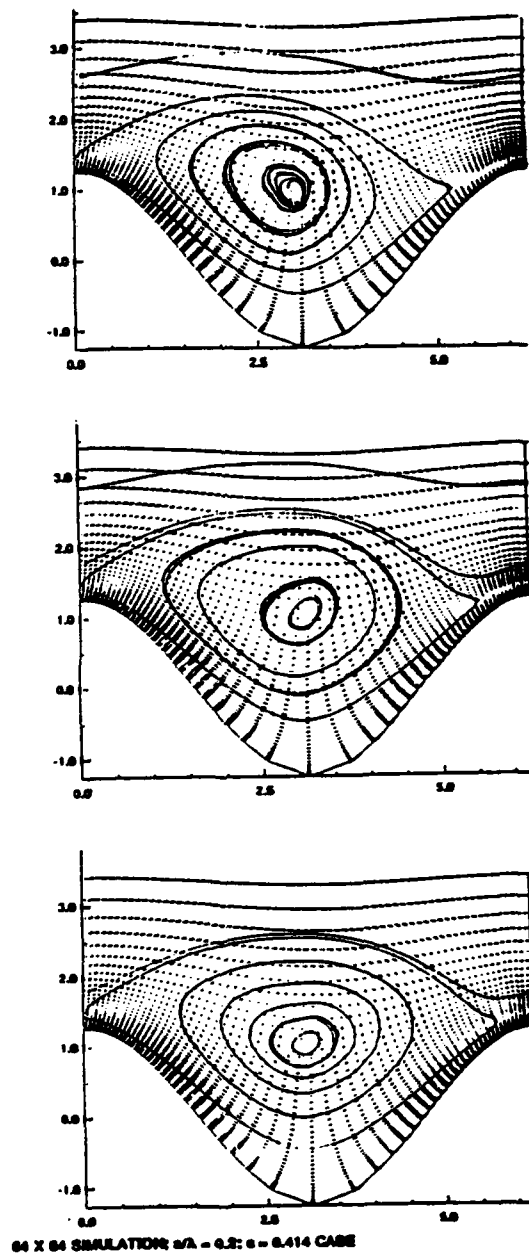
Figure 30. Velocity Distributions Over One Sinusoidal Wave Cavity for Computational Times of 12.5, 15.0 and 17.5, Using Spectral Codes
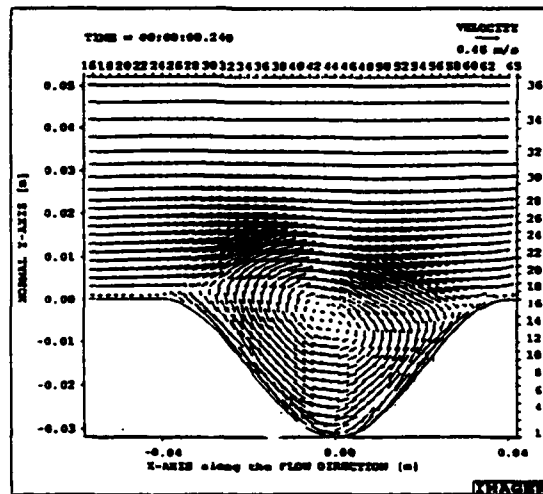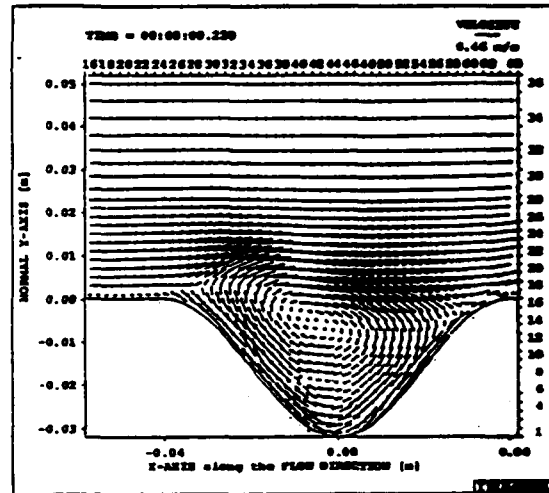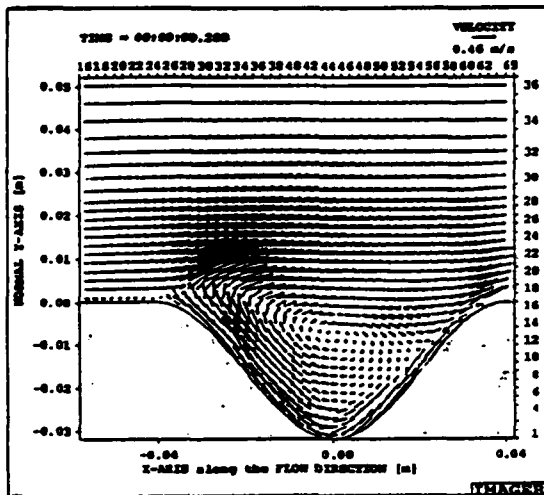
Figure 31.   Velocity Distributions Over One Sinusoidal Wave Cavity for Computational Times of 0.2, 0.22 and 0.24, Using DEM Code

56
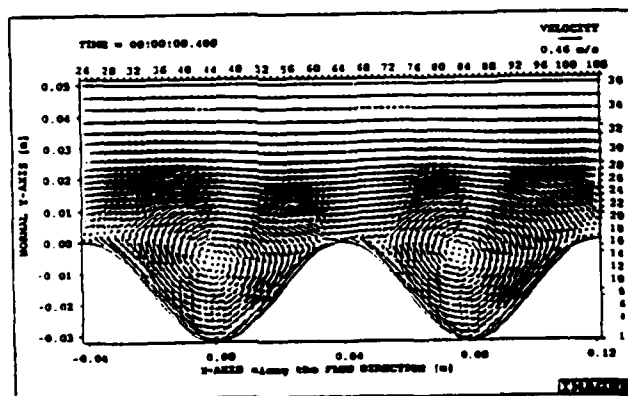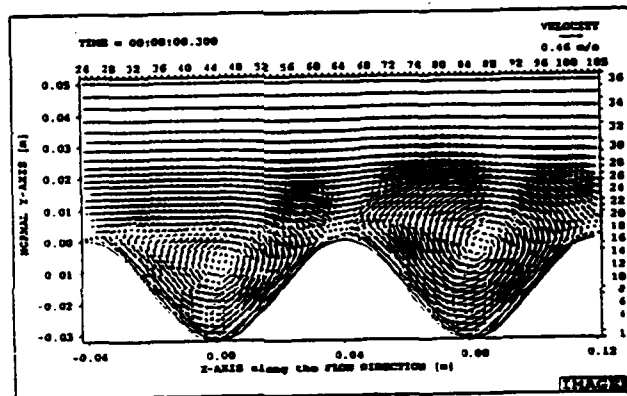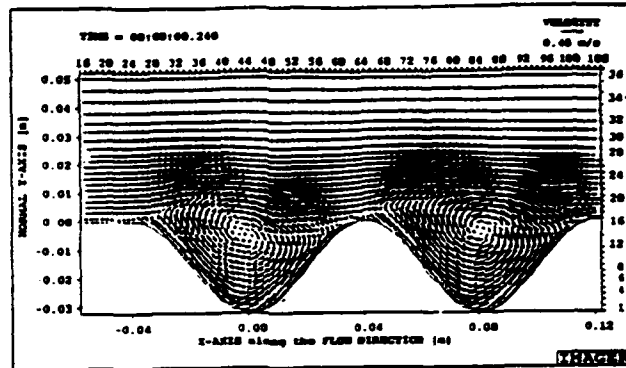
Figure 32. Velocity Distributions Over Two Sinusoidal Wave Cavities for Computational Times of 0.24, 0.3 and 0.4, Using DEM Code

57
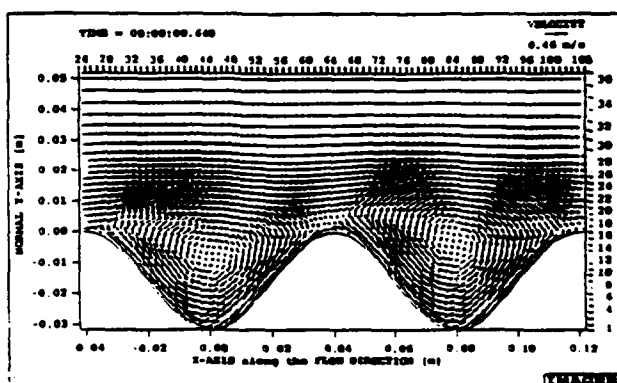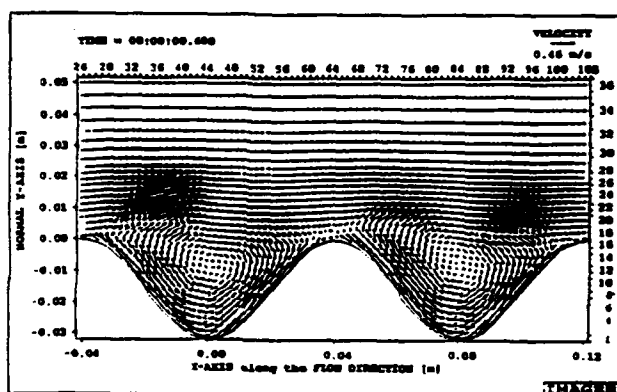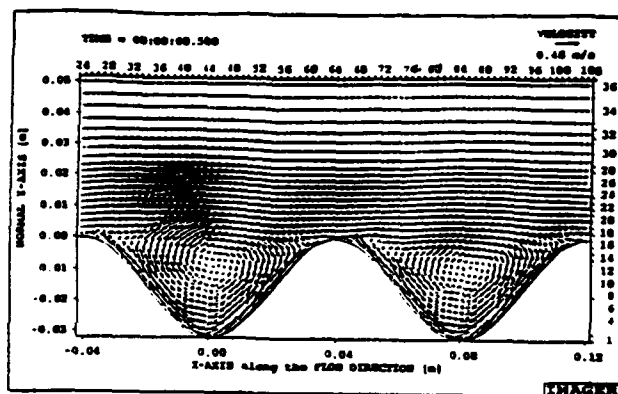
Figure 33.   Velocity Distributions Over Two Sinusoidal Wave Cavities
for Computational Times of 0.5, 0.6 and 0.64, Using DEM
Code
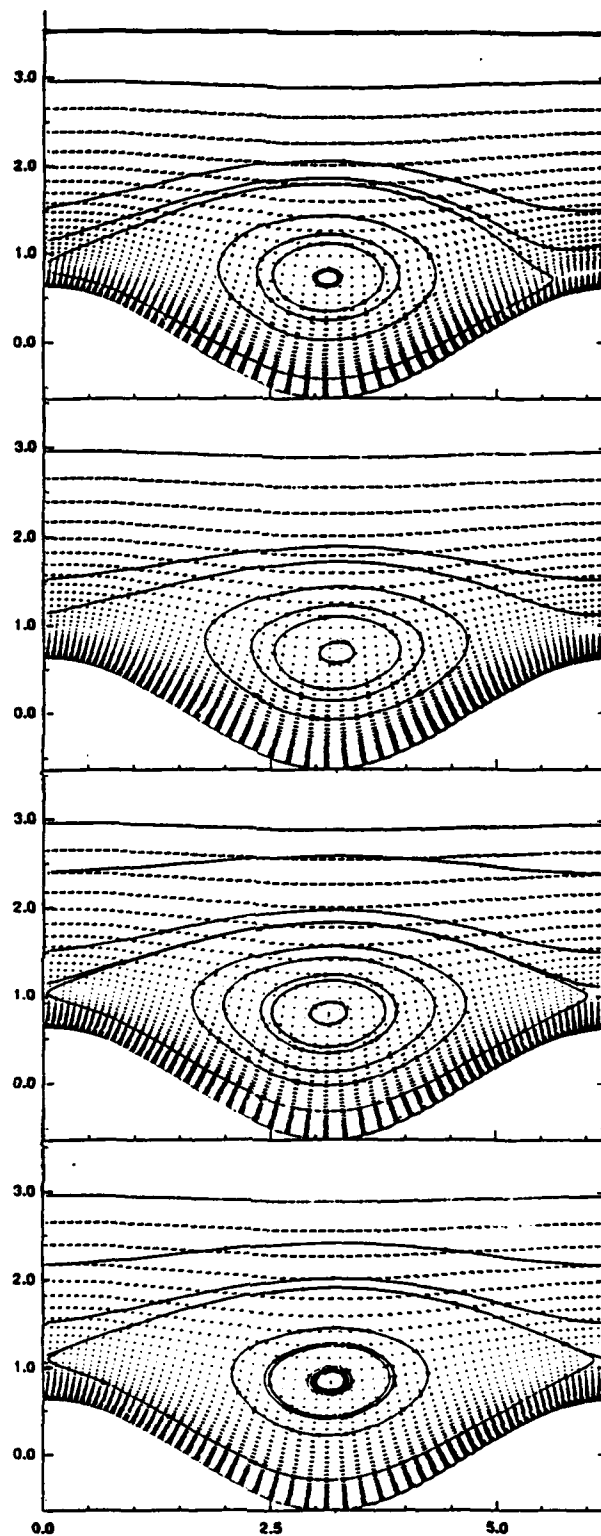
Figure 34.   Velocity Distributions Over One Sinusoidal Wave Cavity for
a/λ = 0.1 and Computational Times of 20, 40, 60 and 80,
Using Spectral Code
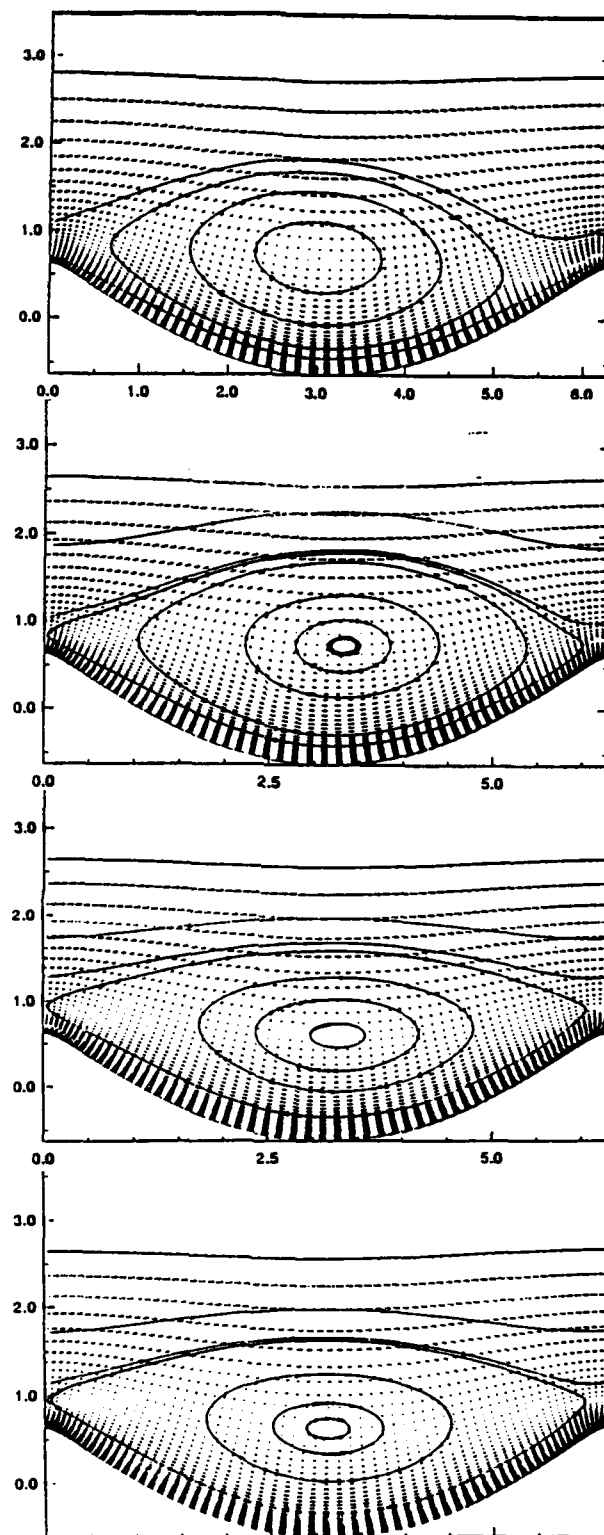
Figure 35. Velocity Distributions Over a Cat's Eye Wave Cavity for Computational Times 20, 25, 45, and 50, Using Spectral Code

60
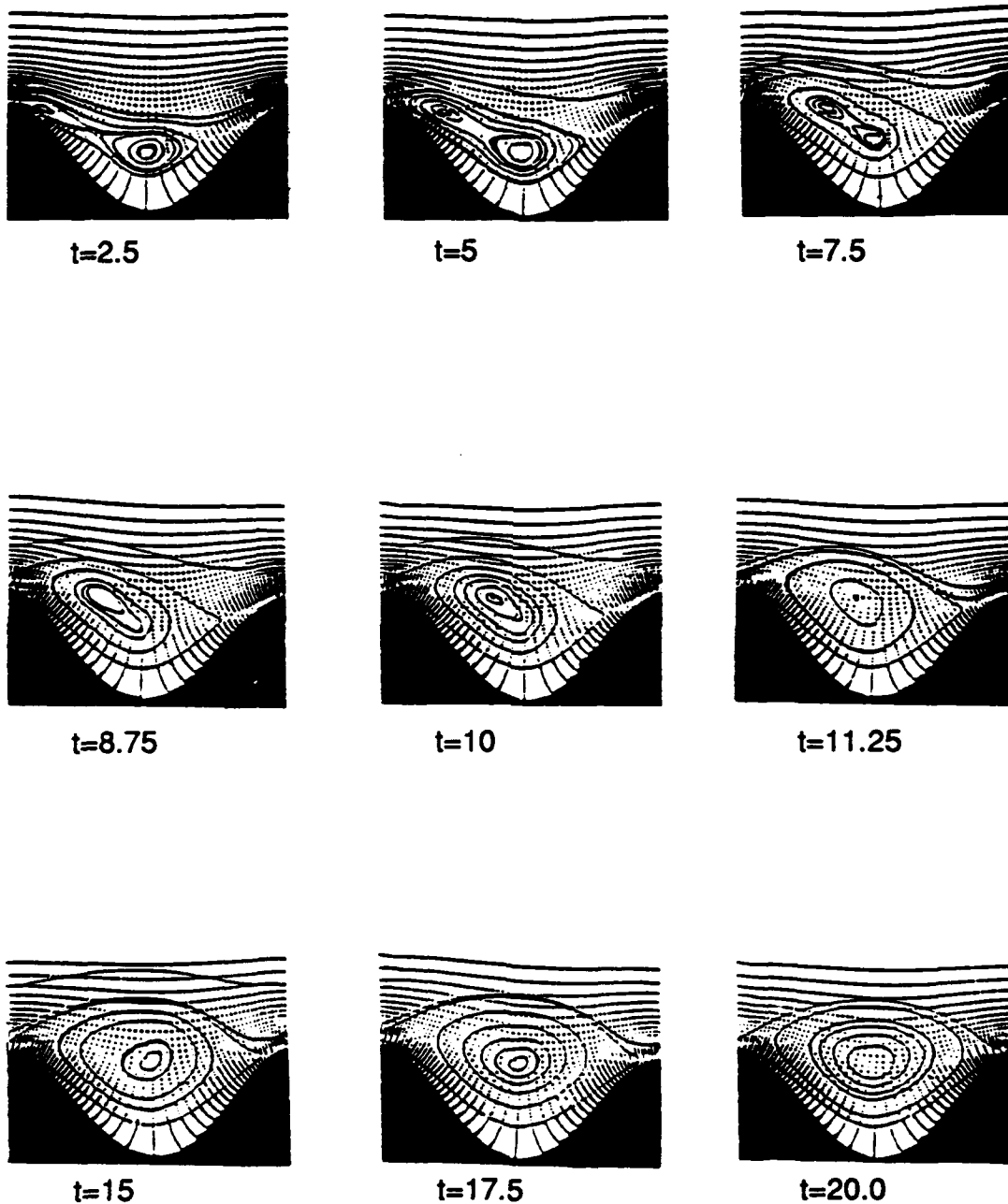
Figure 36.   Computer Simulation of Vortex Formation Sequence for
Computational Times Vary from 2.5 to 20 for a Sinusoidal Wall
Profile with $a/\lambda = 0.2$ and $c/U_\infty = 0.414$ - Spectral Code

61
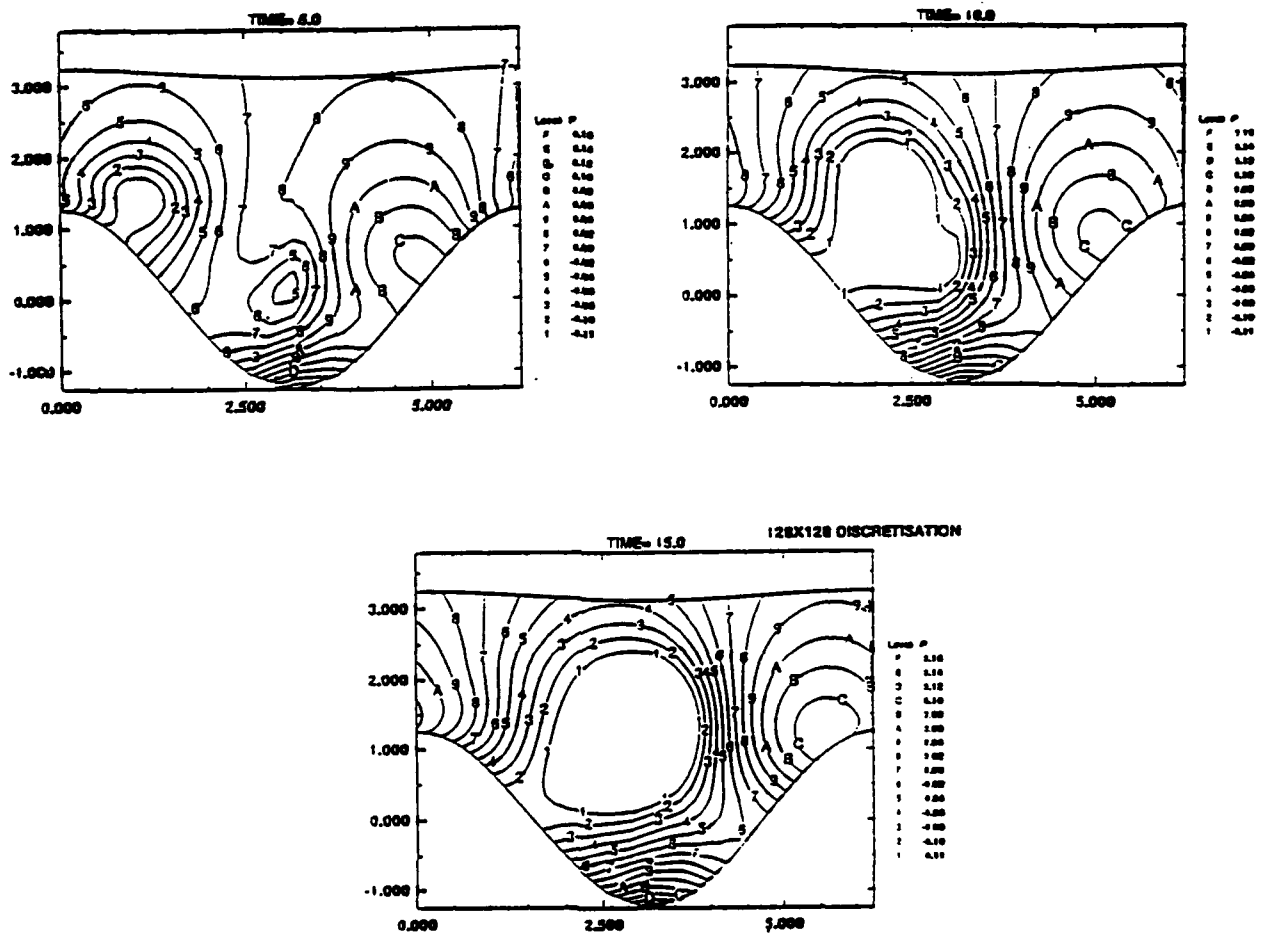
Figure 37.   Pressure Contours Over One Sinusoidal Wave Cavity with
              a/λ = 0.2 and c/U∞ = 0.414 for Computational Times of 5,
              10 and 15, Using Spectral Code
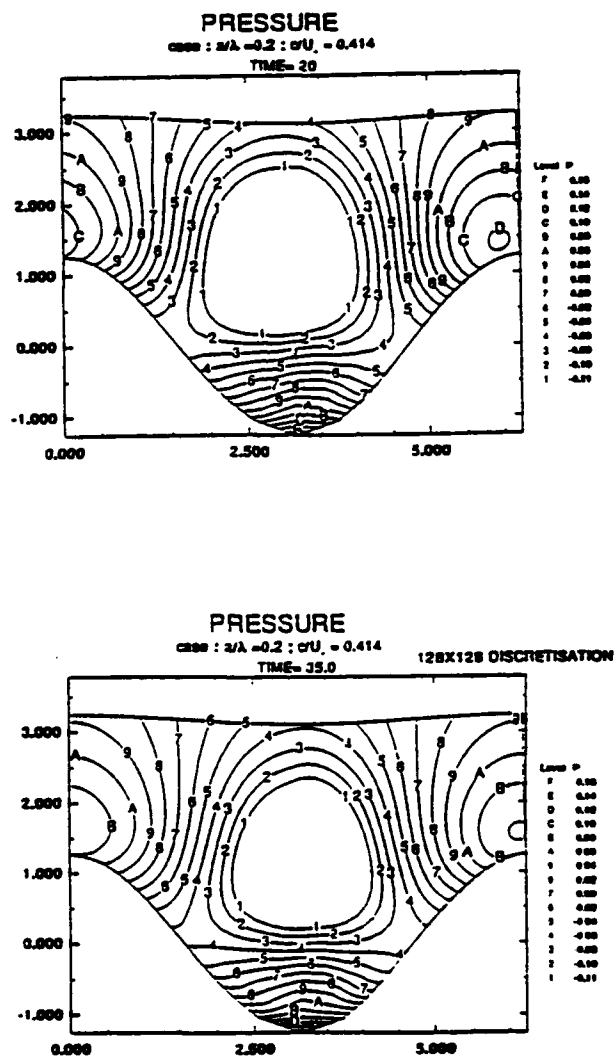
Figure 38.　Pressure Contours Over One Sinusoidal Wave Cavity with a/λ = 0.2 and c/U_∞ = 0.414 for Computational Times of 20 and 35, Using Spectral Code

CAVITATION CONSIDERATION

One of the important design and performance factors for implementation of the traveling wave is cavitation. If the local liquid pressure is dropped below the vapor pressure due to a flow phenomenon, the cavitation occurs. Cavitation may occur in a high-velocity liquid flow, e.g. at the tip of a marine propeller. Since the traveling wave corresponds to ordered vortical flow, any occurrence of cavitation may change the flow configuration at the wall and disorder the whole flow regime. Thus, it is important to design in a such way that minimizes the risk of cavitation.

The likelihood of cavitation onset is generally described by a cavitation index (or cavitation number) σ which is defined by

$$\sigma = \frac{P_\infty - P_v}{\frac{1}{2}\rho U_\infty^2} \tag{31}$$

where P_v is the vapor pressure and P_∞ is the freestream or ambient pressure. The lower σ is, the more likely is the onset of cavitation. It is known (Urick 1983) that for underwater vehicle application if $\sigma < 2$, the flow will definitely cavitate; and if $\sigma > 6$, cavitation is unlikely, so critical values of σ are defined as $2 \leq \sigma_{cri} \leq 6$. Figure 39 presents the limiting cavitation curves for depth versus maximum wave phase velocity. While cavitation is usually considered in terms of tip velocity of a propeller, in the case of traveling wave it can be considered in terms of maximum wall velocity. Maximum wall velocity depends on the wave shape and its parameter (a/λ). For example, for a sinusoidal wall profile, it occurs at 90° and is approximately equal to 1.6c for $a/\lambda = 0.2$ (see Table 4, page 35). These curves (Figure 39) were obtained for values of σ equal to 2 and 6, and describe the safe operational zone, the cavitation zone and the critical zone. The two bottom axes show the actual vehicle velocity U_∞ for values of c/U_∞ equal to 0.4 for sinusoidal with $a/\lambda = 0.2$, and c/U_∞ equal to 0.55 for a cycloidal wall profile with $a/\lambda = 0.1$.

Corresponding zones can be obtained for surface ship application by enlarging the starting portion of the curves on Figure 39. This is presented in Figure 40 which is for smaller tip velocity and depth from the ocean surface. These curves

demonstrate that the traveling wave concept will have only very limited applications for surface ships and, should it prove practicable, can only be exploited to the fullest by deep diving vehicles.
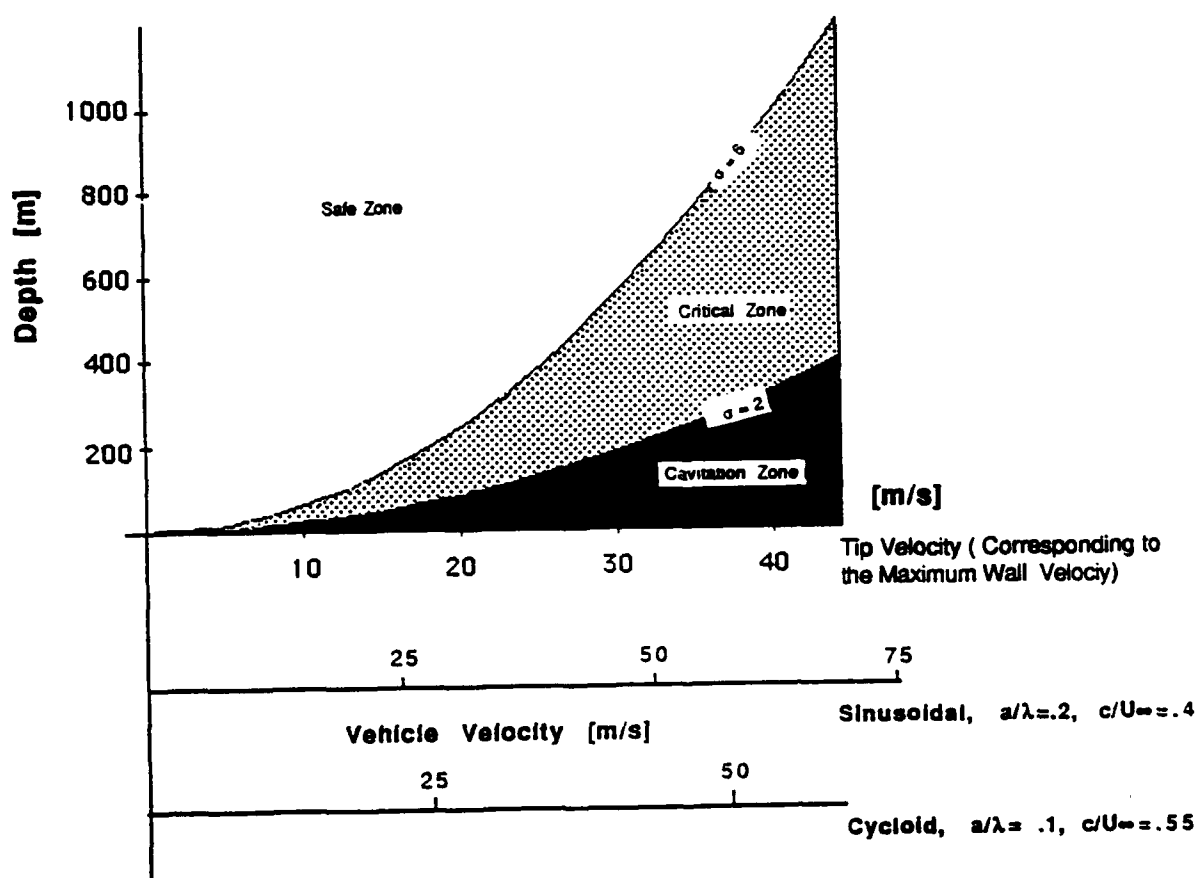
Figure 39. Critical Cavitation Zone - Depth versus Maximum Wall Velocity for Traveling Wave Application
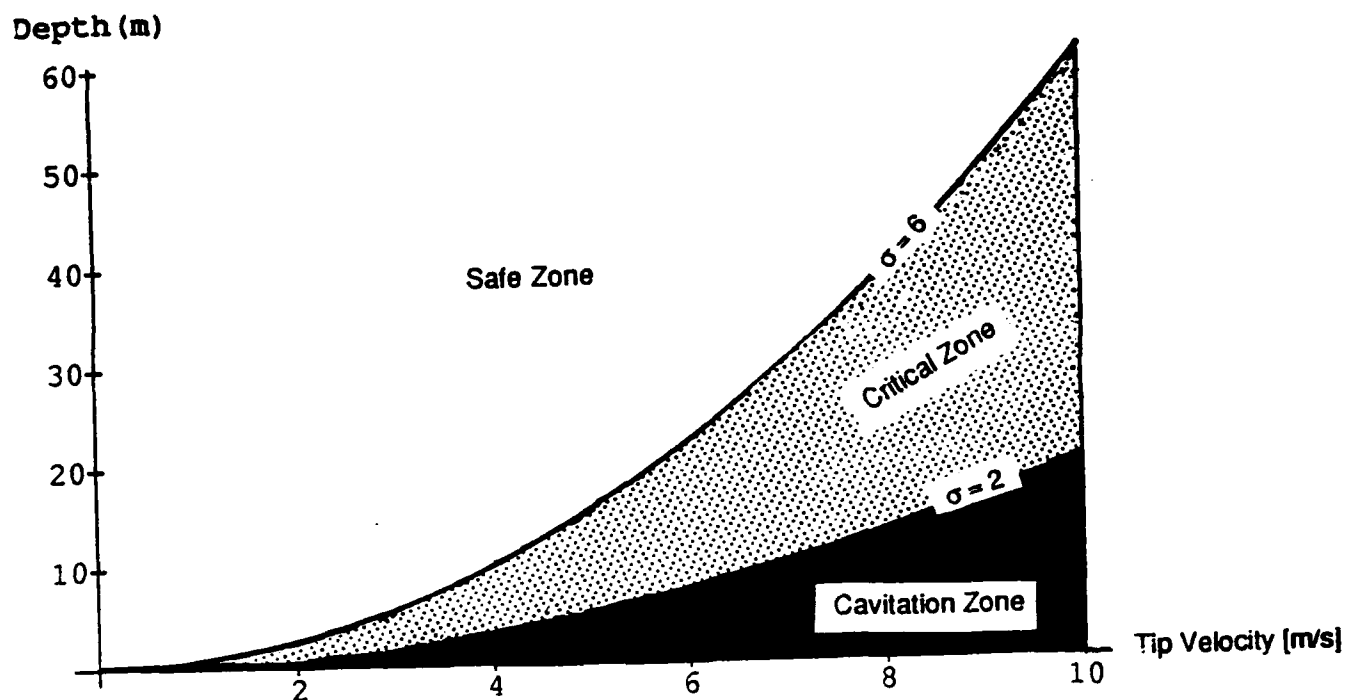
Depth (m)

Figure 40. Critical Cavitation Zone - Depth Versus Tip Velocity for Surface Ship Applications

DRAG CHARACTERISTICS

Comparison of the drag forces of the traveling wave with that of a flat plate can reveal important facts about the potential of the implementation of the traveling wave. Drag characteristics for a sinusoidal wall profile are presented in Figure 41. It is important to note that with the spectral code almost every 6.3 units computation in time corresponds to one wave length (2π) in space. In this Figure the coefficient of the friction drag, C_{Df}, the coefficient of pressure drag, C_{Dp}, and the coefficient of total drag, C_{Dt}, are depicted versus computational time. In order to obtain a meaningful comparison, the drag of a flat plate, C_{Dr}, as a reference drag coefficient, is also shown. In most cases these values are non-dimensionalized with respect to the flat plate values and make the flat plate drag equal to unity. In other words, the growth of the boundary layer has already been taken into account to make the reference drag equal to unity. This Figure indicates that at the initial computational times, there is a rapid increase

66

in drag due to vortex formation. Once the vortex is formed (two vortices merged together), the drag decreases in time with some fluctuation until equilibrium is reached. At later computational times, a fully developed state is established where a vortex is entrapped and maintained in the trough of the wave. The general trend of these curves shows that the friction drag, as well as the pressure drag, are less than that of the flat plate. This is an indication of the feasibility of the traveling wave phenomenon.
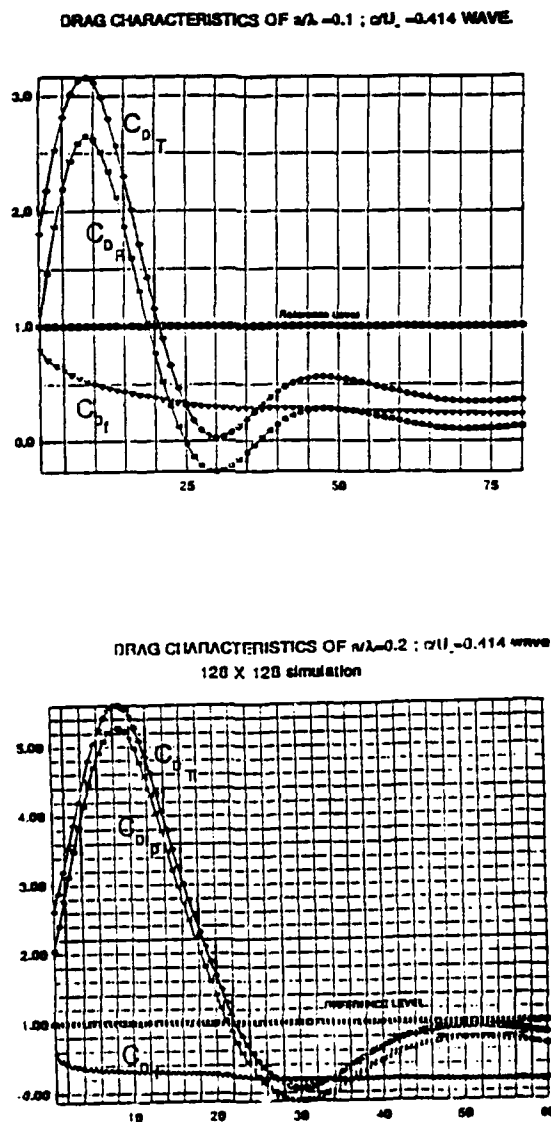
Figure 41.   Drag Characteristics of a Flow over a Sinusoidal Wall Profile Versus Time, for c/U$_\infty$= 0.414 and a/λ of 0.1 and 0.2, Using Spectral Code

The values of drag vary significantly with the wall geometry (wave shape and a/λ) and the flow parameters (c/U_∞). The evolution of drag reduction and generation of thrust versus computational time (corresponding to the number of waves) is presented in Figure 42. This Figure shows the drag characteristics for values of c/U_∞ equal to 0.3, 0.4, 0.5, 0.6 and 0.7, a/λ is 0.1, and Re_λ of 10^3. In these cases it appears that as c/U_∞ increases (more power produced by the wall), the excursions of maximum and minimum pressure drag tend to decrease. Further, it has been shown that at low Re values (1000) where viscous forces are more dominant, the friction drag remains constant with only a modest fluctuation, until the value of c/U_∞ becomes large. For higher Re values (10,000 - 100,000) when inertial forces are more dominant, the friction drag decreases with time even at modest values of c/U_∞.

INFLOW REYNOLDS NUMBER EFFECT

Comparison of the computational results for different Reynolds numbers reveals some interesting points which provide better insight to the traveling wave problem. In order to understand the effect of an inflow Reynolds number, the following cases have been considered:

Case 1:

$$R_x = R_\lambda = 1000 \qquad a/\lambda = 0.1 \qquad \frac{c}{U_\infty} = 0.5$$

Case 2:

$$R_x = 10000, \quad R_\lambda = 1000 \qquad a/\lambda = 0.1 \qquad \frac{c}{U_\infty} = 0.5$$
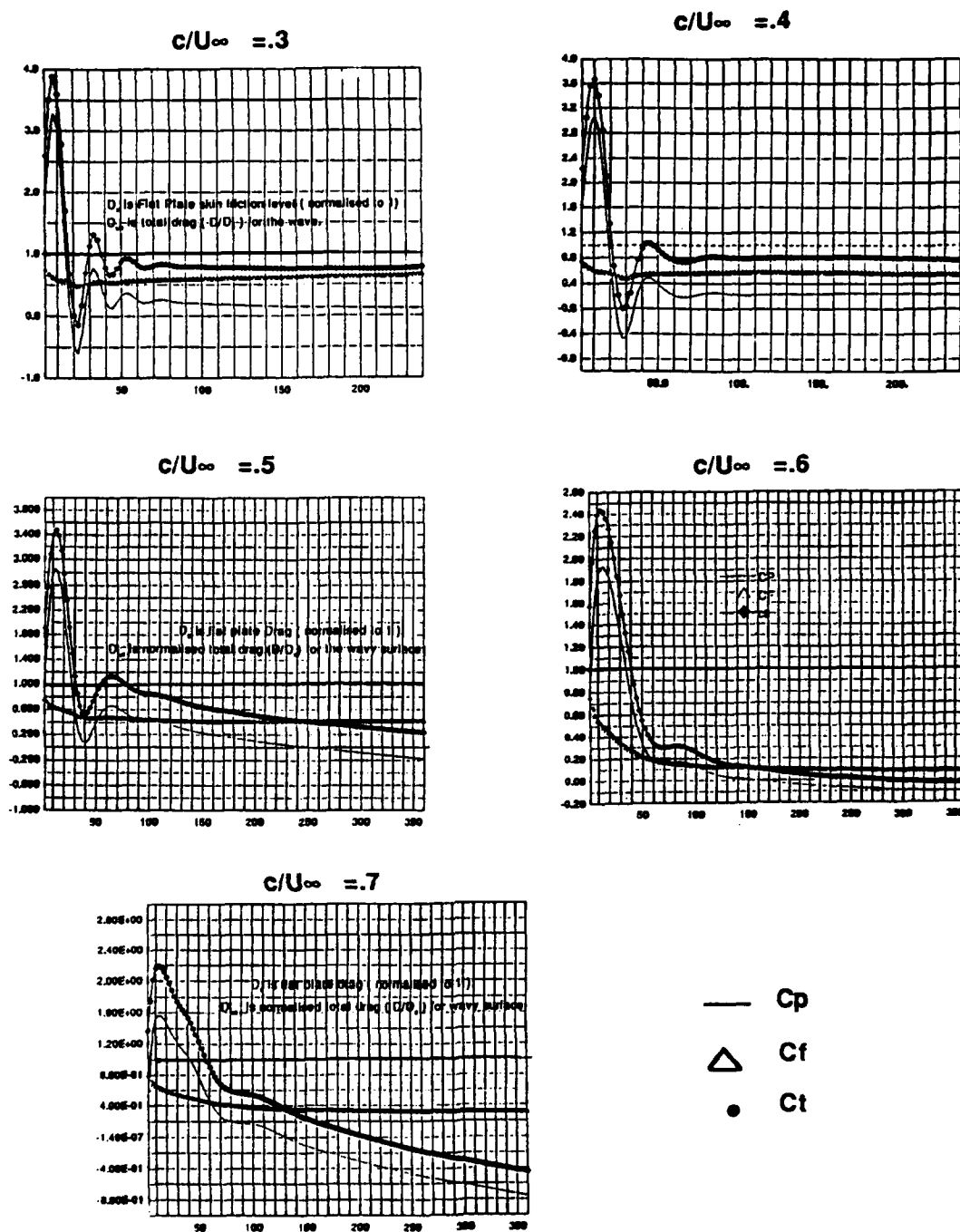
Figure 42.   Drag Characteristics of a Flow over a Sinusoidal Wall Profile Versus Time, for a/λ = 0.1 and c/U∞ = 0.3, 0.4, 0.5, 0.6 and 0.7, Using Spectral Code

It is evident that the two cases are identical with the exception of the inflow Reynolds number. It is assumed that the wave phase velocity c and the free-stream velocity U∞ for both cases are the same. In other words, the effect of

higher Reynolds number is that the characteristic length for Case 2 is 10 times longer than Case 1 (Figure 43) and the flow is more developed.
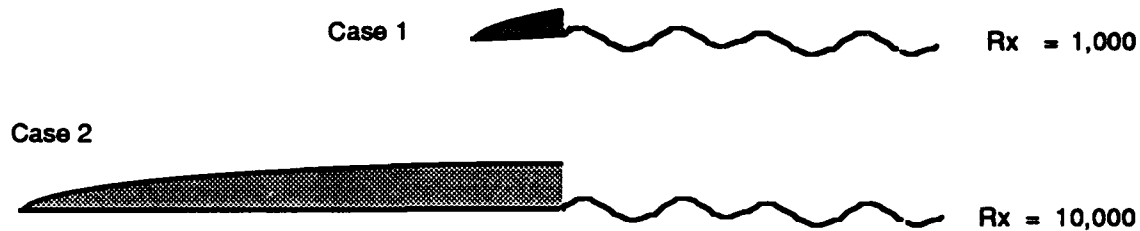
Figure 43. The Inflow Reynolds Number Difference Manifests Itself as Different Characteristic Lengths Which Means a Thicker Inflow Boundary Layer for the Rx = 10,000 Case

This indicates that the thickness of the inflow boundary layers is greater in Case 2 than in Case 1. Since the freestream velocities are the same for both cases, the velocity gradient is steeper in Case 1 than in Case 2 at the point where the wave starts.

By analyzing the x-components of the velocity contours obtained from computational results, it was observed that the rate of change of velocity gradient, $\partial u/\partial y$, for various locations along the wave is greater for Case 1 than for Case 2. As a result, the skin friction drag is higher in Case 1 than Case 2. The height of the vortex center (from the bottom of the trough) was also calculated for various computational times (60, 120, 180 and 240 time units). The calculations showed that the vortex center is higher for Case 2 than for Case 1; and for Case 2 the vortex appears to have a flatter shape than Case 1. These observations indicate that the viscous sub-layer (the so-called isolated layer) is thicker for Case 2, and thus the drag is lesser for this Case. The variations in vortex heights are presented in Figure 44.
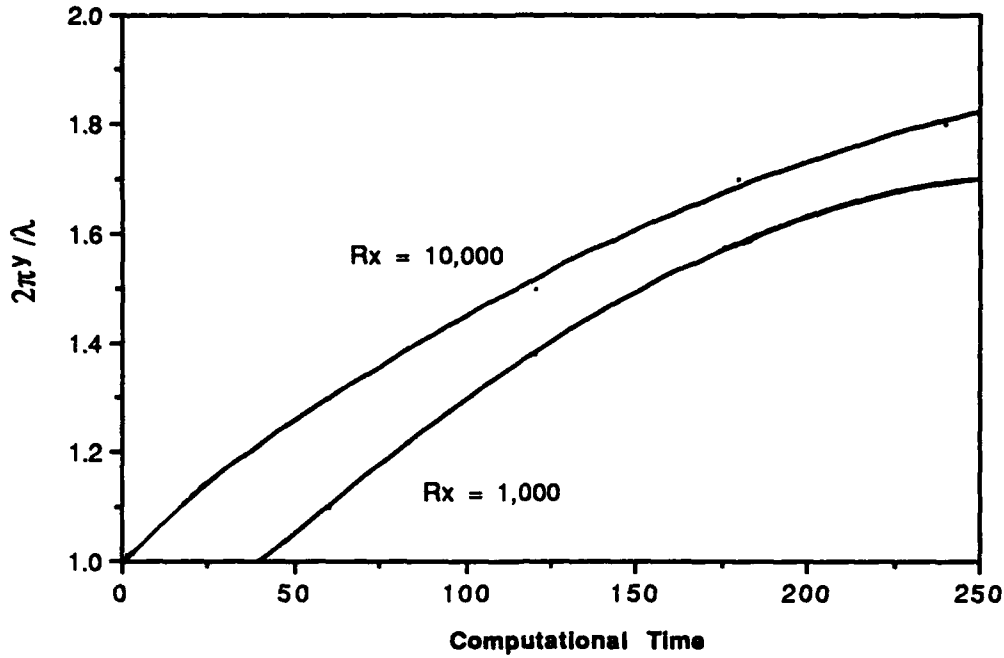
Figure 44.   Variation of the Vortex Center Height Versus Computational Time

Since the characteristic length in non-dimensionalization of the Navier-Stokes equation was chosen to be λ and due to the spatial periodicity (every 2π) of the computational code, the height of the vortex center y is non-dimensionalized by $2\pi/\lambda$.

Circulation was also calculated for the two cases at different computational times. This was made possible by using the x and y component of the velocity contours obtained from the computer results and the definition of circulation Γ:

$$\Gamma = \int_c q.dr = \int_c (udx + vdy)$$ (32)

The calculations showed that the value of circulation is slightly higher for Case 2 ($R_x = 10,000$). This means that the vortex-induced velocity q_v is higher and closer to the wall velocity q_w, and at the upper part it better matches the freestream velocity U_∞. The final result is that the drag is lesser for Case 2 than Case 1 which has already been indicated in the numerical simulations. Thus,

71

the calculation showed that the effect of increasing the inflow Reynolds number is to reduce the skin friction drag and, as a result, the total drag of a traveling wave wall. Further computational simulation is necessary to confirm general trends of Reynolds number effects which is one of the important goals of the future research.

LEGITIMACY OF COMPARISON OF COMPUTATIONAL RESULTS WITH FLAT PLATE

In order to estimate the validity of the numerical results, the relationship between the number of waves and the total length of a reference plate must be obtained. Thus, it is useful to calculate the time corresponding to the starting of the traveling wave (t_s) with respect to the start up of the flow from the leading edge of the reference plate.

Using the time-dependent velocity gradient (Lamb, 1932, Section 334a), one can obtain the shear stress at the wall($y = 0$) as a function of time.

$$\frac{\partial u}{\partial y} = \frac{U_\infty}{\sqrt{\pi \upsilon t}} e^{-y^2/4\upsilon t} \tag{33}$$

$$\tau = \mu \frac{\partial u}{\partial y} \quad \Rightarrow \quad \tau = \mu \frac{U_\infty}{\sqrt{\pi \upsilon t}} \tag{34}$$

The drag coefficient is then:

$$C_f = \frac{\tau}{\frac{1}{2}\rho U_\infty} \quad \Rightarrow \quad C_f = \frac{2}{\sqrt{\pi}}\sqrt{\frac{\upsilon}{t U_\infty^2}} = 1.128\sqrt{\frac{\upsilon}{t U_\infty^2}} \tag{35}$$

If the constant β is defined as:

$$\beta = 1.128\sqrt{\frac{\upsilon}{U_\infty^2}}$$

(36)

then C_f is :

$$C_f = \beta/\sqrt{t}$$

(37)

Now, one can calculate the wave starting time t_s by using the value of C_f at two different computational time steps from the drag characteristics values.

For the case $Re_\lambda = R_x = 1,000$

at $t = t_s$ $C_f = 0.0175$

(38)

at $t = t_s + 240$ $C_f = 0.006$,

(39)

and from Equation 37, C_f is:

$$C_f = \beta/\sqrt{t} \quad \Rightarrow \quad \beta = C_f \sqrt{t}$$

(40)

Now we can solve for t_s and β

$$0.0175 \, (t_s)^{.5} = 0.006 \, (t_s + 240)^{.5}$$

(41)

Thus, $t_s = 31.97$ and $\beta = 0.0989$. With $\upsilon = 1.3 \times 10^{-6}$ (water at 20° C), then $U_\infty = 1.3 \times 10^{-2}$ m/s.

Using the definition of Re_λ, we can find λ

$$Re_\lambda = \frac{U\lambda}{\upsilon} \quad \Rightarrow \quad 1000 = \frac{1.3 \times 10^{-2}\lambda}{1.3 \times 10^{-6}} \quad \Rightarrow \quad \lambda = 0.1m$$

(42)

To calculate the length of the flat plate in 240 time units we have:

$$x_1 = U_\infty t_s = 1.3 \times 10^{-2} (31.97) = .41 \text{ m} \tag{43}$$

$$x_2 = U_\infty (t_s + 240) = 1.3 \times 10^{-2} (31.97 + 240) = 3.53 \text{ m} \tag{44}$$

$$\text{so} \quad \Delta x = x_2 - x_1 = 3.12 \text{ m} \tag{45}$$

and the number of waves for a length of 3.12 m is: $\Delta x / \lambda = 31$.

By similar calculation for the case of $R_\lambda = 1,000$ and $R_x = 10,000$, we obtain the following conditions:

$$\text{at} \quad t = t_s \quad \Rightarrow \quad C_f = 0.00675 \tag{46}$$

$$\text{at} \quad t = t_s + 240 \quad \Rightarrow \quad C_f = 0.0045 \tag{47}$$

$$C_f = \frac{\beta}{\sqrt{t}} \quad \Rightarrow \quad t_s = 192 \quad \Rightarrow \quad \beta = 0.0935 \tag{48}$$

$$\beta = 1.128 \sqrt{\frac{\upsilon}{U_\infty^2}} \quad \Rightarrow \quad U_\infty = 1.375 \times 10^{-2} \text{ m/s} \tag{49}$$

$$R_\lambda = \frac{U\lambda}{\upsilon} = 1000 \quad \Rightarrow \quad \lambda = 9.45 \times 10^{-2} \text{m} \tag{50}$$

$$x_1 = U_\infty t_s = 1.375 \times 10^{-2} (192) = 2.64 \text{m} \tag{51}$$

$$x_2 = U_\infty (t_s + 240) = 1.375 \times 10^{-2} (192 + 240) = 5.94 \text{m} \tag{52}$$

so $\Delta x = x_2 - x_1 = 3.3$ [m] , and the number of waves for the length of the plate is

$$\frac{\Delta x}{\lambda} = \frac{3.3}{9.45 \times 10^{-2}} = 35 \tag{53}$$

This analysis indicates that the comparison of the flat plate and traveling wave results are reasonable because the calculated length of the flat plate is large (i.e. the length is over thirty times the wavelength) so it compares to multi-wave plate. That is, the R_L of an equivalent flat plate would be on the order of 4.5 x 10^4.

V. ROUGH ENERGY CALCULATION

OVERALL DRAG CONSIDERATION

Method for Estimating Overall Drag

As suggested by the analysis, the overall drag for traveling wave walls crucially depends on the configuration of the nose and tail of the finite body. Hence, we are not yet in the position to provide a sufficiently precise estimate of the overall drag (or thrust). However, some rough analysis can be provided and is necessary to guide our future investigation of a finite body. Note that this approximation can only be made for a body of finite length with zero thickness. The central streamline in the wake is assumed to be the continuation of the body shape without any distortion, and the wake vortices are identical to those in the mid-region (Figure 45).
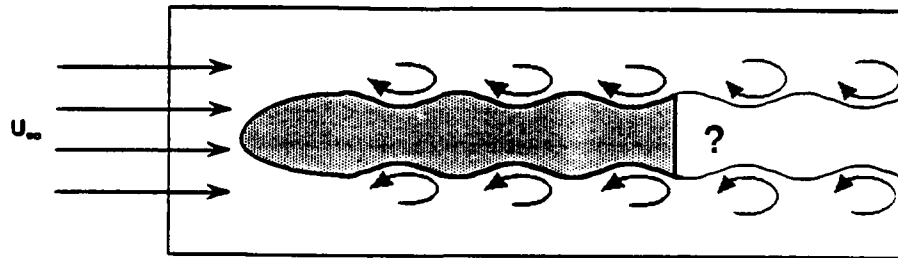
Figure 45.   Approximation of the Wake Form in a Traveling Wave (Rough Estimate)

Kármán's Drag Formulation: The fundamental difference between an ideal infinite traveling wave wall (as is the case of mid-region calculation) and a finite wall is that, in the body-fixed coordinate, vortices will shed off and form a wake for the finite wall; or equivalently, in the wave coordinate system, the leading edge of the wall will continuously move upstream and create new vortices. The rough physical discussion based on Figure 23 (page 39) suggests that if $c < U_\infty$,

then a wake with velocity defect will form, implying a drag. According to that approach a thrust will be possible if $c > U_\infty$, since then the wake will become jet-like. However, that discussion did not explicitly consider a factor, which is of crucial importance for the overall drag, i.e., a shed vortex carries large kinetic energy and can be useful. A typical example is the Kármán vortex-street. The drag formula of Kármán vortex-street (Wu, et al. 1989) is:

$$C_D = 2\,\delta\,(1 - \frac{c}{U_\infty})\left[\frac{\delta}{2\pi}(1 - \frac{c}{U_\infty}) - b\,(1 - \frac{2c}{U_\infty})\right]$$

(54)

where $\delta = 2/\tanh(\pi b)$ and b is the spacing of two rows. The first term approximately reflects the power consumption of creating new vortices and the pressure drop, while the second term is the momentum gain in the wake. Evidently, for proper range of b and c/U_∞ we may have $C_D < 0$. Equation 54 has given quite good estimate for the drag of some bluff bodies; for example, for a circular cylinder, the normalized value of C_D is 0.92 (compared with experimental value 0.93), and for a flat plate normal to the oncoming flow $C_D = 1.6$ (experimental value is 1.7). However, it is not known if this equation is still good enough for $b > 0.281$, which is the case of this study.

Saffman-Schatzman Formulation: While Equation 54 was obtained for point-vortex model, an improved formulation has been derived by Saffman and Schatzman (1982) with finite vortex cores having uniform vorticity inside the core. An estimate based on their formulation is possible by calculating the vortex circulation Γ, core area A, and kinetic energy from numerical data.

According to Saffman and Schatzman the relation between the vortex average kinetic energy and the total drag is

$$D_T = K - \rho\,\frac{\Gamma b}{\lambda}\,(U_\infty - c),$$

(55)

where:

K is the average kinetic energy per unit length over λ;

Γ is the circulation of the vortex; and

b is the spacing of two rows of vortices.

The second term represents the x-momentum increase in the vortices, which produces a thrust component. Subscript T indicates total drag, L or λ indicates the reference length. Thus, for the drag coefficient per unit width we have:

$$C_{D_{TL}} = \frac{D_T}{\frac{1}{2}\rho\, U_\infty^2 L} \quad \text{and} \quad C_{D_{T\lambda}} = \frac{D_T}{\frac{1}{2}\rho\, U_\infty^2 \lambda}$$

(56)

whereby, using Equation 54 (in Equations 56-64, $U_\infty = U$),

$$C_{D_{TL}} = \frac{D_T}{\frac{1}{2}\rho\, U^2 \lambda} = \frac{2K}{\rho\, U^2 \lambda} - 2k\left(1 - \frac{c}{U}\right)\frac{\Gamma}{U\lambda}, \quad k \equiv \frac{b}{\lambda}.$$

(57)

Define dimensionless quantities:

$$\hat{\Gamma} = \frac{\Gamma}{U\lambda} \qquad \hat{K} = \frac{K\lambda}{\rho\Gamma^2} = \frac{K}{\hat{\Gamma}^2 U^2 \lambda \rho}$$

(58)

$$\hat{U}_s = \frac{1}{\hat{\Gamma}}\left(1 - \frac{c}{U}\right),$$

so that Equation 57 reduces to

$$C_{D_{T\lambda}} = 2\hat{\Gamma}^2\left(\hat{K} - k\hat{U}_s\right).$$

(59)

Now, k can be obtained from numerical data. Then there are two ways to estimate $\hat{\Gamma}$, $\hat{K}$ and $\hat{U}_s$:

(1) $\hat{\Gamma}$ is inferred from numerical data, then use known U_∞ - c to get $\hat{U}_s$ and use numerically obtained K, i.e.,

78

$$K = \int_{A_\lambda} \frac{\rho}{2} \left[(u_x - U + c)^2 + u_y{}^2 \right] dA.$$

<div align="right">(60)</div>

(2) Or, $\widehat{\Gamma}$, $\widehat{U}_s$ and $\widehat{K}$ can be inferred from Kármán's theory with finite core correction given by Saffman and Schatzman, as long as k and core area $A(\lambda)$ are known.

Since for the sinusoidal wall profile, the flow has a relatively close analogy with the Kármán street, we expect that the above two approaches will give comparable results for this profile (Table 9a), but the results for the other two wall profiles (the cat's-eye and cycloid) should have agreement within an order of magnitude (Table 9b).

<div align="center">Table 9.   Overall Drag of Two-Side Wavy Walls by
Saffman-Schatzman Formula</div>

<div align="center">Table 9a.</div>

$a/\lambda = 0.2$ $c/U_\infty = 0.414$		Sinusoidal
$C_{D_{T_\lambda}}$	Method 1	−0.204
	Method 2	−0.238

<div align="center">Table 9b.</div>

$a/\lambda = 0.1$ $c/U_\infty = 0.55$		Cat's-eye	Cycloid
$C_{D_{T_\lambda}}$	Method 1	−0.102	-0.196
	Method 2	−0.042	-0.126

* Negative value implies thrust.

It should be noted that since the choice of b is still quite arbitrary in our approach, the specific values in Table 9 may not be important. However, it is important to note that this result reveals the possibility of obtaining very low overall drag or even a thrust by delicately designed tail configuration.

A more realistic estimate of overall drag (or thrust) will be possible only after the numerical calculation of a flow field over a realistic configuration is carried out. We expect that the result will vary strongly with the configuration design.

Comparison with Flat Plate

Generally, one wants to compare the traveling wave wall performance with that of a flat plate. However, such a comparison must be performed very carefully. It would be insufficient to directly compare a segment of one wavelength of a flat plate to the traveling wave wall of one period. Because the frictional drag of a flat plate depends on the local Reynolds number based on the length of the leading edge, the mid-region drag coefficient for the traveling wave wall can achieve $C_{D_{mid-region}} = 0$. Hence, a comparison is only fair for the overall drag of two finite length bodies: a finite flat plate and a body with a traveling wave wall. Moreover, it is well known that even for a thin flat plate, the leading and trailing edge singularities contribute significantly to the total drag (for instance, see Van Dyke, 1975).

Most standard textbooks give the coefficient of friction of a flat plate, C_f, but seldom give $C_{D\ plate}$ because its value depends on the profile in a more complicated fashion. Based on actual measurement on various airfoils, Riegel (1961) deduced the turbulent and laminar flat plate profile drag coefficient C_D which is presented in Figure 46. This value may be used to compare the overall drag of traveling wave wall mid-region considered in this study.

Assume a flat plate of length L, then the profile drag $C_{D\ plate}$ can be expressed as $C_{D\ plate} = a\ (R_{eL})^b$, where a and b are curve fitted to the Riegel C_D value. Thus, let N be the number of waves with wave length λ, spanning entire length of L, and we obtain:

80
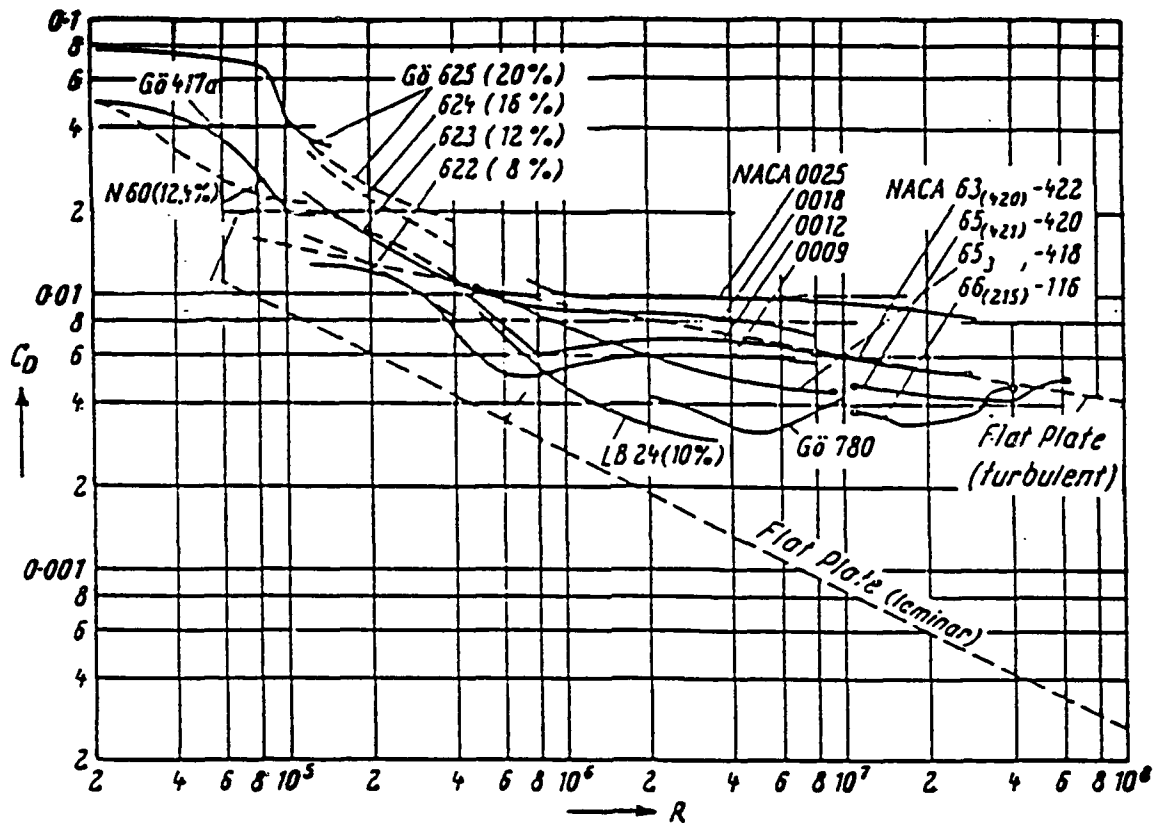
Figure 46. Total Drag Coefficient for a Flat Plate (Riegel, 1961)

$$C_{DT\lambda} \equiv \frac{D_{total}}{\frac{1}{2}\rho\,U^2\,\lambda}\,, \qquad\qquad L = N\lambda$$

(61)

so,

$$C_{DTL} = \frac{C_{DT\lambda}}{N}\,, \quad \text{and}$$

(62)

$$\frac{C_{DTL}}{C_{D\,plate}} = \frac{C_{DT\lambda}}{N a\,(N\,Re_\lambda)^b} = \frac{C_{DT\lambda}}{a N^{1+b}\,N\,Re_\lambda^b}$$

(63)

Note that C_{DTL} is for the mid-region only.

81

Now, let N_{cr} be the critical (required minimum) number of waves which will make the two overall drags equal, thus:

$$N_{cr} = \left(\frac{C_{DT\lambda}}{a\,Re_\lambda^b}\right)^{\frac{1}{1+b}}$$

(64)

The relationship of N_{cr} versus $C_{DT\lambda}$ with Re_λ as a parameter (Equation 64) is plotted in Figure 47 for the known relationship of a turbulent flat plate; that is, a = 0.1120 and b = -0.1816.

The variation of $C_{DTL}/C_{D\,plate}$ versus $C_{DT\lambda}$ for several N waves (Equation 63) is presented in Figure 48. Each curve in this Figure is obtained for a given value of Re_λ ($Re_\lambda = 5.5 \times 10^4$). For instance, in the cat's eye case, the $C_{DT\lambda}$ value is about 0.2 - 0.3, for N = 50 waves and the overall drag of such a traveling wave body would be 50% - 78% of the flat plate. If the the number of waves is increased to N = 100, then the overall drag would be 35% - 45% of the flat plate. As it can be seen from Figure 48, the larger the number of waves, the further reduction of drag would be expected, providing the vortex stability is maintained.
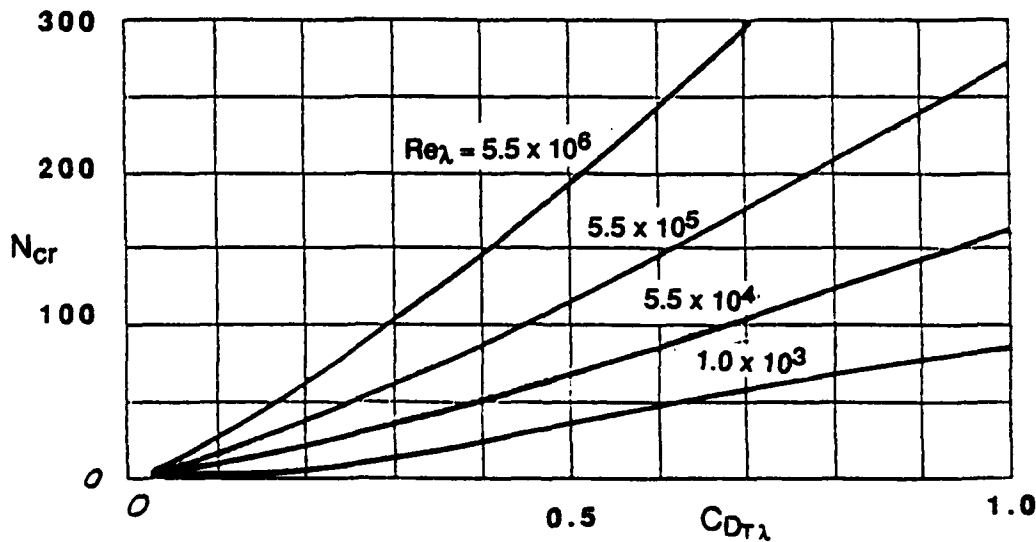
Figure 47. Critical Number of Waves Versus $C_{DT\lambda}$ for Various Re_λ
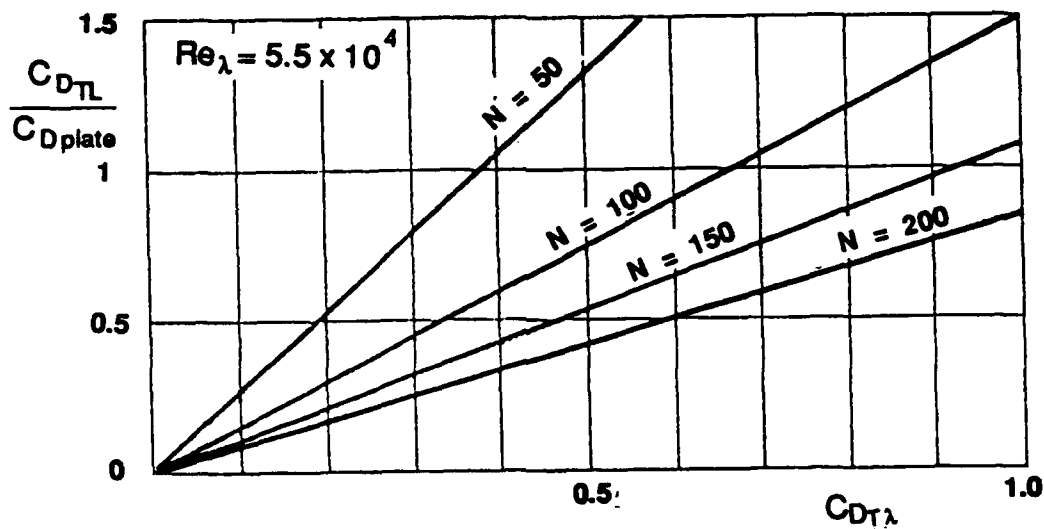
Figure 48.   The Ratio of Total Mid-region Drag for Traveling Wave to
a Flat Plate for Various N

ROLLER BEARING APPROACH

A simplified hydrodynamic energy calculation is provided here. The calculation
is based on the assumption that a vortex can be simulated by a roller bearing.
Each vortex (roller) has the length ℓ and radius r, rotating at angular velocity, ω
in the wave cavity (Figure 49). The wave phase velocity c is assumed to be half
of the freestream velocity, thus:

$$c/U_\infty = 0.5, \quad c=r\omega \quad \text{and} \quad U_\infty=2r\omega. \tag{65}$$
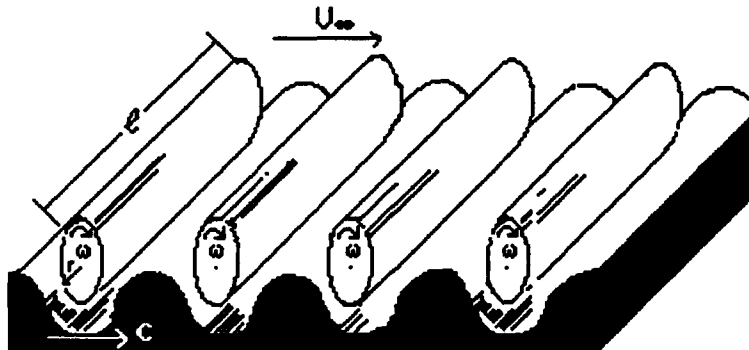
Figure 49. The Vortices are Simulated by a Roller Bearings

83

The total energy to maintain this system of vortices in a traveling wave manner can be divided in three parts:

1. The rate of viscous energy expenditure E_V to maintain the entire vortex system.

2. The rate of translational kinetic energy in the the fluid within the formed vortices E_t.

3. The rate of rotational kinetic energy contained in the vortex system E_r.

A brief derivation of these three energy components is presented below.

Power Due to Viscous Dissipation

We assume that the vortex is a closed loop (a roller) and the wall is part of the streamline that confines the vortex. The moment of the viscous force, M, applied on the boundary of this closed loop vortex can be obtained as the following (Figure 50):
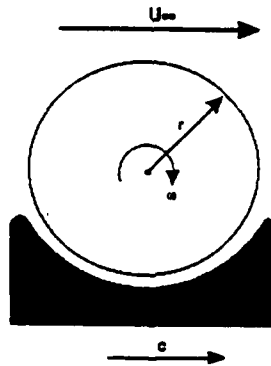
Figure 50. Schematic of a Single Vortex in the Wave Trough

The viscous shear force that acts on the entire surface A is

$$F = \tau.A, \tag{66}$$

the shear stress τ is defined as:

84

$$\tau = \mu \left(\frac{du}{dy}\right) = \mu\, U_\infty/r \tag{67}$$

$$F = \tau.2\pi r \ell, \tag{68}$$

where μ is the viscosity. In terms of angular velocity ω, we can write

$$\tau = 2\mu\omega, \tag{69}$$

thus:

$$F = (2\mu\omega)(2\pi r \ell) = 4\pi r \omega\, \mu\ell \tag{70}$$

and the moment of the viscous forces is

$$M = F.r \tag{71}$$

So:

$$M = 4\pi r^2 \omega\, \mu\ell \tag{72}$$

Taking into account that the specific number of waves $n = L/\lambda$ is added simultaneously on the flow surface of length L and width ℓ, thus, the rate of energy dissipation due to viscous losses of the vortex system in the secondary flow along the entire surface with a traveling wave is:

$$E = nM\omega = 4\pi r^2 \omega^2 \mu\ell\, L/\lambda \tag{73}$$

Power Due to Vortex Translational Motion

The kinetic energy of forward motion of the fluid included in the formed vortices is obtained by subtracting the effect of kinetic energy that is imparted to the fluid by the wall:

85

$$E'_t = (1/2 \; mv^2) = 1/2 \; \rho\pi r^2 \ell \; (U_\infty - c)^2$$

$$= 1/2 \; \rho\ell\pi r2 \; \frac{U_\infty^2}{4} = \rho\pi r^2\ell U_\infty^2/8 \tag{74}$$

The rate of energy per unit time required for the vortex translational motion can be found by multiplying this energy by number of vortices whose centers are moving along the surface at velocity $U_\infty/2$,

$$\frac{dn}{dt} = U_\infty/2\lambda \tag{75}$$

thus:

$$E_t = n \; E'_t = \rho \; \pi r^2\ell U_\infty^3/16\lambda \tag{76}$$

Power Due to Vortex Rotational Motion

The kinetic energy contained in the vortex system due to its rotation at a rate of $\omega = U_\infty/2r$ can be found using the moment of inertia of a circular cross-section of radius r or a simplified inviscid theory for a row of moving vortices (Donaldson, 1989).

The moment of inertia J_0 of a circular cross section about the fixed axis through the origin 0 is:

$$J_0 = \frac{1}{2}\pi r^2 \tag{77}$$

and the rotational kinetic energy is

$$T = \frac{1}{2}J_0\omega^2 = \frac{1}{2}\left(\frac{1}{2}\pi r^4\right)\omega^2 \tag{78}$$

In this case considering the length ℓ and the density ρ of the roller we have:

86

$$T = \frac{1}{2} \rho \ell \left(\frac{1}{2} \pi r^4 \right) \omega^2 \tag{79}$$

The time rate of this rotational energy can be obtained by

$$E_r = T \frac{dn}{dt} = \frac{1}{2} \rho \ell \left(\frac{1}{2} \pi r^4 \right) \omega^2 \left(\frac{U_\infty}{2\lambda} \right) \tag{80}$$

Since $2r\omega = U_\infty$ we have:

$$E_r = \rho \pi r^2 \ell U_\infty^3 / 32\lambda \tag{81}$$

Total Hydrodynamic Energy Rate

By adding the three components of energy rate we can estimate the total hydrodynamic power expenditure for a system of vortices in a traveling wave.

$$E = Ev + Et + Er \tag{82}$$

$$\frac{4\pi \upsilon \rho \omega^2 r_2^2 \ell L}{\lambda} + \frac{2\pi r^2 \rho \ell U_\infty^3}{32\lambda} + \frac{\pi r^2 \rho \ell U_\infty^3}{32\lambda} \tag{83}$$

$$\frac{\pi \rho r^2}{\lambda} \left[4\upsilon\omega^2 \ell L + \frac{3U_\infty^3 \ell}{32} \right] \tag{84}$$

$$R_e = \frac{U_\infty L}{\upsilon} \tag{85}$$

then

$$E = \frac{\pi \rho L \ell U_\infty^2 \upsilon}{\lambda} \left[1 + \frac{3}{32} \left(\frac{r}{L} \right)^2 R_e \right] \tag{86}$$

87

In order to provide a meaningful estimate of this power, a comparison with energy consumption per unit time in a turbulent boundary layer over a flat plate is presented.

$$E_{T.P.} = 0.036 \, L \ell \rho U_\infty^3 \left(R_e\right)^{-\frac{1}{5}} \tag{87}$$

$$\frac{E}{E_{T.P}} = \left(\frac{\pi \rho L \ell U^2 \upsilon}{\lambda} \left[1 + \frac{3}{32}\left(\frac{r}{L}\right)^2 R_e \right] \right) \bigg/ \left(0.036 \, L \ell r U^3 \left[R_e\right]^{-\frac{1}{5}} \right) \tag{88}$$

$$= 87.26 \frac{L}{\lambda} R_e \frac{R_e^{\frac{1}{5}}}{R_e} \left[1 + \frac{3}{32}\left(\frac{r}{L}\right)^2 R_e \right]$$

$$= 87.26 \frac{L}{\lambda} R_e^{\frac{1}{5}} \left[R_e^{-1} + \frac{3}{32}\left(\frac{r}{L}\right)^2 \right] \tag{89}$$

and for high Reynolds number $R_e^{-1} \sim 0$, thus:

$$\frac{E}{E_{T.P}} = 8.18 \frac{r^2}{\lambda L} R_e^{\frac{1}{5}}$$
$$\tag{90}$$

for a typical value of $r/\lambda = 0.25$ and $L/r = 400$ and $Re = 10^7$ the energy ratio is:

$$\frac{E}{E_{T.P}} = 0.128 \tag{91}$$

That means the power expenditure of a traveling wave can be expected to be about one-eighth of the turbulent energy expenditure on a flat plate.

This derivation is similar to Savchenko's (1979) derivation; however, in his derivation, the turbulent energy consumption was taken to be in the order of $(Re)^{-\frac{1}{7}}$ rather than $(Re)^{-\frac{1}{5}}$.

NUMERICAL (SPECTRAL) APPROACHES

A preliminary hydrodynamic energy calculation was performed numerically using spectral code. The components of energy in x and y were calculated first. The x component of the energy includes the x component of wall pressure force plus the frictional force (wall stress). The y component of energy is obtained from the y component of pressure force. In order to calculate the energy rate, the forces were multiplied by pertinent velocities, integrated over the wave length and then were summed to provide the total energy rate. The resultant energy was compared to a reference flat plate moving with the same freestream velocity U_∞. A list of simplified formulation is as follows:

$$E_x = \int_0^\lambda F_x (U_\infty - c)\, dx \tag{92}$$

$$E_y = \int_0^\lambda F_y\, v(x)\, dx \tag{93}$$

$$E_t = E_x + E_y \tag{94}$$

$$E_R = \int_0^\lambda \tau_{fp} U_\infty\, dx \tag{95}$$

where τ_{fp} is the shear stress of a flat plate at the wall.

Figure 51 presents the results of this computation for energy calculation. After initial fluctuations due to the vortex formation, the components of the energy approach their steady state values. The result of a sinusoidal wall profile with $a/\lambda = 0.1$ showed that the total energy is almost 28 percent of a flat plate (Er) at a computational time of 60 seconds and still decreasing as the time passes. The results of c/U_∞ equal to 0.5, 0.6 and 0.7 for longer computational times (up to 350) are very encouraging and are provided in Figure 52. These values are normalized with respect to a reference energy (energy consumption over flat plate at the same condition). This normalization always makes the reference value equal to unity. Thus, any value below 1 represents energy gain for the

traveling wave surface. As can be seen, substantial energy gain is associated for c/U_∞ of 0.6. The energetics for $c/U_\infty = 0.7$ indicates over 90 percent saving of energy with respect to a flat plate at a computational time of 350 and indicates "thrust" for longer computational time. It is important to keep in mind that this is just the total hydrodynamic energy and that the energy required to move the wall is yet to be considered.
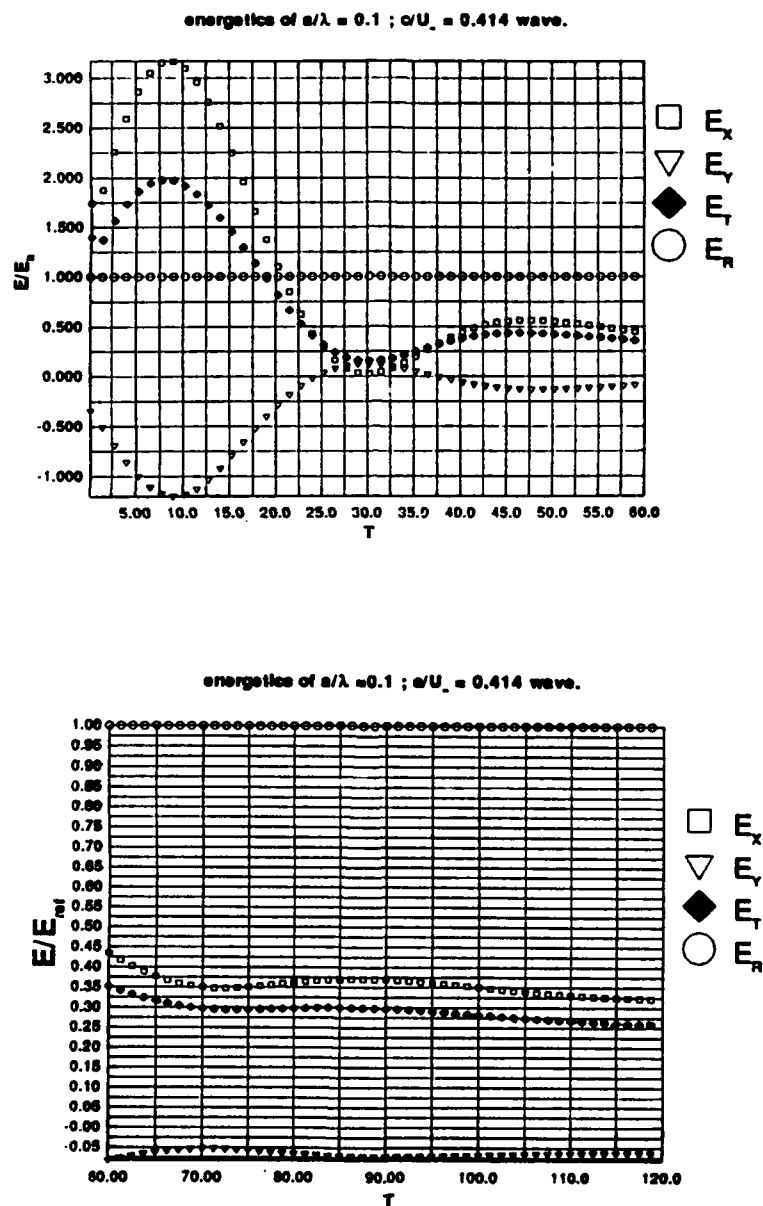
Figure 51.   Flow Energetics for a Sinusoidal Wall Profile Over One Wave Cavity for $a/\lambda = 0.1$ and $c/U_\infty = 0.4$ Versus Time, Using Spectral Code

90
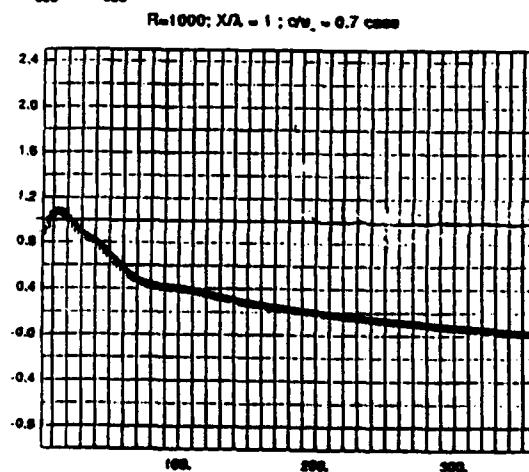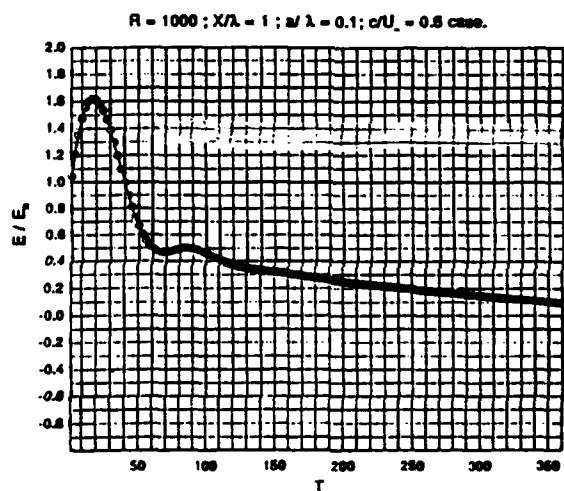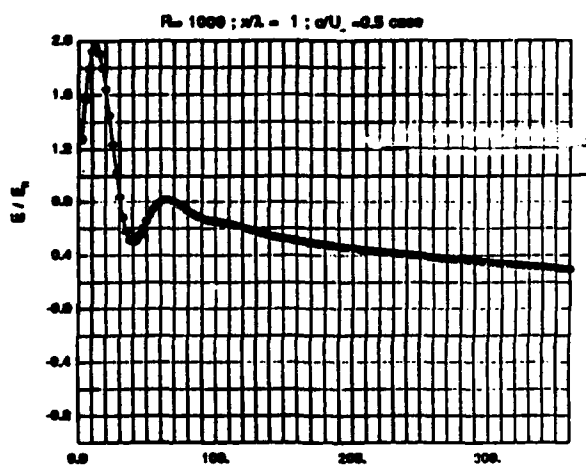
Figure 52. Flow Energetics for a Sinusoidal Wall Profile Over One Wave Cavity for $a/\lambda = 0.1$ and c/U_∞ of 0.5, 0.6 and 0.7

91

VI. ACTIVE WALL TECHNOLOGY

PROPOSED EXPERIMENTAL INVESTIGATION

Background

Following extensive analytical studies of traveling wave behavior, the need to perform an experimental proof-of-concept validation has been identified. The principal experimental objectives are to demonstrate the concept of controlled vortical flow using an active wall device and to obtain an estimate of the associated drag reduction.

In addition to fulfilling the primary objectives stated above, it is hoped that the experimental data will permit a preliminary assessment of the feasibility of utilizing a traveling wave device on an underwater vehicle. The trade-off between the energy required for wall activation and the energy gained through drag reduction is a critical factor. The net energy gain must be significant to justify further investigation of the controlled surface as a practical means of drag reduction for underwater vehicles. In addition, significant drag reduction must be achievable over relatively wide parameter ranges (a/λ, c/U_∞). Alternatively, if the useful parameter ranges are sufficiently "forgiving," implementation of the controlled wall concept could be simplified from a practical engineering standpoint. Implementation in a totally passive mode (wall activation energy derived from the flow) may be envisaged, particularly for vehicles operating at specific depths or speeds.

Soviet researchers have noted that the practical implementation of a coating "containing a device to generate traveling waves is fraught with great difficulties" (Savchenko, 1979). Hence, the mechanism of traveling wave generation in an auto-oscillatory (passive) mode during flow over an elastic shell is of considerable interest. Merkulov (1970) notes that "if the parameters of the elastic plate are so selected that waves with [appropriate phase velocities and wave numbers] can appear on it, we can expect an energy exchange between the fluid and plate, generation of a traveling wave and the forming of secondary flow which, as we conceive it, is capable of reducing hydrodynamic

resistance." In order to implement an auto-oscillatory system, it is important to determine the flow conditions under which a traveling wave with the requisite parameters will propagate in a "self-oscillating regime" (Merkulov, 1970).

Clearly, there are many technological and operational issues to be addressed before the traveling wave concept can be deemed suitable for submarine trials. However, the proposed experimental investigation using an active wall test device in a towing tank is intended to resolve some of the fundamental scientific questions arising from the theoretical study of the traveling wave. The experimental program will allow us to gain some insight into the energy expenditure required to obtain a drag reduction. It must be emphasized that a true energy evaluation, for a system capable of being used at sea, must await the actual development of such a system. The energy budget of this system must then be evaluated under real world operational conditions, which will probably be substantially different from those of the experiment.

Experimental Objectives

The principal objectives of the proposed experimental investigation of traveling wave behavior are as follows:

- To demonstrate vortex entrapment in the troughs of a traveling wave using flow visualization techniques. Both laminar and turbulent starting conditions are to be investigated.
- To determine the effect of flow along a traveling wave wall on overall drag.
- To determine the combinations of wall and flow parameters giving drag reduction. Experimental data will be compared with CFD predictions.
- To assess the trade-off between the energy required for wall activation and the reduction in propulsion energy achieved through drag reduction.

The energy trade-off will be a strong function of the system engineered to activate the wall which will probably be substantially different between

93

experiment and operational implementation. One must be very careful about drawing conclusions based on tests of systems not suitable for at-sea use.

The wall, fluid, and flow parameters likely to influence traveling wave behavior are given in Table 10. The present discussion of active wall systems will focus on the wall parameters required for proof-of-concept experiments. Appropriate parameter values (see below) have been identified on the basis of CFD data and likely values of freestream velocity, Reynolds number (based on wavelength), and wavelength for proposed practical traveling wave applications. The effects of surface roughness will not be addressed in any detail.

Table 10. Experimental Parameters

WALL	FLUID[1]	FLOW
• wavespeed[2], c	• kinematic viscosity, ν	• freestream velocity, U_∞
• wavelength[2], λ	• temperature, T	• turbulence level
• frequency[2], f	• density, ρ	• circulation, Γ
• amplitude, a	• salinity	• pressure, P
• wave profile	• pH	
(sinusoidal, cat's eye, etc.)	• non-Newtonian	
• two or three	additives	
dimensional		
• surface roughness, k_s		

Requirements

Practical demonstration of a controlled vortical flow regime will involve the design and fabrication of some kind of flexible wall device. A traveling wave with specified and controllable phase velocity, amplitude, wavelength and

---

[1] Not all fluid parameters are independent, e.g. both viscosity and density are temperature dependent.

[2] Wavespeed, wavelength and frequency are related, i.e., $c = \lambda f$. Thus, only two of these three parameters can be selected as independent variables.

94

shape will be used to generate and trap vortices in the troughs of a flexible wall. As shown in Figure 53, three main types of flexible wall can be identified. The principal distinction between the three categories is the degree of control afforded the experimenter in determining traveling wave parameters. (See Mattout, 1976, for a more detailed discussion of flexible wall types.)

Compliant walls are passive systems which derive energy from the flow in order to deform. The deformation of a compliant surface is controlled by the flow parameters, the structural configuration of the wall, and the properties of the wall materials. In a critical analysis of compliant wall data, Bushnell and co-workers (Bushnell, Hefner and Ash, 1977), have noted that before any theoretical approach to the question of drag reduction can be validated, "extensive wall motion measurements must be made." For this reason compliant surfaces are not attractive candidates for the proposed traveling wave experiment. Very extensive instrumentation of the flexible surface would be necessary to determine precise values of oscillation amplitude, wavelength, frequency and wavespeed. In addition, for a given flow condition, no parameter optimization is possible using a single flexible wall device. Optimization could only be achieved by constructing a series of compliant wall devices using different materials and/or structural concepts. However, once the range of optimum parameters are identified, it is entirely possible that a compliant wall with controllable mechanical properties may have practical application.

Active walls derive their energy for deformation from an external source, such as mechanical or electrical input. In auto-oscillatory or floating systems, oscillations are injected into the flexible wall in a continuous manner, thereby defining oscillation amplitude, wavelength, and instantaneous frequency. In addition, the flexible wall interacts with the flow in the same way as a compliant surface. Hence, the resulting wall motion is determined by a combination of active and passive effects, and extensive instrumentation would again be required to determine precise values of wave parameters. These parameters could readily be varied by changing the injected oscillation parameters, but the resultant changes in overall wall behavior would not be easily predictable.
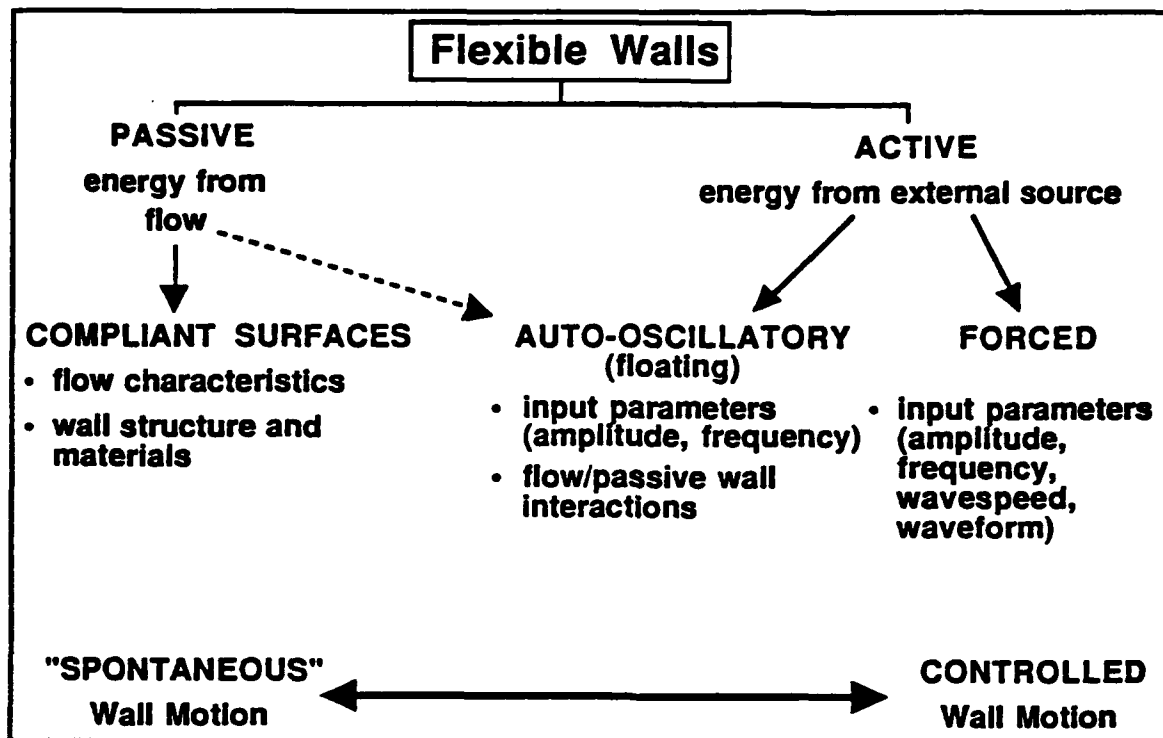
Figure 53. Types of Flexible Wall

In forced active wall devices, the wave parameters can be fully controlled by the experimenter. One of the major design goals for an active wall test plate to investigate traveling wave behavior is that the wave amplitude, together with two of the three related parameters (wavelength, wavespeed and frequency), should be independently controllable. The potential to investigate various waveforms would be an added advantage. Hence, a fully-controlled forced active wall device is deemed necessary for the proposed proof-of-concept experiments. An operational device designed to function at fixed, predetermined parameter values might use a lower-cost auto-oscillatory system.

Active Wall Test Plate

CFD studies of traveling wave behavior have shown that the amplitude-to-wavelength ratio, a/λ, and the ratio of wave velocity to freestream velocity, c/U_∞, are critical parameters influencing vortex entrapment and establishment of a

96

controlled vortical flow. Parameter ranges to be investigated in the proof-of-concept experiment are:

$$0.10 \leq \frac{a}{\lambda} \leq 0.25 \tag{96}$$

$$\frac{c}{U_\infty} \approx 0.5 \tag{97}$$

Target ranges for active wall parameters have been defined on the basis of the above values, together with information on wavelength, freestream velocity, and Reynolds number (based on wavelength) for practical applications. The need to reduce complexity and minimize costs has also been taken into account.

Wavelengths should be in the range

$$\lambda = 5 - 20 \text{ cm} \tag{98}$$

The active plate length, L, should be in the range

$$L \sim 0.5 - 2 \text{ m} \tag{99}$$

such that the active length incorporates at least 10 wavelengths, i.e., $L \geq 10 \lambda$.

Amplitudes of oscillation should be in the range

$$a = 0.5 - 5 \text{ cm} \tag{100}$$

such that Equation (96) is satisfied.

Values of frequency, f, and wave speed, c, should be within the ranges specified below:

$$f = 10 - 100 \text{ Hz} \tag{101}$$

97

$$c = 2 - 5 \text{ m/s} \hspace{4cm} (102)$$

Requirements for an active wall test plate have been summarized in a "specification" document, which has formed a basis for discussions with various organizations interested in the design and construction of an active wall device (see Appendix C).

EXISTING ACTIVE WALL DEVICES

General Remarks

A number of active wall devices have been reported in the literature over the last 20 years. The relevant articles have been reviewed in some detail in order to avoid unnecessary duplication of existing results and to benefit from the experience of previous researchers. A number of important experimental parameters from the different investigations are summarized in Table 11. In addition to information on traveling wave and flow parameters, data relating to the design of active wall devices are included, notably:

- type of actuator system
- wall dimensions
- two-dimensional (2-D) or three-dimensional (3-D) system
- total number of wavelengths
- number of actuator elements per wavelength.

In the ensuing discussion, the active wall systems have been grouped according to the type of actuator employed (mechanical, electromagnetic, etc.). The choice of actuator is critical in determining traveling wave parameters, notably amplitude and frequency. The majority of devices discussed in the literature are mechanically-driven systems. These devices utilize a series of cams positioned on a camshaft with a successive phase difference between adjacent cams. These systems are generally fixed amplitude and wavelength devices, although frequency and wavespeed can be varied by altering the speed of rotation of the camshaft.

Table 11. Characteristics of Active Wall Devices

REFERENCE	ACTUATOR SYSTEM	DIMENSIONS	# OF WAVELENGTHS	ACTUATOR ELEMENTS/λ	TEST MEDIUM	a (cm)	λ (cm)	a/λ	f (Hz)	c (cm/s)	R_λ	U_∞ (cm/s)	c/U_∞	COMMENTS
Kendall 1970	mechanical	60 cm wide, 120 cm active length, 2-D	12	4	air	~0.3	10	0.03	3-30	30-300	$10^4 - 10^5$	≤1600	-0.5 to +0.80	Sinusoidal waveform. Comprehensively documented study, referenced by later investigators.
Merkulov & Savchenko 1970 Savchenko 1979	mechanical	0.8 x 0.4 m, 2-D	4	?	water	2.25	11	0.2	?	?	$2 - 5 \times 10^4$	?	0.33	Details of device obscure. Vortex entrapment observed.
Taneda & Tomonari 1974	mechanical	2.3 x 1.0 m, 2-D	~2	8	air	≤5	120	≤0.04	0.13 - 3.75	15 - 450	$~0.5 \times 10^5$	0 - 2000	0 - 2.5	Vortex entrapment for $c/U_\infty < 1$
	mechanical	20 x 10 cm, 2-D	2	4	water	≤1.5	8	≤0.19	0.01 - 0.5	0.1 - 4	$~0.5 \times 10^3$	0 - 2	0.2 to ∞	Vortex entrapment for $c/U_\infty < 1$
Matoui 1976	mechanical	? 2-D	?	?	water	0.1 and 0.2	4.2 to 50	0.002 to 0.024	0 to 70	≤3500	$~10^5$	150 to 500	-2 to +10	Measured drag reduction and thrust. No flow visualization data.
Ilgamov & Taldykin 1975, 1978	pneumatic	72 cm long, 12 cm diameter, 3-D	6	6	water	≤0.6	12	≤0.05	0-5	≤60	?	?	?	Measurements of thrust
Park, Silvus & Cerwin 1985	piezoelectric	51 mm wide, 40 mm active length, 2-D	4	8	(water)	~0.001	≥1	0.0001	10 to 150	10 to 150	-	-	-	Various waveforms possible. Device never tested due to lack of resources.
Alberty & Jacquet 1970	electromagnetic	-	8	2	water	-	-	-	-	-	-	-	-	Electromagnetic Dermadrive device not built (limited resources).
	mechanical	3-D, dimensions not given	?	?	water	?	?	?	<50	?	?	9-27	?	Inadequately documented. Observed drag reduction/thrust.
Kim, Alonh & Bondarenko 1972	electromagnetic (ferrofluid)	?	?	?	water	?	?	?	?	?	?	?	?	Invention has shipbuilding applications.

99

In general, 2-D active wall devices (i.e., plates) have been used to investigate traveling wave behavior, though Soviet researchers (Ilgamov and Taldykin, 1975; Ilgamov, Suleimanova, Taldykin, and Fedyaev 1978) describe a 3-D pneumatically-driven system (axisymmetric body of revolution). On the basis of the available reports, it is not possible to reach any definitive conclusions regarding the relative merits of 2-D and 3-D systems. It has been postulated that drag measurements may be easier using a towed 3-D device, whereas investigation of ranges of wall and flow parameters and flow visualization experiments may be more readily performed using 2-D test plates.

The number of actuator elements per wavelength is important in determining the wave profile. Since the cost of any traveling wave device increases with the total number of actuators used, it is desirable to select the minimum number of driving elements to achieve the required waveform. Eight actuators per wavelength are generally believed to be necessary to achieve a satisfactory sine wave profile. Nevertheless, it will be seen from Table 11 that a number of researchers have used only four or six actuators per wavelength. Kendall (1970) and Taneda and Tomonari (1974) obtained valuable experimental data (see below) using only four driving elements per wavelength.

Most of the active wall devices described in the literature were designed for amplitude-to-wavelength ratios, a/λ, significantly lower than the desired range identified in the present CFD studies, i.e., $0.10 \le a/\lambda \le 0.25$. However, two experiments (Taneda and Tomonari, 1974, and Savchenko, 1979) have been reported with $a/\lambda \sim 0.2$, and in both cases vortex entrapment in the troughs of the wave train was demonstrated.

Unfortunately, most investigators who claim to have measured a reduction in drag (or even a thrust force) using an active wall device have not documented their experiments in sufficient detail for parameter ranges to be identified unambiguously. However, Mattout (1976) identified three a/λ ranges where drag reduction occurs (see below). Reynolds numbers (R_λ) were typically $\sim 10^5$ - 10^6, but a/λ and c/U_∞ ranges were generally outside the ranges of interest for the present study.

Mechanical Systems

Kendall (1970): One of the first traveling wave devices reported in the technical literature was constructed at the Jet Propulsion Laboratory, Pasadena, CA. The experimental study of the interaction of a turbulent boundary layer with a wavy wall was motivated by an interest in the generation of water waves by wind. Experiments were performed in a low turbulence wind tunnel in the speed range U_∞ = 0-16 m/s. Wall surface pressure, streamwise velocity, and shear stress at the wall were measured, but no flow visualization studies were performed. The details (and problems) of Kendall's traveling wave device are well documented. Kendall's work has been extensively referenced by other researchers investigating active wall systems.

The surface of Kendall's wavy wall was composed of 1/4 inch (0.6 cm) thick neoprene rubber sheet with a surface smoothness comparable to writing paper. The rubber sheet comprised the last 4 feet (~ 1.2 m) of the floor of the test section, and was supported from below by 49 ribs spaced at 1 inch (2.5 cm) intervals in the streamwise direction. Each rib extended the full width of the test section. Below each rib was a circular cam of 1/8 inch (0.3 cm) eccentricity. Each cam was positioned on a common camshaft extending the length of the wall and driven by a variable speed motor. The phase difference between adjacent cams was 90°. The traveling wave parameters obtained using this mechanical device are summarized in Table 11.

The ribs were attached to the rubber sheet by a small filet of rubber adhesive forming a compliant fixture. The interval of arc length along the rubber was set equal to 1.02 inch to avoid a net stretching of the rubber. Despite this precaution, a distortion component in the wave profile was observed near the conclusion of the experiment. This component had a wavelength equal to the rib spacing (1 inch, 2.5 cm) and a maximum amplitude of ~ 0.003 inch (0.08 mm). Clearly, any future traveling wave device of this type designed for long-term operation must use a fatigue-resistant flexible skin material to avoid distortion of the waveform by the higher harmonic components.

Kendall also addressed the question of the length of wavy wall required to attain equilibrium behavior. An attempt was made to assess the distance

equilibrium after the abrupt onset of surface waviness. The 4-foot long flexible wall was preceded by a 5-foot smooth wood section, at the leading edge of which was a boundary-layer trip for the purpose of fixing the site of transition. Some difficulties were experienced in interpreting pressure and drag coefficient data due to the scatter of experimental points. However, it was concluded that at least over the latter half of the wall, the pressure values depended only upon local conditions and not on the history of the boundary condition; i.e., approximately 6 wavelengths were required to attain equilibrium. From these and other data, e.g., Taneda and Tomonari (1974), it would appear that the number of wavelengths necessary for equilibrium depends upon various conditions, including wall and flow parameters and the abruptness of the onset of surface waviness. The target value of at least ten wavelengths for a traveling wave test plate has been selected as a reasonable compromise between cost and technical requirements.

Merkulov and Savchenko (1970): An experimental investigation of fluid flow along a traveling wave has been reported by researchers from the Institute of Hydromechanics in Kiev. A mechanically-driven active wall device using a series of rotating cylinders under a smooth fairing is described by Merkulov and Savchenko (1970). Emphasis is placed upon modeling a traveling wave "in a translational system of coordinates." Unfortunately, it is not possible to obtain the wave parameters from the data provided or to understand the wave-generating mechanism in any detail. However, a later review by Savchenko (1979) references the earlier experimental investigation and provides some parameter values (Table 11). The details of the active wall device remain obscure.

As noted earlier, a/λ is approximately 0.2; i.e., within the range of interest identified in the present study. Vortex entrapment was demonstrated (see Figure 54), although it is unclear from the photographs provided whether or not vortices were observed in all four wave troughs; the distance required to attain an equilibrium flow condition is not determined. The experiments apparently demonstrated that the value of c/U_∞ is critical in obtaining stable periodic flow; a value of 0.33 is identified as the lower bound of the optimal range. The results of drag coefficient measurements have already been discussed (Chapter I).
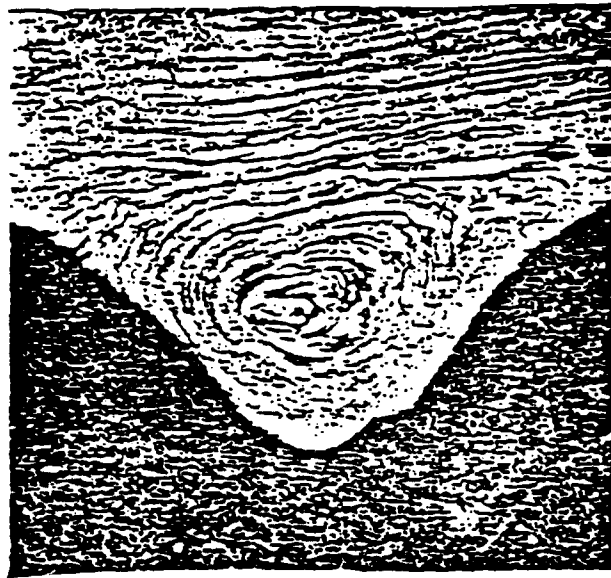
Figure 54.   Vortex Entrapment in Trough of Traveling Wave
              (Savchenko, 1979)

Taneda and Tomonari (1974): "Wave machines" similar to the one developed by Kendall (1970) were constructed by researchers at Kyushu University in Japan to investigate the "effect of swimming motion on the boundary layer" in wind tunnel and water tank tests. Important experimental parameters are summarized in Table 11. Although the traveling wave motion was generated by a mechanical system similar to Kendall's, it is important to note that the transition to a wavy wall was continuous (see Figure 55), rather than abrupt as in the Kendall experiment.
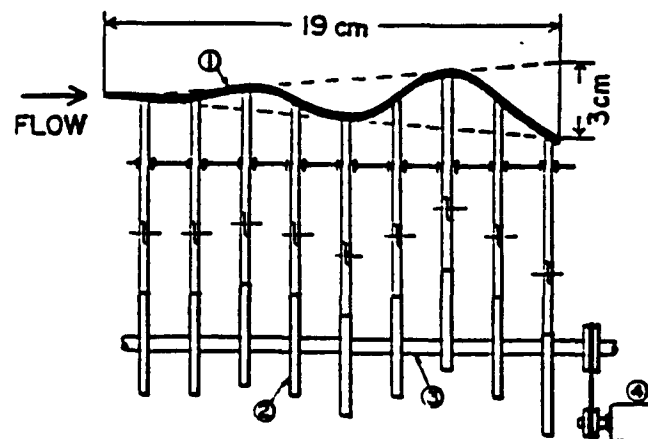
Figure 55. Wave Machine Used in Water Tank (Taneda and Tomonari, 1974)
            (1=rubber, 2=cam, 3=camshaft, 4=motor)

103

In the water tunnel experiment, Taneda and Tomonari were able to demonstrate vortex entrapment "at each (wave) trough" for $c/U_\infty = 0.23$ (see Figure 2, page 6), suggesting that with a suitable combination of parameters and boundary conditions, equilibrium controlled vortical flow can be established without the need for a long transition region. This result is clearly of importance for the design of an active wall test device. No data on "edge effects" or on the location of the wavy wall in the wind/water tunnel are provided.

Mattout (1976): A series of experiments has been performed at the TH2 SOGREAH hydrodynamic tunnel in Grenoble, France to assess the possibility of reducing drag using flexible walls. A mechanically-activated system was used to generate a 2-D wave system transverse to the flow. The active wall device was integrated into one wall of the test section, and was placed on a wall balance with fluid bearings (Bertin and Cie 70-Ab-04 balance). A sketch of the model is shown in Figure 56 (de Loof, 1974). A membrane is stretched on a hollow box containing the activating mechanism, which is very similar to that used by Kendall (1970). A series of transverse bars, each attached via a push-rod to a cam and common camshaft, are in contact with the inner surface of the membrane.
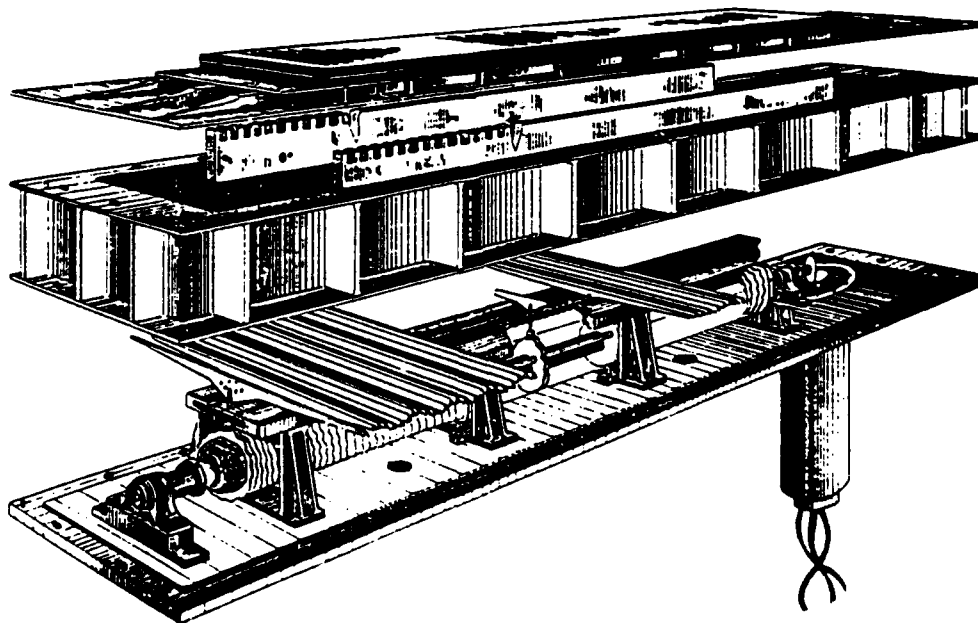
Figure 56. Active Wall Device (Mattout, 1976; de Loof, 1974)

It is noted that the parameter ranges achievable with the model are narrower than those identified as desirable in theoretical studies. The parameter ranges investigated in the experiment are given in Table 11. Inspection of these values suggests that the reported variations in a/λ were obtained by selecting discrete values of wave amplitude (0.1 or 0.2 cm) and continuously varying wavelength over the specified range. This is somewhat surprising, since other mechanically-driven active wall devices described in the literature are fixed wavelength systems. Recent designs (see Mechanical Actuators) can incorporate an option to change wavelength, but this is generally a time-consuming process involving manual repositioning of the cams on the camshaft. In contrast, methods have been devised to change wave amplitude both quickly and easily.

Drag reduction on the order of 25 percent was measured for various parameter combinations, and a "special propulsion effect" (i.e., thrust) was observed for very small a/λ values (.02 to 0.004 as reported by Mattout). It is concluded that more accurate definition of favorable parameter ranges is desirable, particularly in conjunction with flow visualization experiments to illustrate the associated flow behavior in the turbulent boundary layer. There is also a need to assess the trade-off between the energy required for wall activation and the energy gained by drag reduction.

Pneumatic Systems

Reports from the Kazan Technical Physics Institute, USSR describe a pneumatically-activated, wave-generator model used to determine the propulsion generated by the model in water (Taldykin and Ilgamov, 1975; Ilgamov, Suleimanova, Taldykin and Fedyaev, 1978). Reference is made to the investigations by Kendall (1970) and Taneda and Tomonari (1974), and it is noted that in these flat plate experiments it is not possible to measure the force exerted on the plate; hence, the requirement for a 3-D device in an experiment designed to measure thrust.

The wave-generator model used by Taldykin and Ilgamov is an elongated cylindrical body tapering at both ends. Wave parameter data are summarized in Table 11. A cross-section through part of the body is illustrated in Figure 57.

105

The traveling wave motion on the surface of the body is generated by inflating and deflating the toroidal rubber shells using compressed air; i.e., the device is activated pneumatically. There are six toroidal rubber shells (actuators) per wavelength. Sequential inflation/deflation of these shells is achieved by the use of a six-cylinder compressor in which the pistons perform harmonic oscillations with 60° phase shift. The wave amplitude can be varied by modifying the air flow. In addition, amplitude was found to decrease with increasing submergence depth due to hydrostatic pressure effects, and was influenced by frequency effects (see below). Thus, it was necessary to determine the wave amplitude photographically for any given combination of experimental parameters.
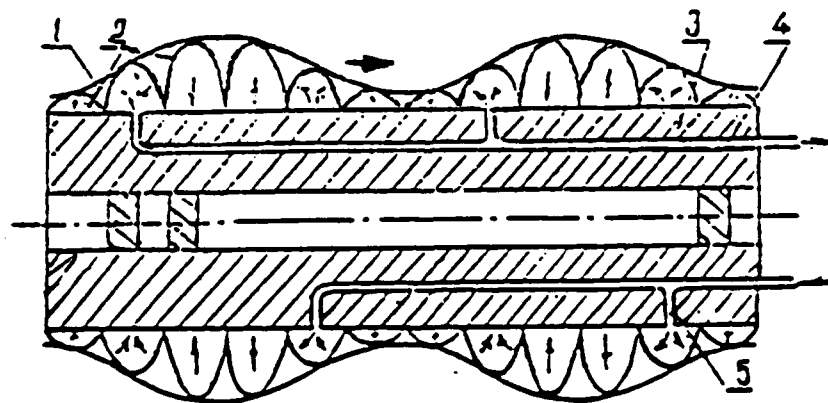
Figure 57. Wave-Generator Model (Ilgamov et al., 1975, 1978)

Key 1 = rubber outer shell, 0.8 mm thick   3 = styrofoam body

     2 = toroidal rubber shell   4,5 = airlines

The most serious limitation of the model was the restriction on frequency due to heating of the air lines. Although the device was designed to operate in the frequency range 0-5 Hz, in practice frequencies were limited to ≤ 4 Hz by heating effects. In addition, wave amplitude was found to decrease significantly

at higher frequencies. This phenomenon was attributed to weakened pumping and bleeding on account of the long feed lines.

Further difficulties were encountered due to intense vibration of the model at several frequencies, and associated problems in measuring thrust. Damping plates were attached to the hull model to reduce horizontal and vertical vibrations.

Despite the practical problems associated with the wave-generator model, thrust force was measured (apparently satisfactorily) as a function of frequency and wave velocity at various submersion depths. Nonetheless, the use of a pneumatically-activated traveling wave device appears fraught with difficulties and is not recommended for future investigations.

Piezoelectric Systems

An active wall device, nominally designed for the cancellation of Tollmien-Schlichting waves in a laminar boundary layer in water, has been developed by researchers at Southwest Research Institute in San Antonio, Texas (Park, Silvus and Cerwin, 1985). Piezoelectric ceramic actuators have been used in preference to a mechanically-driven system. In this way, amplitude, frequency and velocity of the traveling wave are all independently controllable. In the absence of active wall boundary layer calculations as a basis for selecting values of traveling wave parameters, data on Tollmien-Schlichting waves and membrane models were used to select parameter ranges.

As can be seen from Table 11, wave amplitudes are small (≤ 13 microns) and a/λ values are three orders of magnitude less than present requirements. Unfortunately, the maximum deformation amplitude attainable using piezoelectric actuators is less than 0.1 mm (see Candidate Actuator Systems). The lead zirconate titanate actuators selected by Park and co-workers were chosen because they had the highest available piezoelectric strain constant (274 pm/V). Due to technology limits on the sizes of sheet piezoelectric materials, the maximum amplitude of deformation was estimated to be 25 microns, using a peak applied voltage of 300V. In practice, amplitudes of approximately half this value can be obtained.

Despite the limitations on wave amplitude, the piezoelectric active wall device constructed at Southwest Research Institute is extremely flexible in terms of frequency and wavespeed ranges (Table 11). In addition, the waveform is not limited to a sinusoid; the use of an electronic drive system permits generation of a traveling surface wave of essentially arbitrary shape. Due to funding limitations, the device has never been used for water tunnel experiments.

Electromagnetic Systems

Dermadrive: Traveling wave propulsion for underwater vehicles was the subject of a student project at the University of Michigan (Alberty and Jacquet, 1970). The student report describes Dermadrive (i.e., skin drive), "a new concept in silent underwater propulsion" which eliminates the need for a propellor. The Dermadrive concept was apparently inspired by the propulsion systems of fish such as the gymnotid and the skate which have flexible fins. The propulsive force in these creatures is understood to be derived from a traveling wave pattern that progresses along their ribbon-like fins (Figure 58). A more formal treatment of balistiform and gymnotiform locomotion has been published recently by Lighthill and co-workers (Lighthill and Blake, 1990; Lighthill, 1990).
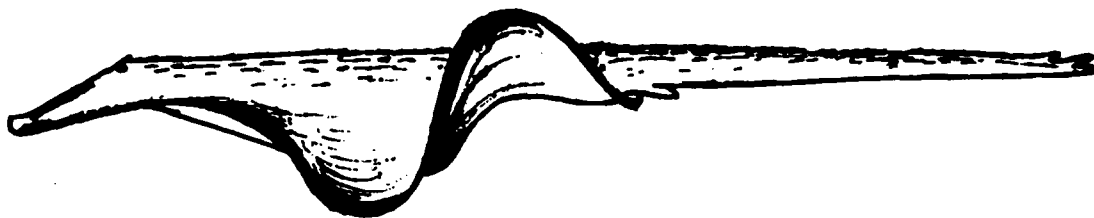
SKATE

GYMNOTID

Figure 58. Two Fish That Utilize Traveling Waves for Propulsion

The proposed Dermadrive submarine has a flexible skin-like shell surrounding the hull. The hull length is divided into 16 equal segments by 17 actuator systems. Each system is comprised of two sets of concentric, segmented magnetic rings. The inner electromagnetic ring is attached to the hull, and the permanently magnetized outer ring is attached to the inside of the flexible skin. By alternating the current in the electromagnetic rings, the resultant magnetic field can be made to repel and attract the outer rings alternately. Hence, the flexible skin executes an oscillatory motion. By suitable phasing of the current to each actuator, the circumferential traveling wave can be made to move aft along the length of the hull (Figure 59). In order to permit maneuverability of the submarine, each quadrant of the electromagnetic ring is independently controlled.
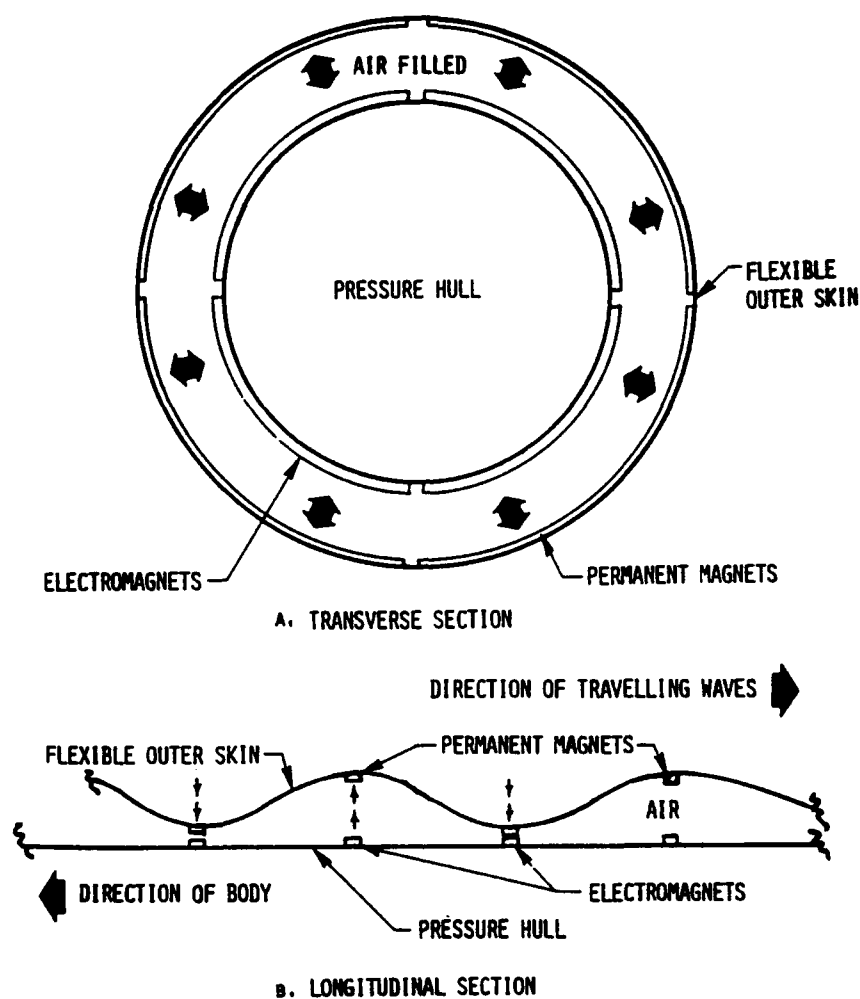
Figure 59.   Submarine Sections Illustrating Electromagnetic System
of Skin Oscillation (Not to Scale)

Unfortunately, plans to build a scale model of an electromagnetically propelled traveling wave submarine had to be abandoned due to time and financial limitations. Limited experimentation was performed using a working model with a mechanical cam system to generate and propagate the traveling wave pattern. Interestingly, the electromagnetic Dermadrive system is described in some detail in the Soviet literature (Chernikov, 1978).

Results obtained using the mechanical system are summarized in Figure 60, which illustrates the measured resistance (drag) or thrust as a function of the

110

rpm of the drive system. Regrettably, the investigation was inadequately documented and it is not possible to determine any of the traveling wave parameters from the student report. However, pronounced minima in resistance are observed at rpm values of 40 to 50. It is noted that the Dermadrive system is "not as well behaved" as a conventional propeller which generates thrust at all non-zero rpm values. In fact, the University of Michigan findings appear to be in qualitative agreement with the present traveling wave study, in that they indicate a reduction in drag only for specific combinations of wave and flow parameters.
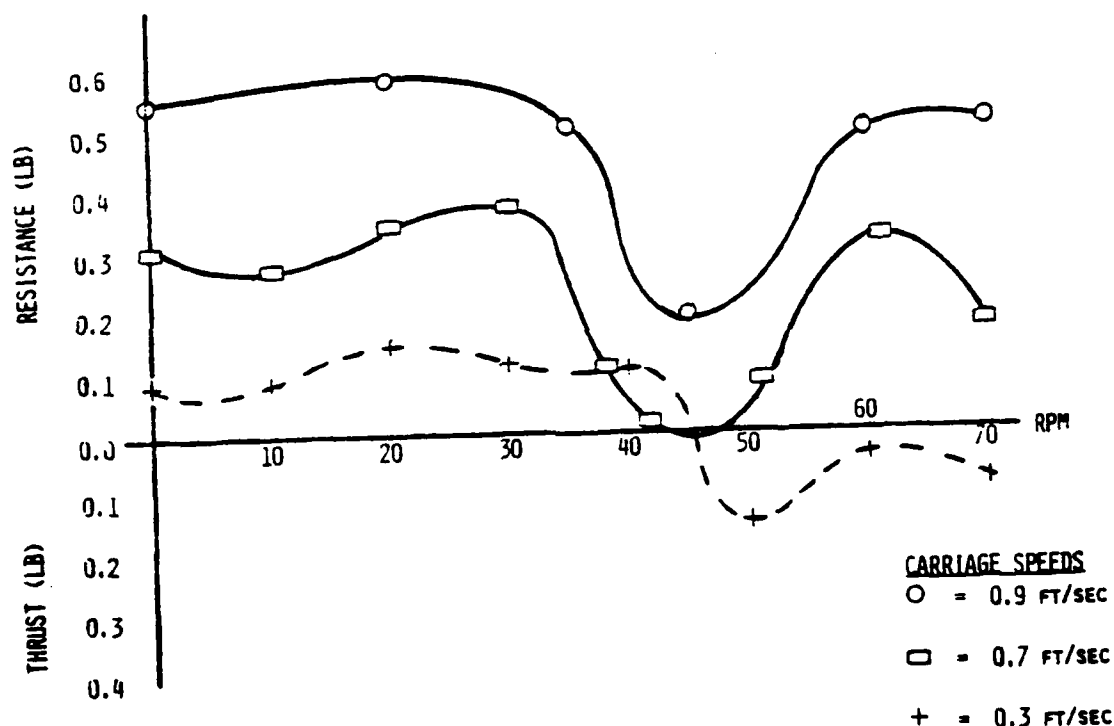
Figure 60. Drag/Thrust Characteristics of Mechanical Dermadrive Model

Drag Reduction Device for Underwater Vessels: A Soviet Inventor's Certificate from the Institute of Electrodynamics, Ukrainian Academy of Sciences (Kim, Afonin and Bondarenko, 1972) describes an electromagnetic device "for reducing the frictional drag of underwater vessels." The device, illustrated schematically in Figure 61, generates a "moving mechanical wave" (i.e., traveling wave).

The device may be constructed with an elastic ferromagnetic outer casing and a non-ferromagnetic damping fluid. Alternatively, if the elastic casing is made of a non-ferromagnetic material, then a damping fluid with suspended ferromagnetic particles (i.e., ferrofluid) is used to fill the cavities.

The passage of an electric current through the inductor results in interaction between the ferromagnetic material (casing or ferrofluid) and the inductor-generated electromagnetic field. The electromagnetic force of attraction is a maximum at points beneath the momentary poles of the inductor. As a result of this force the casing is deformed, creating wave troughs at the positions of the instantaneous poles.
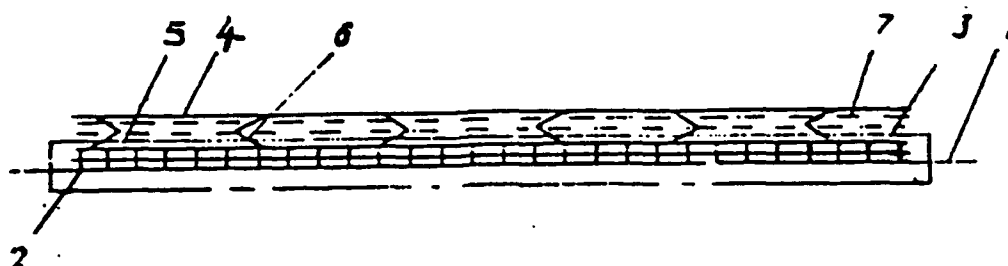
Figure 61.   Schematic of Soviet Electromagnetic Traveling Wave Device
(Inventor's Certificate Number 457629)

Key   1 = hull   5 = cavity between elastic casing and body
       2 = hull-mounted inductor   6 = resilient partition between cavities
       3 = sheath around inductor   7 = damping fluid (ferrofluid when casing is non-
       4 = (ferromagnetic) elastic casing   ferromagnetic)

Wave crests are created when the damping fluid is put under pressure in the regions of momentary poles and flows to lower pressure regions. Translation of the momentary inductor poles results in translation of the wave troughs and peaks, creating a moving mechanical wave.

Unfortunately, no information is provided on typical ranges of wave parameters achievable with this system. The principles of the device are not dissimilar from those of the Dermadrive system described above. In both cases, a hull-mounted electromagnet interacts with a permanent magnet mounted on or

enclosed in a flexible skin. The Soviet device is somewhat more sophisticated in that it incorporates a ferro-magnetic fluid, rather than air, in the cavities between the hull and the flexible casing.

CANDIDATE ACTUATOR SYSTEMS

General Comments

The preceding review of existing active wall systems, together with information on state-of-the-art actuator materials (see below), indicates that selection of an actuator system is a critical element in active wall design. In particular, the present requirements for wave amplitudes ≥ 0.5 cm and frequencies in the range 10 to 100 Hz impose severe technical restrictions on candidate actuator systems. In general, the requirement for wavelengths on the order of 10 cm can readily be accommodated.

Ongoing research on adaptive and "smart" structures is extremely relevant to present active wall requirements, as may be seen from the following discussion. Actuator materials such as piezoelectrics, shape memory alloys, and magnetostrictors are currently attracting considerable attention, and significant developments have been reported in the last five years. However, it is important to bear in mind that the principal objective of the proposed experiment is to investigate basic traveling wave behavior for specified ranges of wave and flow parameters. In the short term, it is desirable to design an active wall device which can be developed with minimum technical risk, while focusing attention on a range of experimental issues, such as drag measurement techniques and boundary conditions.

Mechanical Actuators

Inspection of the data presented in Table 11 shows that mechanically-driven active wall devices have generally been favored by earlier researchers. Wave amplitudes of 0.1 to 2.3 cm are reported, with wavelengths of 4 to 120 cm. Frequencies are generally ≤ 30 Hz, although Mattout (1976) reports frequencies up to 70 Hz, albeit with low amplitudes (0.1 and 0.2 cm). With one exception

113

(Alberty and Jacquet, 1970), the traveling wave devices were apparently two-dimensional (plates).

Available information indicates that most of the devices were based on the rotating cam design developed by Kendall (1970). With such a system, wavespeed and frequency can be changed easily by changing the speed of rotation of the camshaft. Modifying amplitude and wavelength is much harder.

Cortana Corporation has received preliminary designs for active wall test devices from EG&G Washington Analytical Services Center, Inc., Rockville, MD, and from NorthWest Research Associates, Inc., Bellevue, WA. In both cases, mechanical actuators were selected in order to obtain the required parameter values (see Appendix C) with minimum .echnical risk. Both devices utilize a rotating camshaft arrangement. Some design details are proprietary.

The EG&G design is for a 2-D plate to be mounted on top of a flow channel. The simplest (and cheapest) option is for a fixed amplitude and fixed wavelength device, with variable wavespeed (and frequency)[3]. A more sophisticated option would provide for variable wavelength and wavespeed (plus frequency), with fixed wave amplitude. In the ideal case, amplitude, wavelength, and wavespeed could all be varied independently. However, the feasibility of having this degree of control with a mechanical system has not yet been demonstrated, and such a system will likely be expensive.

A number of technical challenges and risks have been identified by EG&G engineers. It is thought that the challenges can be met by applying well-known engineering techniques to produce a workable design. Issues to be addressed include the following:

- Cam set design to ensure safe mass/stiffness/critical speed relationships
- Control system design and implementation

---

[3] Wavespeed is the independent variable which is controlled by the speed of rotation of the camshaft. At a given wavelength, variation in wavespeed results in a variation in frequency (dependent variable).

- Cost efficient fabrication processes
- Cam/follower design
- Mechanical dynamics of cam/follower and membrane linkages
- Packaging wiring/sliprings for 240 steppermotors
- Cam loads on internal motors and gears/component size
- Design for operability and maintainability.

In contrast, significant development will likely be necessary in order to address the technical risks, which include the following:

- Membrane material and design considerations
- Load/Drag force measurement and implications for structure/mechanism
- Ensuring wave form fidelity where critical.

The other proposed design is for a mechanically-driven 3-D device (axisymmetric body of revolution). Again, the simplest option will be a fixed amplitude, fixed wavelength device with variable wavespeed (and frequency). An option to vary amplitude (discrete rather than continuous variation) can be incorporated. The wavelength can be changed by repositioning the actuators manually; this process is estimated to require one manday of effort. Some difficulties are anticipated in performing flow visualization studies, given the need to move lights and cameras along the water tank at the wave velocity (c), rather than at the freestream velocity (U_∞). However, a towed 3-D model was chosen in preference to a fixed 2-D plate in order to facilitate drag measurements.

Pneumatic Actuators

A 3-D pneumatically-driven active wall device has been used by Soviet researchers to measure the thrust generated by a traveling wave system (Taldykin and Ilgamov, 1975; Ilgamov et al., 1978). As noted earlier, frequencies were severely limited (≤ 4 Hz), and amplitude and frequency were not independent of each other. Stability problems were also encountered with the model. Somewhat surprisingly in view of these experimental difficulties, the

115

variation in thrust force as a function of wave velocity appears to have been measured satisfactorily. Nonetheless, a pneumatically-driven device is not an attractive option for future traveling wave investigations.

Hydraulic Actuators

A literature search for active wall devices has not revealed any hydraulically-activated systems, i.e., systems operated by fluid under pressure. However, in view of the considerable expertise which already exists in hydraulically-operated, variable-geometry systems, (i.e. swing-wing aircraft), this option was considered worthy of investigation.

Dowty Signature Management has manufactured wing slot seals for variable geometry aircraft such as the B1-B bomber, the General Dynamics F111, and the Panavia Tornado. Thus, Dowty personnel are familiar with both design and operational aspects of hydraulically-activated, variable-geometry systems. Following discussions with Dowty of active wall requirements for a traveling wave proof-of-concept experiment, it was concluded that hydraulic actuators are unsuitable for the proposed application because of frequency limitations. Difficulties are anticipated in obtaining wave frequencies much above 10 Hz, resulting in undesirable limitations on the parameter ranges which can be investigated.

Piezoelectrics

Piezoelectric materials generate a charge in response to a mechanical deformation, or, conversely, undergo mechanical strain when an electric field is applied across them. Hence, piezoelectrics may be used as electrical-to-mechanical or mechanical-to-electrical transducers. Various piezoelectric actuator materials, notably ceramics, and different actuator geometries have been investigated. In view of their small size, piezoelectric actuators can be incorporated into structures in a non-invasive fashion. Quasi-static shape control of plates with surface-mounted piezoelectrics has been demonstrated. As an alternative to surface bonding, piezoelectrics can be embedded inside composite laminates, as shown in Figure 62. The main advantages of embedding as opposed to surface mounting are an enhancement of the load

116

transfer from the actuator to the host structure and a surface structure free of fragile components and connections. When piezoelectrics are embedded in an electrically-insulating material such a glass/epoxy composite, they can be embedded directly without the need for any protective coating. However, if they are embedded in graphite/epoxy or some other conducting material, they must be electrically insulated to avoid short-circuiting of the actuator by the surrounding material.
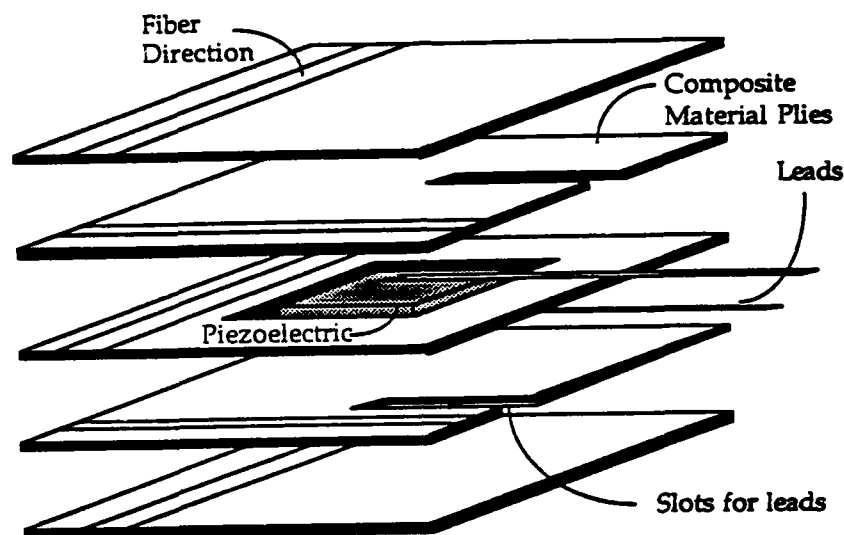
Figure 62.   Piezoelectrics Embedded in a Glass/Epoxy Laminate
(Hagood, Crawley, Luis and Anderson, 1988)

The relationship between the applied electric field and the mechanical response is described by a series of piezoelectric constants characteristic of the particular material being employed. For a longitudinal-extension element (actuator) of the type required for an active wall,

$$\sigma = d_{31} E \tag{103}$$

where σ is strain, E is electric field, and d_{31} is the piezoelectric strain constant. It should be noted that the applied field is in direction 3, and the mechanical response is in direction 1; hence, the piezoelectric strain constant is designated d_{31}. The above relationship may be rewritten in terms of actuator elongation, $\Delta\ell$, actuator length, ℓ, applied voltage, V, and actuator thickness, t, i.e.,

117

$$\Delta \ell = (d_{31} \, \ell V) \, / \, t \tag{104}$$

In practice, it is desirable to maximize $\Delta \ell$ (target value ≥ 0.5 cm for the proposed application), while minimizing the applied voltage and keeping the actuator dimensions, ℓ and t, within reasonable bounds. Both positive (expansion) and negative (contraction) values of strain are generally possible with piezoelectric actuators, depending on the sign of the applied voltage.

For applications requiring only small induced strains, piezoceramics such as PZT (lead zirconate titanate) behave linearly. However, in high strain applications material nonlinearities can cause difficulties in predicting the response of a piezoelectrically controlled structure, and hysteresis effects are observed. The variation of piezoelectric strain constant, d_{31}, as a function of strain for a typical material is shown in Figure 63.
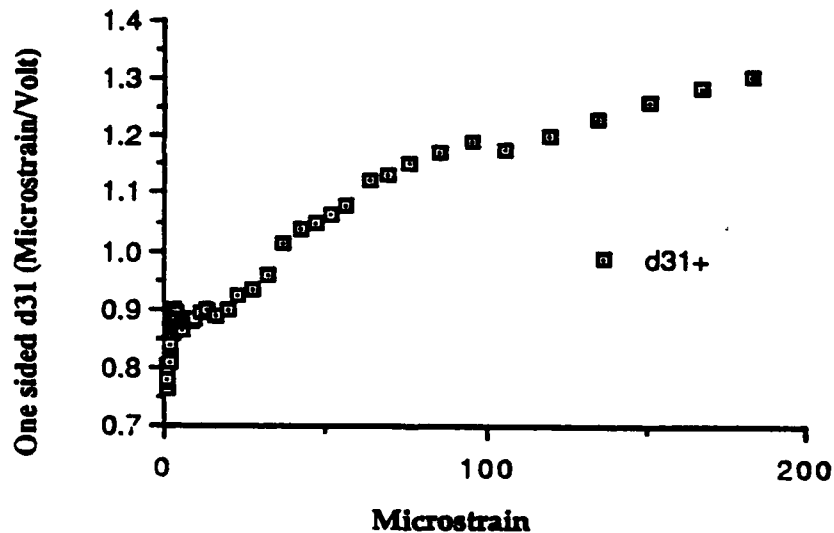
Figure 63. Variation of d_{31} as a Function of Material Strain

The general characteristics of piezoelectric actuators may be summarized as follows:

- maximum strain levels ~ 0.1 percent;
- high response speed (~ 10 μs);
- high applied electric fields (~ 1kV/mm); and
- high generative force (typically 400 kgf/cm^2).

For the proposed active wall application, the principal limitation is the maximum strain level. Park, Silvus and Cerwin (1985) selected a PZT ceramic as an actuator material, since this had the highest available piezoelectric strain constant (d_{31}). However, materials technology limitations on the sizes of sheet piezoelectrics restricted the maximum achievable deformation to ~10-20 μm. The peak applied voltage was 300V. Other researchers report problems with the reliability and durability of piezoelectric actuators, due in part to difficulties in materials preparation.

Recent developments at Pennsylvania State University have resulted in significant improvements in piezoelectric actuator materials, notably in terms of increased maximum strain values and reduced activation voltages. Strain levels of ~0.3 percent and activation voltages of 50-100V (~10-fold reduction compared to previous values) have been reported. Nonetheless, the strains are still too low to be of practical use for an active wall device required to generate waves of amplitude $\geq$0.5 cm. Hence, state-of-the-art piezoelectric actuators are not suitable candidates for the current application, despite their desirable features, such as precision displacement control, good frequency response, and demonstrated capability when used with sophisticated electronic control systems.

Electrostrictors

Electrostrictive materials undergo mechanical strain in an applied electric field. The induced strain in piezoelectrics is proportional to the applied field ($\Delta \ell / \ell \propto E$), whereas electrostriction is a second-order effect, and the induced strain is proportional to the square of the applied field ($\Delta \ell / \ell \propto E^2$). Thus, electrostrictors are monopolar rather than bipolar actuators. (Reversing the electric field does not alter the sign of the resulting strain.)

Until recently, electrostriction was considered a small effect of little interest for practical applications. However, newly developed materials based on lead magnesium niobate (PMN) exhibit electrostrictive strains up to 0.1 percent without hysteresis. The absence of hysteresis is a significant advantage of electrostrictors as compared to piezoelectrics. In addition, the non-linear relation between strain and electric field can be used to tune the piezoelectric

(electrostrictive) coefficient, d_{33}, as illustrated in Figure 64. The slope of the strain-electric field curve gives the value of d_{33}, which is seen to be zero in the absence of an applied field, but which increases to its maximum value under a bias field of ~3.7kV/cm. This maximum value is about twice the piezoelectric strain constant in PZT.
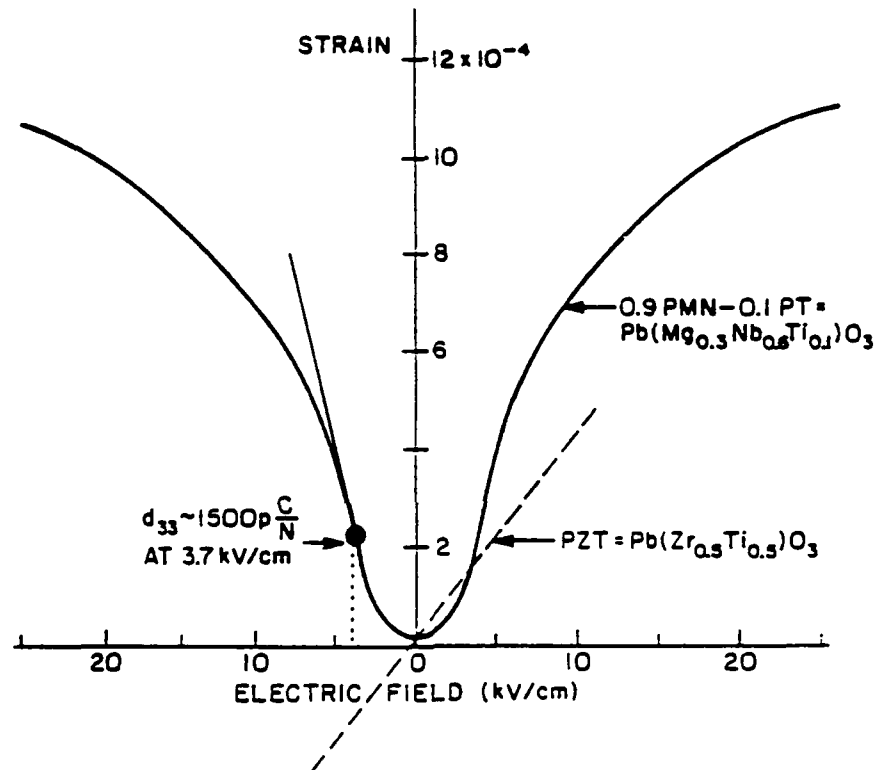
Figure 64. Strain Versus Electric Field for PMN-based Electrostrictor

Electrostrictive actuators have been used in shape control of mirrors and other optical surfaces. In common with piezoelectrics, electrostrictors are suited to applications requiring accurate control of displacements on the order of 10^{-5} m (0.001 cm). However, the maximum strain values are too low for the proposed active wall application requiring displacements ≥ 0.5 cm.

Shape Memory Alloys

Shape memory alloys, or SMAs, exhibit a temperature-induced deformation resulting from microstructural modifications associated with a martensitic transformation. A material which is plastically deformed below its martensitic transformation temperature has a "memory," and returns to its original shape when heated above the transition temperature. The martensite/austenite phase transformation produces significant forces as the alloy recovers its original shape, and SMAs can be used as actuators converting thermal energy to mechanical energy.

The Nitinol[4] series of nickel/titanium shape memory alloys has been widely studied, but a number of other materials also show shape memory behavior, e.g. copper/zinc, copper/aluminum/nickel and nickel/aluminum alloys. Nitinol shape memory actuators have been successfully used in robots, radiator valves, greenhouse vents, and liquid/gas switches. The use of SMAs for active vibration control is currently being investigated.

For the purposes of the proposed active wall application, the most important characteristics of SMA actuators are the following:

- magnitude of deformation (target > 0.5 cm)
- frequency response (target 10 - 100 Hz)
- ease of actuation (transformation temperature, actuation voltage).

Simple, straight actuator configurations lend themselves to the generation of small deflections. Helical actuator configurations are more suitable for producing large deformations. A deformation of 0.95 cm is reported using a helical Nitinol actuator with a total length of 85 cm, corresponding to a strain of ~1.1 percent (Baz, Iman and McCoy, 1987). This is significantly less than the plastic strains of 6 - 8 percent which can be completely recovered on heating small samples of SMA, but indicates that displacements on the order of 1 cm are achievable using state-of-the-art SMA actuators.

---

4   Nitinol is an acronym for Nickel Titanium Naval Ordnance Laboratory.

Phase transformation temperatures for Nitinol alloys are generally in the range 40-50°C, and the above actuator required an activation voltage of ~5 V. Hence, Nitinol actuators are suitable for operation at temperatures close to ambient, and do not require unacceptably high voltages for activation.

The frequency response of Nitinol actuators has been investigated by a number of researchers, and in all cases difficulties in rapidly cooling the SMA wires have limited frequencies to a few Hertz. Increasing the length of the wire improves the cooling response time by increasing the surface area over which heat dissipation occurs, and by reducing the power consumption for a given voltage. However, increasing the length also decreases the maximum strain achievable in practice, as shown by the data for helical Nitinol actuators given in Table 12.

Table 12. Strain Data for Helical Nitinol Actuators[5]

ACTUATOR LENGTH (cm)	DISPLACEMENT (cm)	STRAIN (%)
11.8	0.20	1.70
32.4	0.14	0.43
44.2	0.08	0.18

Alternatively, the speed of response to cooling can be significantly improved by using forced convection, i.e., by blowing cold air onto the actuator. This does not adversely affect either the response to heating or the maximum deflection amplitude. Nonetheless, the frequency response of SMA actuators with forced cooling is limited to a few Hertz, making these materials unsuitable for the proposed active wall application.

Electromagnetic Systems

Background: The possibility of using the attractive and repulsive forces between electromagnets, or between an electromagnet and a permanent

---

[5] Baz, Iman and McCoy, 1987.

magnet, has been proposed as a means of generating a traveling wave. The Dermadrive system (Alberty and Jacquet, 1970) incorporates permanent magnets attached to a flexible outer skin and hull-mounted electromagnets. An air gap separates the hull and outer skin. Although an electromagnetic Dermadrive device was never constructed, an analogous mechanically-driven system was built and used in water tunnel tests. Difficulties were encountered with an air-filled model, and the device had to be flooded to eliminate the hydrostatic load on the cams. Originally, the model was to have been air-filled with a pressure-regulating system to equalize internal and external pressures at depth. However, in practice the thin outer skin was unable to contain the local pressure distribution associated with expansion and deformation. It was noted that the internal fluid displacement accompanying traveling wave generation probably had an adverse effect on propulsive characteristics. Air, which is 800 times less dense than water, would offer less inertial resistance to the fluid displacement associated with the expansion and contraction of the outer skin.

In view of the practical problems encountered with an air-filled model, a related Soviet device which uses damping fluid rather than an air-gap appears more promising (Kim, Afonin and Bondarenko, 1972). Two variants of this device are proposed. In both cases, a hull-mounted inductor provides a variable electromagnetic field. One option employs a non-magnetic damping fluid enclosed between the hull and ferromagnetic elastic casing. Alternatively, a non-magnetic elastic casing is used in conjunction with a ferrofluid. The following section on ferrofluids describes the basic properties and behavior of these materials, and addresses some of the important issues associated with a ferrofluid traveling wave device.

Ferrofluids: A ferrofluid is a stable colloidal suspension of single domain ferromagnetic particles in a liquid carrier (Figure 65). The magnetic particles are generally iron oxide or cobalt oxide. A number of different carrier fluids can be used, including hydrocarbons, water and esters. The magnetic particles are generally 40-200 Å in diameter, and are coated with a dispersing agent to prevent agglomeration. Each particle is surrounded by a surfactant film one molecule thick. The repulsive force between the hydrophilic surfactant tails gives rise to an energy barrier which keeps the particles apart, even in a strong magnetic field gradient (Figure 66). The saturation magnetization of a ferrofluid

increases with increasing particle concentration. However, viscosity also increases with particle concentration, and for practical purposes particle loadings are generally limited to less than 15 percent by volume. A typical ferrofluid contains approximately 10^{23} particles per cubic meter.
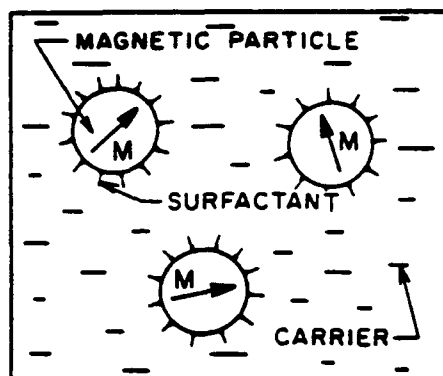
Figure 65. Components of a Ferrofluid
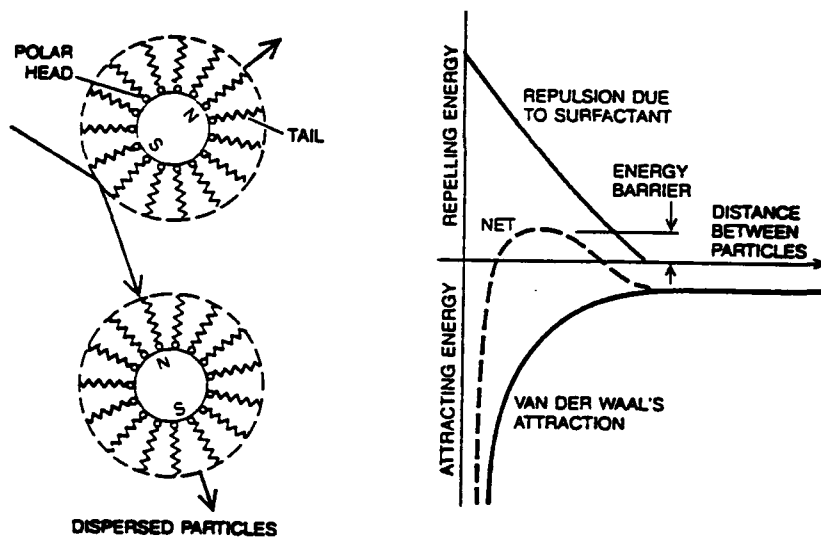
Figure 66. Surfactant Film on Magnetic Particles

Ferrofluids behave as normal homogeneous fluids, but are also highly susceptible to magnetic fields. The chemical, mechanical, and other physical properties of a ferrofluid correspond very closely to those of the carrier liquid. For example, ferrofluids utilizing organic carrier liquids are essentially non-conductive and have good lubrication properties. In the absence of an external magnetic field, the ferromagnetic particles are randomly oriented. In a uniform field, the particles align with the field direction according to the Langevin theory

124

of paramagnetism. The saturation magnetization is greater than that of a paramagnetic solid, but less than that of the ferromagnetic particle component. The magnetic properties of ferrofluid are described as superparamagnetic.

In a magnetic field gradient, the ferromagnetic particles in a ferrofluid experience a force which causes them to move through the carrier fluid. The drag associated with the particle motion causes the fluid to flow, and the ferrofluid appears to respond as a homogeneous magnetic liquid which moves to the region of highest field. The particles are not removed entirely from the carrier, since the particle flux in the direction of the field is balanced in the steady state by back diffusion. Ferrofluid behavior can be described mathematically by a modified Bernoulli equation with an added term to account for magnetic energy. The general form of the ferrohydrodynamic Bernoulli equation is

$$\text{pressure} + \begin{array}{c}\text{kinetic}\\ \text{energy}\end{array} + \begin{array}{c}\text{gravitational}\\ \text{energy}\end{array} + \begin{array}{c}\text{magnetic}\\ \text{energy}\end{array} = \text{constant} \qquad (105)$$

The most widespread commercial use of ferrofluids is in sealing devices, for example to prevent leakage in the gap between a rotating shaft and a cylindrical permanent magnet that forms a collar around it. The magnet poles are shaped so as to produce an intense magnetic field. The fluid creates an impermeable ring around the shaft while allowing it to rotate with negligible friction. Seals of this kind have been used for vacuum furnaces, gas lasers, motors and blowers.

As discussed earlier, a traveling wave device based on ferrofluids has been patented by researchers at the Institute of Electrodynamics, Ukrainian Academy of Sciences in Kiev. The invention applies to "shipbuilding, particularly to devices for reducing the frictional drag of a body moving in water." Cavities formed between an elastic casing and hull-mounted inductor are filled with ferrofluid. When an electric current passes through the inductor, an associated magnetic field is generated. Motion of the ferrofluid occurs towards the regions of highest field. By varying the current, and hence the magnetic field, the displacement of the ferrofluid can be made to generate a moving mechanical wave in the casing.

In the absence of any information on wave parameters, it is difficult to assess the practical feasibility of the Soviet ferrofluid traveling wave device. Two items which need to be assessed are the stability of the ferrofluid and its rheological properties. Popplewell and Charles (1981) discuss ferrofluid stability in terms of changes in particle concentration. For a ferrofluid to be stable, the changes in particle concentration resulting from an applied magnetic field should not be so great as to cause detrimental increases in viscosity or particle/carrier separation. The stability criterion depends upon the particular application envisaged, and should also take account of the time required to reach steady state conditions, which should be small compared to the time the ferrofluid is in a given field gradient.

The flow characteristics of ferrofluids in an applied magnetic field are also important in determining the ability of a ferrofluid to follow field variations. The rheological properties of ferrofluids will affect the amplitude and frequency parameters of any traveling wave device. Kamiyama, Koike and Wang (1987) have investigated the rheological behavior of ferrofluids with different carrier liquids. In the case of hydrocarbon-based magnetic fluids, the apparent viscosity increases with applied magnetic field, but is unaffected by shear rate, i.e., the fluid exhibits Newtonian behavior even in an external magnetic field. In contrast, water-based and diester-based magnetic fluids show Newtonian behavior in the absence of an external field, but exhibit the flow characteristics of a pseudo-plastic fluid in an applied field. The apparent viscosity is affected not only by the magnetic field, but also by shear rate.

In view of the limited resources available for the present study of active wall technologies, it has not been possible to search for additional Soviet reports on ferrofluid traveling wave devices. However, Soviet researchers are clearly of the opinion that the frictional drag of a body moving in water can be reduced using a traveling wave device, and have at least considered using ferrofluids as actuators for active wall systems.

Magnetostrictors

Magnetostrictive materials exhibit strains when subjected to a magnetic field. These strains occur as anisotropic magnetic domains within the material attempt to align with the local magnetic field. Iron, cobalt and nickel exhibit magnetostrictive properties with maximum strains on the order of 10^{-5} (0.001 percent). Recently a series of iron-lanthanide alloys known as Terfenol-D[6] has been developed; these materials exhibit magnetostrictive strains greater that 10^{-3} (0.1 percent). The general composition of Terfenol alloys is $Tb_xDy_{1-x}Fe_2$, where x~0.3. Alteration of the stoichiometry often allows optimization of the strain-versus-magnetic field curve for the various applications. The following properties are reported for a typical Terfenol alloy:

- Young's modulus 2.5 - 3.5 x 10^4 MPa (4-5 x 10^3 ksi)
- tensile strength 28 MPa (4.1 ksi)
- compressive strength 700 MPa (102 ksi)
- density 9.25 g/cm^3 (~0.33lb/in^3)
- Curie temperature 400°C (750°F).

In practice it has been found that Terfenol operates most effectively as a precision actuator by inducing a uniform magnetic field and then varying field strength about this constant value. This results in increases and decreases in length around a mean value. For large strains at high frequencies, Terfenol actuators must be placed in compression to avoid dynamic fracture caused by inertial forces. In a prestressed condition, good frequency response up to 1 kHz may be possible.

Figure 67 shows FSZM (free stand zone melt) Terfenol-D response curves for two stoichiometries (Goodfriend & Shoop, 1991). The magnetostrictive strain is given in parts per million (ppm). The width of the curve represents hysteresis. Terfenol actuators exhibit linear behavior for displacements smaller than ~0.05mm. Linear operation with peak-to-peak displacement amplitudes of

---

[6] The name "Terfenol" comes from the symbols for the elements in the alloy and for the Naval Ordnance Laboratory (NOL, now NSWC) where the material was first investigated.

0.025mm has been demonstrated for 25mm long devices. Larger amplitudes are theoretically possible using longer actuators, but it appears extremely unlikely that displacements on the order of 0.5cm would be feasible, particularly since actuator behavior is non-linear for large displacements. Thus, magnetostrictors do not appear to be suitable candidate actuator materials for the proposed active wall device.
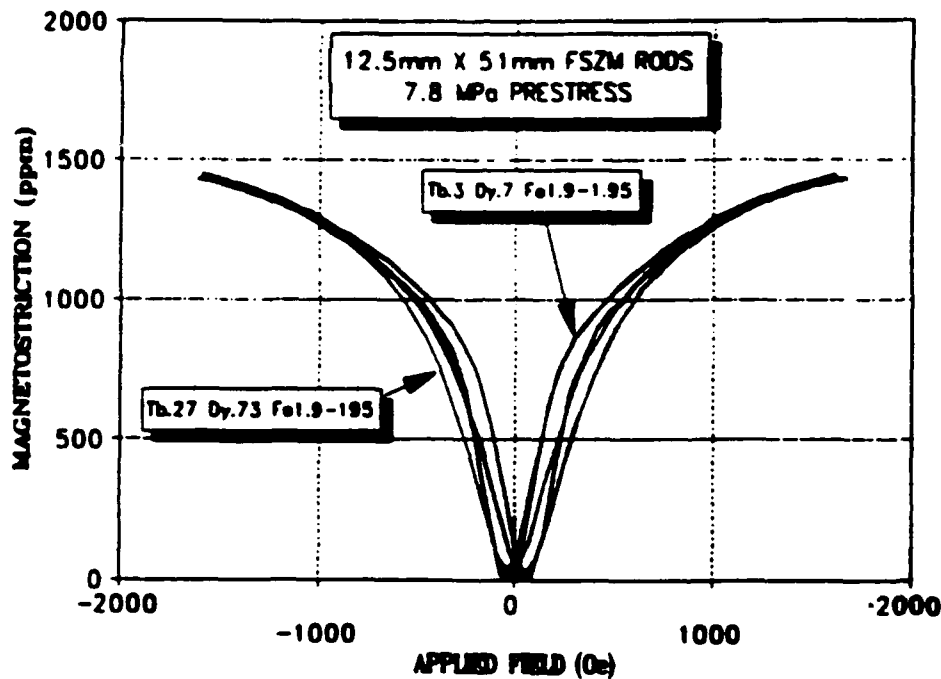
Figure 67. Terfenol-D Response Curves for Two Stoichiometries

Electrically Conductive Polymers

Electrically conductive polymers exhibit conductivities approaching those of metals. For example, the conductivity of polyacetylene has been reported as high as 1.5×10^5 siemens/cm (typical value ~ 2×10^4 siemens/cm), compared to 6.0×10^5 siemens/cm for copper. The electrical conductivities of insulating polymers are typically in the range 10^{-15} to 10^{-20} siemens/cm.

Electrically conductive polymers are generally made by doping of insulating polymers which have a conjugated backbone structure consisting of alternating single and double chemical bonds. In the doping process, mobile charge

carriers are introduced via redox reactions. Electron delocalization along the polymer backbone provides a pathway for charge carriers, and a resulting increase in electrical conductivity of 20 to 25 orders of magnitude. Doping can be achieved in several ways:

- exposure of insulating polymer to dopant gases such as bromine and iodine;
- covalent bonding of the dopant (e.g. sulfonic acid) to the polymer; and
- application of a voltage between the polymer and dopant (electrochemical doping).

In the case of electrochemical doping, the applied voltage causes dopant ions, such as boron tetrafluoride, to penetrate the insulating polymer, making it conducting. Reversal of the applied voltage "dedopes" the polymer which reverts to its insulating state. The ability to switch the polymer between its insulating and conducting states has many potential applications, including electromechanical actuators.

Certain dopant/polymer combinations exhibit dimensional changes of up to 10 percent in length associated with the insulating/conducting transition. Hence, these materials may be used as actuators converting electrical to mechanical energy. The associated technology is immature, but researchers at Allied Signal Inc. have proposed a variety of extensional devices. Conductive polymers are understood to offer increased work capacity per cycle at an order of magnitude less voltage than piezoelectric actuators.

Conductive polymer electromechanical actuators have not yet been sufficiently investigated to be considered serious candidates for an active wall test plate. However, quoted strain values ($\leq$ 10 percent) are encouraging, as are data on actuator efficiency. (In principle, for a strain of 10 percent, a deformation of 0.5 cm is obtained using an actuator 50 cm long.) The frequency response of conductive polymer actuators will depend upon the insulating/conducting transition rate, which is a function of the migration rate of dopant ions. It would therefore appear that frequencies of 10-100 Hz should be readily achievable. Thus, conductive polymer actuators could be attractive long-term options for active wall devices.

CONCLUSIONS AND RECOMMENDATIONS

On the basis of the preceding reviews of existing traveling wave devices and state-of-the-art actuator systems, a number of recommendations can be made regarding an active wall device for a traveling wave proof-of-concept experiment. The principal objective of this experiment is to demonstrate that it is possible to generate and sustain stable vortices in the troughs of a traveling wave, such that both viscous shear forces at the wall and pressure drag are nearly zero. Ideally, the associated ranges of flow and wall parameters would also be identified.

Regrettably, available data from traveling wave experiments are often ambiguous and inconclusive, particularly with respect to drag reduction. Flow visualization data are sparse, but it is interesting to note that in the two cases where flow visualization was investigated (Table 13), vortex entrapment was successfully demonstrated for a/λ values within the range identified in the present study, i.e. $0.10 \leq a/\lambda \leq 0.25$. c/U_∞ values were slightly lower than the present target values of about 0.5. Drag reduction data are more numerous but also less consistent. Wide ranges of a/λ and c/U_∞ values have been investigated, although not all parameter values have been fully documented in every case. It would appear that drag reduction, and even thrust, can be obtained using a traveling wave device. Such effects are only observed for specific parameter ranges/combinations, but available data do not permit identification of critical parameters and values. Hence, further experimental investigation is required, particularly to quantify drag reduction effects and to identify associated parameter values.

Table 13. Summary of Experimental Data

REFERENCE	SECONDARY FLOW	DRAG REDUCTION/THRUST
Kendall (1970)	no flow visualization	no drag measurements
Merkulov & Savchenko (1970) Savchenko (1979)	vortex entrapment demonstrated $c/U_\infty = 0.33$, $a/\lambda = 0.2$	measured drag reduction associated with formation of secondary flow
Taneda & Tomonari (1974)	vortex entrapment demonstrated $c/U_\infty = 0.23$, $a/\lambda = 0.19$	no drag measurements
Mattout (1976)	no flow visualization	measured drag reduction/thrust
Ilgamov et al. (1975, 1978)	no flow visualization	measured thrust
Park, Silvus & Cerwin (1985)	no experimental data	no experimental data
Alberty & Jacquet (1970)	no flow visualization	measured drag reduction/thrust
Kim, Afonin & Bondarenko (1972)	no information available	reduction in frictional drag claimed

In the near term, an active wall device for traveling wave proof-of-concept experiments must be developed with low technical risk. Items such as noise and magnetic signature, which would be critical in practical submarine applications, need not be addressed at this stage. However, solutions are required to a number of unresolved issues, including the following:

- Are drag measurements best performed using a 2-D (plate) or 3-D (body of revolution) device? Although none of the traveling wave reports cited above mention problems associated with drag measurement, discussions with a number of researchers have indicated that great care is needed in order to measure drag accurately with any type of active wall device.

- Further investigation of boundary conditions is required, e.g. nature and extent of transition from flat to active wall, closure of a 3-D active wall device. Kendall (1970) considers the length of active wall required to establish equilibrium flow conditions, but

131

other researchers do not address the influence of the given boundary conditions upon their experimental data.

In any traveling wave study, careful documentation of parameter values and experimental details is extremely important, particularly in view of the present incomplete understanding of traveling wave phenomena. For example, it is not clear whether there is a relationship between the abruptness of the flat/wavy wall transition and the number of wavelengths required to establish equilibrium flow conditions. Reported studies are not documented in sufficient detail to shed any light on this issue.

The properties of candidate actuators for an active wall device are summarized in Table 14. Inspection of these data shows mechanical actuation to be the only viable, low risk, short-term option to achieve target traveling wave amplitude and frequency values. Technical barriers to the implementation of a number of other actuator systems have been identified. Pneumatic, hydraulic, and shape memory alloy systems are all subject to severe frequency limitations (<10 Hz), while piezoelectric, electrostrictive, and magnetostrictive actuators are only suitable for deformation amplitudes on the order of 0.001 cm. Electromagnetic systems may provide an alternative to mechanical actuation, but no satisfactory practical implementation of the proposed designs has been reported. Consequently, mechanical actuators are preferred for a near-term proof-of-concept experiment where low technical risk is important in minimizing costs. Available data indicate that actuators based on electrically conductive polymers may be attractive candidates in the long term, but the associated technology is presently in its early development stages.

The frequencies of mechanically-driven active wall devices described in the technical literature are generally ≤ 30 Hz, although frequencies up to 70 Hz have been reported for small wave amplitudes (0.1 and 0.2 cm). Some difficulties may be anticipated in combining amplitudes on the order of 1 cm with frequencies greater than ~30 Hz. A mechanical device designed to operate under these conditions would need to be reasonably robust, and researchers are understandably apprehensive about forecasting the useful lifetime of a high frequency, high amplitude, mechanically-actuated traveling wave device.

132

Table 14. Summary of Actuator Characteristics

ACTUATOR TYPE	FREQUENCY (TARGET 10-100 Hz)	WAVELENGTH (TARGET 5-20 cm)	AMPLITUDE (TARGET 0.5-5 cm)	ACTUATION MECHANISM	COMMENTS
Mechanical	≤70 Hz demonstrated	4-120 cm demonstrated	0.1 - 2.3 cm demonstrated	rotating camshaft	• low-risk option to obtain target parameter values
Pneumatic	≤5 Hz	12 cm demonstrated	0.5 & 0.6 cm demonstrated	flow of compressed air	• frequency limited due to heating of air lines • amplitude depends on depth & frequency
Hydraulic	≤10 Hz	?	?	flow of pressurized fluid	• frequency limited
Piezoelectric	10 - 150 Hz demonstrated	1 cm demonstrated, longer wavelengths possible	~0.001 cm demonstrated	electric field, voltages ~ 50-100V	• amplitude limited, maximum strain for SOA materials ~ 0.3%
Electrostrictor	similar to piezoelectrics	target values achievable	~0.001 cm	electric field ~10 kV/cm	• amplitude limited, maximum strain ~ 0.1%
Shape Memory Alloy	limited to a few Hz	target values achievable	≤ 1 cm	temperature (resistive heating)	• frequency limited by cooling rates
Electromagnetic	?	target values should be achievable	?	magnetic attraction/ repulsion	• no practical demonstration of concept
Magnetostrictor	≤ 1 Hz	target values should be achievable	≤ 0.005 cm	magnetic field	• amplitude limited
Electrically Conductive Polymer	Target values should be achievable	target values should be achievable	?	electrochemical doping/dedoping	• strain values up to 10% demonstrated • long-term option, immature technology

Note: Shaded boxes indicate technical barriers to use of actuators for traveling wave device.

133

Ideally, a traveling wave test device would be designed such that wavespeed, amplitude and frequency could be varied independently. However, the feasibility of achieving this degree of flexibility with a mechanically-driven device has not been demonstrated to date. Nonetheless, an active wall system (2-D or 3-D) using mechanical actuators has been identified as the most promising candidate for a proof-of-concept experiment.

The most cost-effective, near-term option for an active wall device appears to be a mechanically-driven system with variable wavespeed and frequency, together with variable amplitude or wavelength. Thus, values of a/λ could be varied while either a or λ remained constant. Parameter ranges should be selected on the basis of theoretical data presented in earlier sections of the present report. Items which require further study prior to the construction of any traveling wave device are 1) the relative merits of 2-D and 3-D systems, and 2) the likely influence of different inflow (leading edge) boundary conditions.

VII. SUMMARY

VORTEX ENTRAPMENT

Physical models based on von Kármán vortex street and Kelvin-Stuart cat's eye analogies have been developed for the traveling wave. It has been shown that upon the proper choice of flow parameters and wall geometry, it is possible to capture vortices in the wave troughs and generate a nearly stable secondary flow, with a resulting reduction in total drag. An important characteristic of this type of flow condition is that the external flow is not in direct contact with the wall. A shear layer exists between the wall and the vortices, as well as between the freestream and the vortex. The controlled vortical flow regime cannot be classified as conventional laminar, transitional or turbulent flow.

COMPUTATIONAL APPROACH

As an aid in understanding the physics of the traveling wave, several different codes have been utilized (chiefly spectral and finite element). It was realized that the solutions are sensitive to grid size and that resolution is an important factor. Due to the periodic nature of the wall wave and the need for computational efficiency, some type of periodic scheme was always imposed in the computational analysis. It is believed that in a real application periodicity is achievable by properly energizing the wall. For exact periodicity of the flow in the mid-region, the total drag for the steady state approaches zero. The investigations to date have been limited to Reynolds numbers between 10^3 and 10^5, based on wavelength. However, recent experimental investigation indicates that the phenomenon is also applicable for turbulent flow.

DRAG REDUCTION

Results of the numerical computations for several parameter sets indicate that the entrapped vortices are not very sensitive to the exact flow condition and wall geometry. It was also shown that for an exact periodic flow at the leading and

135

trailing edges of each wave, the total drag of the mid-region is indeed equal to zero. This is due to the fact that, from a control volume viewpoint, the in-flow and out-flow conditions are the same. Therefore, there is no momentum deficit at the edges of the control volume. Drag characteristics for values of $c/U_\infty \sim 0.5$ suggest substantial drag reduction.

WALL PROFILE

Simulation studies based on sinusoidal, Kelvin-Stuart cat's eye, and cycloid wall profiles demonstrated the capability of reducing the drag with respect to that of a flat plate. However, evidence based on the results of the numerical study suggests that these may not be the optimum profiles and that further investigation is necessary. In fact, it has been conjectured that, for a wall shape corresponding to a minimum energy state (viewed from the traveling frame of reference), the induced vortex velocity, q_v, must approach the wall velocity, q_w, to minimize the slip velocity and the shear stress. The ratio q_v/q_w appears to be an important criterion which merits further study.

ENERGY

Hydrodynamic energy calculations for a traveling wave with a sinusoidal wall profile for $a/\lambda = 0.1$ and $c/U_\infty = 0.4$, 0.5, 0.6 and 0.7 indicate that the mid-region energy requirement is substantially less than that of a flat plate in laminar flow. In fact, calculation for $c/U_\infty = 0.7$ suggests over 90% energy savings at 350 time units for the spectral code. This case also indicates the onset of "thrust" at longer computational times. These calculations involved integrating the pressure and stress forces over one complete cycle for several different times. A simplified model indicated substantial energy savings in comparison to turbulent energy consumption over a flat plate.

136

ACOUSTIC PHENOMENA

Acoustic phenomena associated with the traveling wave have not been addressed in this report. It is believed that due to the unsteady nature of the pressure forces accompanying initial vortex formation, noise will be radiated. Since the acoustic energy radiated is proportional to the second time-derivative of the pressure, the fluctuating wall may also be an acoustic source. A simplified calculation should reveal the relative importance of this factor. More detailed calculation of radiated noise will need to be considered later.

EXPERIMENTAL VERIFICATION

Experimental verification of the traveling wave concept has been identified as important for future study. Although exact periodicity is required to minimize drag, it is important to investigate experimentally the feasibility of achieving periodic conditions in real flow.

Design and materials aspects of active wall systems have been investigated with a view to constructing a traveling wave test device for water tunnel experiments. The majority of traveling wave devices reported in the literature use mechanical actuators. Despite recent progress in developing actuator materials, such as shape memory alloys, piezoelectrics and electrostrictors, a mechanically-driven active wall device remains the only option presently available for generating waves with amplitudes on the order of 1cm. Although a mechanically-actuated traveling wave device is unsuited to practical submarine applications, valuable data could be obtained using a system of this type for laboratory experiments. Preliminary designs and order of magnitude cost estimates have been obtained for 2-D and 3-D mechanically-driven traveling wave test devices.

APPLICATIONS

The principal objective of the present study has been to investigate the physics of the traveling wave. However, in summarizing the investigations to date it is appropriate to mention briefly some potential applications.

The ultimate goal of this research is to apply the traveling wave technique to specific areas of a moving body. For our purposes, underwater vehicles, such as torpedoes and submarines, are the main candidates for utilizing the traveling wave to reduce drag. Depending upon the local pressure drop relative to the cavitation pressure, surface ships may also utilize this technique on submerged hull surfaces. Non-military and commercial applications must also be considered. These include high speed commercial surface ships and long pipelines to transport water, oil and other chemicals. The traveling wave could also be applied to the broad field of aerodynamics and wherever a reduction in skin friction is required.

Passive areas of a surface that contribute to the drag and act as negative work regions could become active and contribute to the total positive work. Formation of vortical flow in the wave train with production of a secondary flow and the so-called "fluid wall" will reduce wall pressure and make the skin friction nearly zero. Preliminary results of the numerical computations indicate the potential application of the traveling wave for a laminar in-flow regime. In order to achieve the optimum conditions, it is important to investigate the best location on the whole body surface for the traveling wave to be implemented. It is also necessary to identify the limitations to practical application of the traveling wave.

Traveling wave generation in an auto-oscillatory mode is of considerable interest for practical applications. A suitable combination of elastic coating properties and flow parameters can result in energy exchange between the fluid and coating such that a traveling wave develops on the coating surface. The implications of an auto-oscillatory system should become more evident with increased understanding of traveling wave phenomena.

138

REFERENCES

1.   Aizin, L.B., and Volodin, A.G. "Stability of the Boundary Layer Above the Surface of a Wave Travelling Over a Plate." Journal of Applied Mechanics and Technical Physics 20, 5 (September-October 1979): 562-565.

2.   Babenko, V.V. "A Flow-Around Mechanism in Aquatic Animals." Bionika 17 (1983): 39-45.

3.   Babenko, V.V. "Interaction of Flow with Elastic Surface." Stratifitsirovanyye i Turbulentnyye Techeniya. Sbornik Nauchnykh Trudov (1979): 292-300.

4.   Balasubramanian, R., and Orszag, S.A. Numerical Simulation of Flow Over Wavy Walls. New York, N.Y.: American Institute of Aeronautics and Astronautics, [1980].

5.   Balasubramanian, R., and Orszag, S.A. Numerical Studies of Laminar and Turbulent Drag Reduction - Part II. Hampton, VA: NASA Scientific and Technical Information Branch, 1983.

6.   Balasubramanian, R., and Orszag, S.A. Numerical Studies of Laminar and Turbulent Drag Reduction. Hampton, VA: NASA Scientific and Technical Information Branch, 1981.

7.   Baz, A.M.; Iman, K.R.; and McCoy, J.J. Active Control of Flexible Space Structures Using Nitinol Shape Memory Actuators. AD-A205 928. Silver Spring, MD: Statcon, Inc., [1987].

8.   Benjamin, T. Brooke. "Effects of a Flexible Boundary on Hydrodynamic Stability." Journal of Fluid Mechanics 9 (1960): 513-532.

9.   Benjamin, T. Brooke. "Shearing Flow Over a Wavy Boundary." Journal of Fluid Mechanics 6 (1959): 161-205.

10.   Benjamin, T. Brooke. "The Threefold Classification of Unstable Disturbances in Flexible Surfaces Bounding Inviscid Flows." Journal of Fluid Mechanics 16 (1963): 436-450.

11.   Berezovskii, A.A., and Kaplanskii, F.B. "Rising Vortex Ring in a Viscous Fluid." Izvestiya Akademii Nauk SSSR. Mekhanika Zhidkosti i Gaza 24, 3 (May-June 1989): 42-48.

12.   Berkovskiy, B.S., and Puchkova, T.G. "A Thin Profile Deformable in Accordance with the Laws Governing Variable Amplitude Traveling Waves." Bionika 15 (1981): 21-35.

13.   Blackburn, B.R., and Moore, K.J. Reynolds Number Modification with Compliant Coatings. Falls Church, VA.: Cortana Corp., [1980].

14.   Burdé, G.I. "An Exact Solution of the Navier-Stokes Equations." Izvestiya Akademii Nauk SSSR. Mekhanika Zhidkosti i Gaza 24, 4 (July-August 1989): 168-169.

15.   Bushnell, Dennis M. Turbulent Drag Reduction for External Flows. New York, N.Y.: American Institute of Aeronautics and Astronautics, [1983].

16.   Bushnell, Dennis M.; Hefner, Jerry N.; and Ash, Robert L. "Effect of Compliant Wall Motion on Turbulent Boundary Layers." Physics of Fluids 20, 10 (October 1977): 31-48.

17.   Bushnell, Dennis M., and Moore, K.J. "Drag Reduction in Nature." Annual Review of Fluid Mechanics 23 (1991): 65-79.

18.   Carpenter, P.W., and Garrad, A.D. "The Hydrodynamic Stability of Flow Over Kramer-Type Compliant Surfaces. Part 1. Tollmien-Schlichting Instabilities." Journal of Fluid Mechanics 155 (1985): 465-510.

19.   Carpenter, Peter W., and Gajjar, Jitesh S.B. "A General Theory for Two- and Three Dimensional Wall-Mode Instabilities in Boundary Layers over Isotropic and Anisotropic Compliant Walls." Theoretical and Computational fluid dynamics 1, 6 (1990): 349-378.

20.   Chernikov, V. "Bionics in Relation to Naval Research and Development Discussed." Voyennyye Znaniya 8 (August 1978): 42-43.

21.   de Loof, J.P. "A Synthesis on Drag Reduction Experiments at Bertin from Compliant Surfaces and Gas Film to Polymers." In: International Conference on Drag Reduction, p. F3-37-52. Bedford, England: BHRA Fluid Engineering, [1974].

22.   Demekhin, E.A., and Kaplan, M.A. "Stability of Stationary Traveling Waves on the Surface of a Vertical Film of Viscous Fluid." Izvestiya Akademii Nauk SSSR. Mekhanika Zhidkosti i Gaza 24, 3 (May-June 1989): 33-41.

23.   Dombrov, B.M., and Sorokodum, Ye.D. "The Kinematics of a Flexural-Oscillating Plate." Bionika 12 (1978): 62-67.

24.   Domm, Ulrich. "The Stability of Vortex Streets with Consideration of the Spread of Vorticity of the Individual Vortices." Journal of the Aeronautical Sciences 22, 11 (November 1955): 750-754.

25.   Donaldson, Coleman D. "Analysis of Moving Wavy Wall." Research notes, May 1989.

26.   Donaldson, Coleman D. Private communication, September 1990.

27.   Dovgiy, S.A., and Kayan, V.P. "On a Procedure for Determining the Thrust Developed by an Oscillating Wing." Bionika 15 (1981): 70-76.

28.   Dyke, M. van. Perturbation Methods in Fluid Mechanics. Stanford, CA: The Parabolic Press, 1975.

29.   Ericsson, L.E. Dynamic Omnipresence of Moving Wall Effects, a Selective Review. New York, N.Y.: American Institute of Aeronautics and Astronautics, [1987].

30.   Fedyaev, V.L. "On the Dynamic Interaction of an Elastic Shell with a Viscous Incompressible Fluid." In: Non-Linear Problems in Aerohydroelasticity. Kazan, R.S.F.S.R., 1979.

31.   Ffowcs Williams, J.E., and Purshouse, M. "A Vortex Sheet Modelling of Boundary-Layer Noise." Journal of Fluid Mechanics 113 (1981): 187-220.

32.   Ffowcs Williams, J.E., and Zhao, B.C. "The Active Control of Vortex Shedding." Journal of Fluids and Structures 3 (1989): 115-122.

33.   Goodfriend, M.J. and Shoop, K.M. "Adaptive Characteristics of the Magnetostrictive Alloy, Terfenol-D, for Active Vibration Control." In: Proceedings of the Conference on Recent Advances in Active Control of Sound & Vibration, p. 199-209. Edited by: C.A. Rogers and C.R. Fuller. Blacksburg, VA: Technomic Publishing Co., 1991.

34.   Goodman, W.L. The Effect of Opposing-Unsteady Vorticity on the Turbulent Structures in Wall Flow. New York, N.Y.: American Institute of Aeronautics and Astronautics, [1985].

35.   Gorodtsov, V.A. "'Slipping' of Turbulent Flow on Elastic Film." Stratifitsirovanyye i Turbulentnyye Techeniya. Sbornik Nauchnykh Trudov (1979): 345-349.

36.   Gottlieb, David, and Orszag, Steven A. Numerical Analysis of Spectral Methods. Arlington, VA: Office of Naval Research, [1977].

37.   Hagood, N.W.; Crawley, E.F.; de Luis, J.; and Anderson, E.H. "Development of Integrated Components for Control of Intelligent Structures." In: Smart Materials, Structures, and Mathematical Issues, p. 80-104. Edited by Craig A. Rogers. Lancaster, PA: Technomic Publishing Co., 1988.

38.   Hansen, R.J.; Hunston, D.L.; Ni, C.C.; and Reischman, M.M. "An Experimental Study of Flow-Generated Waves on a Flexible Surface." Journal of Sound and Vibration 68, 3 (1980): 317-334.

39.   Haque, Muhammad I., and Mahmood, Khalid. "Analytical Study on Steepness of Ripples and Dunes." Journal of Hydraulic Engineering 112, 3 (March 1986): 220-236.

40.   Haque, Muhammad I., and Mahmood, Khalid. "Geometry of Ripples and Dunes." Journal of Hydraulic Engineering 111, 1 (January 1985): 48-63.

41.   Holm, Darryl D.; Marsden, Jerrold E.; and Ratiu, Tudor. "Nonlinear Stability of the Kelvin-Stuart Cat's Eyes Flow." Lectures in Applied Mathematics 23 (1986): 171-186.

42.   Howard, F.G.; Goodman, W.L.; and Walsh, M.J. Axisymmetric Bluff-Body Drag Reduction Using Circumferential Grooves. New York, N.Y.: American Institute of Aeronautics and Astronautics, 1983.

43.   Hoyt, J.W. "The Effect of Additives on Fluid Friction." Transactions of the ASME Journal of Basic Engineering (June 1972): 258-285.

44.   Ilgamov, M.A.; Suleimanova, M.M.; Taldykin, M.V.; and Fedyaev, V.L. "A Wave-Generator Model." Soviet Physics Doklady 23, 7 (July 1978): 479-481.

45.   Ilgamov, M.A., and Fedyaev, V.L. "On Stationary Flow Induced by Surface Oscillations of a Cylinder." Paper presented at the Seminar on Shell Theory, Kazan, R.S.F.S.R., 1975.

46.   Ilgamov, M.A., and Taldikin, M.V. "Deformation Control of Cylindrical Shells in a Fluid." Paper presented at the Seminar on Shell Theory, Kazan, R.S.F.S.R., 1975.

47.   Ilgamov, M.A.; Suleimanova, M.M.; and Taldikin, M.V. "On One Model of a Wave Propulsive Device." Reports of the USSR Academy of Sciences 241, 2 (1978): 1-6.

48.   Ivashchenko, B.D.; Il'ichev, K.P.; and Postolovskii, S.N. "Hydrodynamic Effect of a Traveling Wave." Fluid Dynamics 10, 1 (January-February 1975): 122-124.

49.   Kalugin, V.N., and Panchuk, V.I. "Viscous Incompressible Fluid Flow Along a Traveling Wave (Numerical Experiments)." Bionika 4 (1970): 104-110.

50.   Kamiyama, Shinichi; Koike, Kazuo; and Wang, Zhi-Shan. "Rheological Characteristics of Magnetic Fluids." JSME International Journal 30, 263 (1987): 761-766.

51.   Kanarskiy, M.V.; Babenko, V.V.; Kozlov, L.F. "Experimental Investigation of Turbulent Boundary Layer on Elastic Surface." Stratifitsirovanyye i Turbulentnyye Techeniya. Sbornik Nauchnykh Trudov (1979): 56-67.

52.   Kazennov, A.K.; Karlikov, B.L.; Khomiakov, A.N.; Cherniavskii, F.N.; and Sholomovich, G.I. "Fishtail Type Motor Model with Flexible Carcass and Shell - Has Carcass with Longitudinal Cut-Out and Cantilever Curved Rod." Opisanie Izobreteniia k Avtorskomie Svidetel'stvie (August 1980).

53.   Kendall, James M. "The Turbulent Boundary Layer Over a Wall With Progressive Surface Waves." Journal of Fluid Mechanics 41, pt. 2 (1970): 259-281.

54.   Kida, Shigeo. "Stabilizing Effects of Finite Core on Kármán Vortex Street." Journal of Fluid Mechanics 122 (1982): 487-504.

55.   Kidun, S.M. "Investigating the Propagation Speed of Oscillations on the Skin of the Dolphin." Bionika 13 (1979): 52-58.

56.   Kim, K.I.; Afonin, A.A.; and Bondarenko, V.I. "Ustroistvo dlia Snizheniia Soprotivleniia Treniia Dvizhushchegosia v Vode Ob'ekta" ["Device for Reducing Frictional Drag of a Body Moving in Water"]. Opisanie Izobreteniia k Avtorskomy Svidetel'stvy 3 (26 June 1975).

57.   Korennaya, L.I. "Components of Viscous Drag of Undulating Body." Bionika 21 (1987): 53-58.

58.   Korennaya, L.I. "Method of Designing a Wave Propulsion Device." Bionika 15 (1981): 77-83.

59.   Kozlov, L.F., and Korennaya, L.I. "Measurement of the Thrust of a Plate with Wavy Deformation." Izvestiya Akademii Nauk SSSR, Mekhanika Zhidkosti i Gaza 20, 1 (January-February 1985): 186-188.

60.   Kozlov, L.P.; Korobov, V.I.; and Babenko, V.V. "The Effect of an Elastic Wall on a Boundary Layer." Reports of the Ukrainian Academy of Sciences, Series A, Physical, Mathematical, and Technical Sciences (January 1983): 45-47.

61.   Kramer, Max O. "Boundary-Layer Stabilization by Distributed Damping." Journal of the Aerospace Sciences 24 (1957): 459.

62.   Kramer, Max O. "Boundary-Layer Stabilization by Distributed Damping." Journal of the American Society of Naval Engineers 72 (1960): 25-33; Journal of Aeronautics/Space Sciences 27 (1960): 69.

63.   Kramer, Max O. "Hydrodynamics of the Dolphin." Advances in Hydroscience 2 (1965): 111-130.

64.   Krolenko, S.I., and Malkin, M.F. "Fishtail Propulsor Theory." Sudostroyenive 10 (1981): 14-18.

65.   Kuznetsov, N.G.   "Asymptotic Expansions for the Surface Waves Generated by a Submerged Body Moving with Rapidly Oscillating Velocity." Izvestiya Akademii Nauk SSSR, Mekhanika Zhidkosti i Gaza 20, 3 (May-June 1985): 138-145.

66.   Lamb, Horace.   Hydrodynamics.   London: Cambridge University Press, 1932.

67.   Landahl, M.T.   "On the Stability of a Laminar Incompressible Boundary Layer Over a Flexible Surface." Journal of Fluid Mechanics 13 (1962): 609-632.

68.   Lessen, Martin, and Gangwani, Santu T.   "Effect of Small Amplitude Wall Waviness Upon the Stability of the Laminar Boundary Layer." Physics of Fluids 19, 4 (April 1976): 510-513.

69.   Levy, H., and Forsdyke, A.G.   "The Stability of an Infinite System of Circular Vortices." Proceedings of the Royal Society of London Series A, 114 (May 1927): 594-604.

70.   Levy, H., and Hooker, S.G.   "Vortex System in the Wake of a Cylinder in a Fluid." Philosophical Magazine 9, 7th series, 57 (March 1930): 489-502.

71.   Lighthill, James, and Blake, Robert.   "Biofluiddynamics of Balistiform and Gymnotiform Locomotion.   Part 1. Biological Background, and Analysis by Elongated-Body Theory." Journal of Fluid Mechanics 212 (1990): 183-207.

72.   Lighthill, James.   "Biofluiddynamics of Balistiform and Gymnotiform Locomotion.   Part 2. The Pressure Distribution Arising in Two-Dimensional Irrotational Flow From a General Symmetrical Motion of a Flexible Flat Plate Normal to Itself." Journal of Fluid Mechanics 213 (1990): 1-10.

73.   Lighthill, James.   "Biofluiddynamics of Balistiform and Gymnotiform Locomotion.   Part 3. Momentum Enhancement in the Presence of a Body of Elliptic Cross-Section." Journal of Fluid Mechanics 212 (1990): 11-20.

74.   Lighthill, James.   "Biofluiddynamics of Balistiform and Gymnotiform Locomotion.   Part 4. Short-Wavelength Limitations on Momentum Enhancement." Journal of Fluid Mechanics 213 (1990): 21-28.

75.   Lin, J.C.; Walsh, M.J.; Watson, R.D.; and Balasubramanian, R. Turbulent Drag Characteristic of Small Amplitude Rigid Surface Waves. New York, N.Y.: American Institute of Aeronautics and Astronautics, [1983].

76.   Logvinovich, G.V.   "Hydrodynamics of a Thin, Flexible Body (Evaluation of Hydrodynamics of Fish)." Bionika 4 (1970): 5-11.

77.   Mahmood, Khalid, and Haque, Muhammad I.   "Bedform Length and Velocity Pulsations in Alluvial Channels." Journal of Waterway, Port, Coastal, and Ocean Engineering 114, 3 (May 1988): 315-330.

78.   Mattout, R. Reduction of Drag By Flexible Walls. NASA TT F-17089. Washington, D.C.: NASA, [1976].

79.   Mattout, R., and Cottenceau, B. Experimental Study of Activated Compliant Surface in Water Tunnel. Global Measures. Z.I. des Gâtines, France: Bertin et cie, 1972.

80.   Merkulov, V.I. "Flow of a Viscous Fluid Along a Traveling Wave." Izvestiya Akademiia Nauk SSSR. Sibirskoe Otdelenie. Seriia Tekhnicheskikh Nauk 2, 8 (1967).

81.   Merkulov, V.I. "On the Possibility of Body Motion Undisturbing Ideal Fluids." Paper presented at the 5th Mechanics Congress, Varna, Bulgaria, September 1985.

82.   Merkulov, V.I. "Traveling Wave on an Elastic Body Moving in an Ideal Fluid." Bionika 4 (1970): 95-104.

83.   Merkulov, V.I., and Savchenko, Yu.I. "Experimental Investigation of Fluid Flow Along a Traveling Wave." Bionika 4 (1970): 116-120.

84.   Nikishova, O.D. "Stability of Boundary Layer on Body of Actively Moving Aquatic Animals." Bionika 17 (1983): 31-35.

85.   Nikishova, O.D., and Babenko, V.V. "Flow of Liquid Around Flexible Bodies." Bionika 9 (1975): 55-60.

86.   Oossanen, P. van. "Hydrodynamic Resistance Characteristics of Humans, Dolphins and Ship Forms." Schip en Werf 15, 24 (November 1988): 501-510.

87.   Oshima, Yuko. "Motion of Vortex Rings in Water." Journal of the Physical Society of Japan 32, 4 (April 1972): 1125-1131.

88.   Osipenko, S.B.; Savchenko, Yu.N.; and Chernyy, I.M. "On the Efficiency of a Hydroreactive Propulsion System with a Changeable Shape." Bionika 13 (1979): 95-104.

89.   Park, Joel T.; Silvus, H. Stanley, Jr.; and Cerwin, Steve A. "Active-Wall Device for the Generation of Small Traveling Surface Waves." Review of Scientific Instruments 56, 5 (May 1985): 732-739.

90.   Pearson, C. Frederick, and Abernathy, F.H. "Evolution of the Flow Field Associated with a Streamwise Diffusing Vortex." Journal of Fluid Mechanics 146 (1984): 271-283.

91.   Pershin, S.V. "A Flapping Wing as a Vane Machine for the Forced Circulation of a Medium." Bionika 15 (1981): 84-94.

92.   Popplewell, J., and Charles, S.W. "Ferromagnetic Liquids — Their Magnetic Properties and Applications." IEEE Transactions on Magnetics Mag-17, 6 (November 1981): 2923-2928.

93.   Pyatetskiy, V.Ye., and Khatuntsev, V.N. "Efficiency of Cetacean Propulsion Complex." Bionika 19 (1985): 43-47.

94.   Riegel, F.W. Airfoil Section. London: Butterworth, 1961.

95.   Rousseau, A. Hydrodynamic Properties of Dolphin Skin. Z.I. des Gâtines, France: Bertin et cie, 1972.

96.   Saffman, P.G., and Schatzman, J.C. "An Inviscid Model for the Vortex-Street Wake." Journal of Fluid Mechanics 122 (1982): 467-486.

97.   Saffman, P.G., and Schatzman, J.C. "Stability of a Vortex Street of Finite Vortices." Journal of Fluid Mechanics 117 (1982): 171-185.

98.   Savchenko, Yu.N. "Hydrodynamic Effects of a Travelling Wave." Bionika 13 (1979): 19-24.

99.   Savchenko, Yu.N. "Some Characteristics of the Hydrodynamics of an Engine of the 'Flapping Wing Type.'" Bionika 5 (1971): 11-19.

100.   Schlichting, Hermann. Boundary Layer Theory. New York, N.Y.: McGraw-Hill, 1979.

101.   Sen, P.K., and Arora, D.S. "On the Stability of Laminar Boundary-Layer Flow Over a Flat Plate with a Compliant Surface." Journal of Fluid Mechanics 197 (1988): 201-240.

102.   Sergeev, V.S. "Stability of the Motion of a Rigid Body in an Unsteady Flow." Izvestiya Akademii Nauk SSSR, Mekhanika Zhidkosti i Gaza 23,3 (May-June 1989): 18-22.

103.   Sidorov, A.F. "Two Classes of Solutions of the Fluid and Gas Mechanics Equations and Their Connection to Traveling Wave Theory." Zhurnal Prikladnoi Mekhaniki i Tekhnicheskio Fiziki 2 (March-April 1989): 34-40.

104.   Stuart, J.T. "On Finite Amplitude Oscillations in Laminar Mixing Layers." Journal of Fluid Mechanics 29 (1967): 417-440.

105.   Taneda, Sadatoshi, and Tomonari, Yoshimasa. "An Experiment on the Flow Around a Waving Plate." Journal of the Physical Society of Japan 36, 6 (June 1974): 1683-1689.

106. Tovstykh, L.Ye.; Smirnova, A.G.; Zhurava, V.M.; and Faddeyev, Yu.I. "Estimation of Pressures on the Surface of a Deformable Ellipsoid of Revolution." Bionika 9 (1975): 51-55.

107. Tyndall, Juliet. "A Numerical Study of Flow Over Wavy Walls." (M.S. thesis, University of Iowa, 1988)

108. Urick, Robert J. Principles of Underwater Sound. 3rd ed. New York: McGraw-Hill Book Co., ©1983.

109. Vakili, A.D.; Wu, J.M.; and Bhat, M.K. High Angle of Attack Aerodynamics of Excitation of the Locked Leeside Vortex. Warrendale, PA: Society of Automotive Engineers, Inc., 1988.

110. Voropayev, G.A., and Svirskaya, Ye.A. "Boundary Conditions for Turbulent Flow on Viscoelastic Boundary." Bionika 16 (1982): 47-53.

111. Voskresenskii, V. "Underwater Flight." Nauka i Tekhnika 8 (1976): 20-25.

112. Wehrmann, O.H. Physics of Fluids 8 (1965): 1389.

113. Weinstein, L.M., and Balasubramanian, R. Second International Conference on Drag Reduction. Cranfield, England: British Hydromechanics Research Association Fluid Engineering, 1977.

114. Wille, R. "Kármán Vortex Streets." In Advances in Applied Mechanics, pp. 273-287. Edited by H.L. Dryden and T. von Kármán. New York, N.Y.: Academic Press, 1960.

115. Wu, J.M.; Wu, J.Z.; Wu, C.J.; and Vakili, A.D. "Preliminary Study of Nonlinear Flow Over Traveling Wave Wall." Paper presented at the International Symposium on Nonsteady Fluid Dynamics, ASME Fluid Engineering Division Meeting, Toronto, Canada, June 4-7, 1990.

116. Wu, J.Z., and Wu, J.M. Guiding Principles for Vortex Flow Control. New York, N.Y.: American Institute of Aeronautics and Astronautics, [1981].

117. Zubarev, V.M. "Boundary Layer on the Moving Surface of a Cylinder." Fluid Dynamics 18, 6 (November-December 1983): 862-866.

APPENDIX A
SPECTRAL CODE

The two-dimensional Navier-Stokes equations to be solved for the traveling wave problem in physical coordinates are:

$$\rho\left(\frac{\partial u}{\partial t} + u\frac{\partial u}{\partial x} + v\frac{\partial u}{\partial y}\right) = -\frac{\partial p}{\partial x} + \mu\left(\frac{\partial^2 u}{\partial x^2} + \frac{\partial^2 u}{\partial y^2}\right) \tag{A-1}$$

$$\rho\left(\frac{\partial v}{\partial t} + u\frac{\partial v}{\partial x} + v\frac{\partial v}{\partial y}\right) = -\frac{\partial p}{\partial y} + \mu\left(\frac{\partial^2 v}{\partial x^2} + \frac{\partial^2 v}{\partial y^2}\right) \tag{A-2}$$

$$\frac{\partial u}{\partial x} + \frac{\partial v}{\partial y} = 0, \tag{A-3}$$

For the traveling wave, we use the Galilean Transformation to transform the flow over a wave moving with a phase velocity c to that in a coordinate system that is fixed at a point on the wave; i.e.

$$\begin{aligned} X &= x\text{-}ct \\ Y &= y \\ T &= t, \end{aligned} \tag{A-4}$$

Note that with this transformation the field variables are

$$\begin{aligned} U &= u\text{-}c \\ V &= v \\ P &= p + 1/2\,(U_\infty^2 - (U_\infty - c)^2 \end{aligned} \tag{A-5}$$

Substituting these relations (equation A-5) in equations A-1 through A-3, it is seen that under Galilean Transformation, the Navier-Stokes equations take the form

$$\rho\left(\frac{\partial u}{\partial T} + (u - c)\frac{\partial u}{\partial X} + v\frac{\partial u}{\partial Y}\right) = -\frac{\partial p}{\partial X} + \mu\left(\frac{\partial^2 u}{\partial X^2} + \frac{\partial^2 u}{\partial Y^2}\right) \qquad (A\text{-}6)$$

$$\rho\left(\frac{\partial v}{\partial T} + (u - c)\frac{\partial v}{\partial X} + v\frac{\partial v}{\partial Y}\right) = -\frac{\partial p}{\partial Y} + \mu\left(\frac{\partial^2 v}{\partial X^2} + \frac{\partial^2 v}{\partial Y^2}\right) \qquad (A\text{-}7)$$

$$\frac{\partial u}{\partial X} + \frac{\partial v}{\partial Y} = 0. \qquad (A\text{-}8)$$

If one were to substitute the relation of equation A-6 in equations A-7 and A-8, one would obtain an equation system A-1 through A-3, except that the field variables are now U, V, P, i.e.,

$$\rho\left(\frac{\partial U}{\partial T} + (u - c)\frac{\partial U}{\partial X} + V\frac{\partial U}{\partial Y}\right) = -\frac{\partial P}{\partial X} + \mu\left(\frac{\partial^2 U}{\partial X^2} + \frac{\partial^2 U}{\partial Y^2}\right) \qquad (A\text{-}9)$$

$$\rho\left(\frac{\partial V}{\partial T} + (u - c)\frac{\partial V}{\partial X} + V\frac{\partial V}{\partial Y}\right) = -\frac{\partial P}{\partial Y} + \mu\left(\frac{\partial^2 V}{\partial X^2} + \frac{\partial^2 V}{\partial Y^2}\right) \qquad (A\text{-}10)$$

$$\frac{\partial U}{\partial X} + \frac{\partial V}{\partial Y} = 0. \qquad (A\text{-}11)$$

The Galilean Transformation thus allows for the solution of the flow over a moving wave train in a grid system which is fixed on the wave itself (crest of wave is typically chosen as the origin of this coordinate system), thereby simplifying the analysis of the flow. If the flow does not contain streamwise periodicity, the Galilean Transformation does not yield any advantages since the computational box occupies differing positions at various times (owing to the transformation X = x - ct); thus analyses using Galilean Transformation should and must only be conducted in periodic flow cases.

BOUNDARY AND INITIAL CONDITIONS

$$V(X, Y, T) = V(X + 2\pi, Y, T)$$
$$U(X, Y, T) = U(X + 2\pi, Y, T) \qquad \text{(A-12)}$$
$$P(X, Y, T) = P(X + 2\pi, Y, T)$$

Wall Boundary Conditions:

at $y_w = f(X, T)$.

$$U(X, f(X, T), T) = -c$$

$$V(X, f(X, T), T) = -c\frac{\partial Y}{\partial X}w \qquad \text{(A-13)}$$

and at $Y = \infty$,

$$U(X,Y,T) = U-c$$
$$V(X,Y,T) = 0 \qquad \text{(A-14)}$$
$$P(X,Y,T) = 0$$

Initial Conditions prescribed for the flow field:

$$U(X,Y,0), V(X,Y,0) \qquad \text{(A-15)}$$

Thus, the system of equations are integrated in time to get the evolution of flow from T=0 to any given time. Conventionally, the flow equations are solved in non-dimensional flow variables such as,

$$\widehat{X} = 2\pi X/\lambda$$
$$\widehat{Y} = 2\pi Y/\lambda \qquad \text{(A-16)}$$
$$\widehat{T} = 2\pi U_\infty T/\lambda$$

Therefore, a non-dimensional time $2\pi = 6.28$ represents typically one wavelength of evolution of flow at free-stream (X=U*T = 1 *2*π = 1 wavelength).

A-3

If the bottom wall $Y_w = 0$, i.e., the bottom is a flat surface, the solution of the equations represents the classical Rayleigh problem as long as the initial conditions are that the wall starts from rest. If the initial conditions happen to be that of a flow with a particular memory, such as a boundary layer with a given thickness (Blasius/laminar flow or turbulent flow) the time evolution on the flat surface closely parallels that of flat plate boundary layer, as long as correlation such as

$$L = L_0 + c_0 T \tag{A-17}$$

is used to relate the reference length that forms the characteristic Reynolds number (subscript 0 represents initial values).

The velocity c represents the phase velocity and can be obtained by calibration of flat plate evolution data with a boundary layer flow. This approach thus relates a temporarily evolving flow to a spatially evolving flow to a spatially evolving steady flow and is used to calibrate the reference plate drag characteristics in the numerical computations.

APPENDIX B
DISCRETE-ELEMENT METHOD

The fundamental algorithm is based on the artificial-compressibility hypothesis which is implemented in terms of two user-controlled constant parameters, i.e.,

D : Dilatation-factor

β : Pseudo-compressibility-factor,

which are selected on the basis of the requirements of each specific application.

The N-S system of PDEs for two-dimensional applications consists of

$$\frac{1}{D}\frac{\partial \varphi}{\partial t} + \frac{\partial V_x}{\partial x} + \frac{\partial V_y}{\partial y} = 0 + \left[\Delta t^2 A_\varphi \left(\frac{1}{N_{CFL,\beta,D}}\right)\left(\frac{2^{m+n}}{\partial x^m \partial y^n}\right)(V_x, V_y)\right] \quad \text{(B-1)}$$

$$\frac{\partial V_x}{\partial t} + \frac{\partial}{\partial x}(V_x V_x) + \frac{\partial}{\partial y}(V_y V_x) = -\frac{\partial p}{\partial x} + \frac{\partial T_{xx}}{\partial x} + \frac{\partial T_{yx}}{\partial y}$$

$$+ \left[\Delta t^2 A_x \left(\frac{1}{N_{CFL,\beta,D}}\right)\left(\frac{2^{m+n}\varphi}{\partial x^m \partial y^n}\right)\right] \quad \text{(B-2)}$$

$$\frac{\partial V_y}{\partial t} + \frac{\partial}{\partial x}(V_x V_y) + \frac{\partial}{\partial y}(V_y V_y) = -\frac{\partial p}{\partial x} + \frac{\partial T_{xy}}{\partial x} + \frac{\partial T_{yy}}{\partial y}$$

$$+ \left[\Delta t^2 A_y \left(\frac{1}{N_{CFL,\beta,D}}\right)\left(\frac{2^{m+n}\varphi}{\partial x^m \partial y^n}\right)\right] \quad \text{(B-3)}$$

where $m + n = 3$

The pressure p is formulated in terms of the dilatation φ and the pseudo-compressibility factor β, i.e.,

$$p = \beta\varphi. \tag{B-4}$$

The stress components T_{ij} can be considered as Laminar and/or Turbulent by using an algebraic-closure submodel based on Prandtl-Blasius power-law form and the local element-Reynolds number. A_φ, A_x, and A_y represent the "artificial-dispersion" terms of Δt^2-order and 3rd-order and 3rd-derivative form, "only as required" for damping out high-frequency oscillations (temporal and/or spatial). For the current application, the artificial-dispersion terms are not required. The computational algorithm can be implemented as a complete 2nd-order-accurate scheme for wave, advection and diffusion; i.e., all artificial-diffusion terms can be eliminated. Furthermore, it can also be implemented as a 3rd-order-accurate scheme, by implementing A_φ, A_x, and A_y; i.e., all artificial-dispersion terms can be minimized.

It is important to note that the dilatation-factor, D, and the pseudo-compressibility-factor, β, introduce an artificial-wave-speed, $C_{\beta,D}$ as,

$$C_{\beta,D} = \sqrt{\beta D} . \tag{B-5}$$

In all applications of the computational model, D and β are selected appropriately to guarantee an artificial-wave-speed $C_{\beta,D}$ much higher than the flow velocity (V_x, V_y), i.e.,

$$C_{\beta,D} \gg \max(V_x, V_y); \ C_{\beta,D} > 10 \max(V_x, V_y), \tag{B-6}$$

in order to guarantee high-speed wave phenomena which cannot compete with the advection and diffusion (viscous) effects. As a consequence of the artificial-wave-speed, $C_{\beta,D}$, the explicit timewise-integration algorithm requires a CFL number, $N_{CFL,\beta,D}$.

$$N_{CFL,\beta,D} = \frac{\Delta t \, C_{\beta,D}}{2 \min(\Delta x, \Delta y)} < 1, \tag{B-7}$$

for the stability of the computational results. Therefore, with β and D selected by the user, on the basis of the non-interference criterion for a specific application, the required time step Δt can be established by considering the selected spatial-resolution accuracy ($\Delta x, \Delta y$). The computational algorithm does not require any iteration (with "artificial time") between the "physical time" steps; and therefore, the computational results always represent "time-accurate" simulations of the transient flow conditions.

APPENDIX C
ACTIVE WALL TEST PLATE

Variables

1. Subject to towing tank limitations:

   - Length of plate (> active length, L)
   - Velocity of plate (U_∞)

2. Dependent on active wall configuration:

   - Wave speed (c)
   - Wavelength (λ)
   - Frequency (f)
   - Amplitude (a)
   - Waveform (sinusoidal, cat's eye, etc.)

Notes

- Variables are not all independent. The following relationships are defined:

$$c = \lambda f \tag{C-1}$$

$$Re = \lambda U_\infty / \nu \tag{C-2}$$

   where Re = Reynolds number
   ν = viscosity of water
   (1.3×10^{-6} m^2 s^{-1})

- Complexity and cost of the active wall configuration are likely to increase with increases in the following parameters:

   - number of wavelengths in active length, L/λ
   - amplitude, a

- frequency, f
- complexity of waveform

- One of the major design goals for the active wall test plate is that the wave amplitude, together with two of the three related parameters - wavelength, speed and frequency - should be independently controllable. Most active wall schemes reported in the literature permit arbitrary control of one or two of these parameters. Since the amplitude/wavelength ratio, a/λ, is a critical test parameter, it is particularly important that either amplitude or wavelength should be independently controllable to permit investigation of a/λ values in the range of interest (0.10 - 0.25). In practice it may be difficult to vary wavelength; mechanically-driven wall devices described in the literature are fixed-wavelength systems.

Requirements

- $\lambda \geq 5$ cm   (C-3)

- Active length of plate incorporates at least 10 wavelengths, i.e. $L \geq 10 \lambda$

- $0.10 \leq a/\lambda \leq 0.25$ (C-4)

- $c/U_\infty \geq 0.5$ (C-5)

- $10^5 < Re < 3 \times 10^6$ (C-6)

Test Parameters

Values of plate and active wall parameters for the tests can be defined as follows on the basis of requirements specified above and the desirability of minimizing complexity and cost of test systems.

Wavelengths should be in the range

    $\lambda = 5\text{-}20$cm   (C-7)

The active plate length should be in the range

$$L \sim 0.5\text{-}2m \qquad\qquad\qquad (C\text{-}8)$$

such that the condition $L \geq 10\lambda$ is satisfied for the wavelength value(s) selected.

Amplitudes of vibration should be in the range

$$a = 0.5\text{-}5cm \qquad\qquad\qquad (C\text{-}9)$$

such that $0.10 \leq a/\lambda \leq 0.25$ for the selected wavelength value(s).

Values of frequency, wave-speed, and plate velocity should be within the ranges specified below, subject to the limitation that $c/U_\infty \geq 0.5$.

$$f = 10\text{-}100 \text{ Hz.} \qquad\qquad\qquad (C\text{-}10)$$
$$c = 2\text{-}5 \text{ m.s}^{-1} \qquad\qquad\qquad (C\text{-}11)$$
$$U_\infty = 4\text{-}10 \text{ m.s}^{-1} \quad (\sim 8 - 20 \text{ knots}) \qquad\qquad (C\text{-}12)$$

The minimum value of Reynolds number ($\lambda = 5cm$, $U_\infty = 4$ m.s^{-1}) is 1.5×10^5.
The maximum value of Reynolds number ($\lambda = 20cm$, $U_\infty = 10$ m.s^{-1}) is 1.5×10^6